ADVANCED POLYMERIC MATERIALS FOR THE ENHANCED PERFORMANCE OF ENERGY STORAGE DEVICES

WANG JINGWEI

PhD

The Hong Kong Polytechnic University

This programme is jointly offered by The Hong Kong
Polytechnic University and Harbin Institute of
Technology, Shenzhen

2021

The Hong Kong Polytechnic University
Department of Mechanical Engineering
Harbin Institute of Technology, Shenzhen
School of Materials Science and Engineering

Advanced Polymeric Materials for the Enhanced Performance of Energy Storage Devices

Wang Jingwei

A thesis submitted in partial fulfillment of the requirements for the degree of Doctor of Philosophy

August 2020

CERTIFICATE OF ORIGINALITY

I hereby declare that this thesis is my own work and that, to the best of my knowledge and belief, it reproduces no material previously published or written, nor material that has been accepted for the award of any other degree or diploma, except where due acknowledgement has been made in the text.

Wang Jingwei

Abstract

This thesis reports the utilization of polymeric materials in the improvement of electrochemical devices. A sodium-ion conducting PVA-based gel electrolyte was first developed for the application of electric double-layer capacitors (EDLCs). Sodium triflate (NaTf) was selected as the electrolytic salt and NMP was employed as the solvent of PVA and NaTf. The composite (PVA with 30% NaTf and 10% EMITf) showed a high ionic conductivity of 3.8×10^{-3} S cm^{-1} and good thermal stability up to 150 °C. It was thus employed in the fabrication of EDLCs by using a spinning-casting method, serving as both ion-conducting electrolyte and separator. The capacitor showed almost 100% coulombic efficiency and stable charge-discharge cyclic property with almost 100% capacity retention after 1000 cycles, when charging up to 1.6 and 2.0 V with a capacity of 103.7 and 127.8 F g^{-1}, respectively.

The PEDOT-PDMS co-polymer was then synthesized to have good electrical conductivity from PEDOT and flexibility because of the amorphous nature and conjugated structure. The synthesis was made through the hydrosilylation and dehydrocoupling reaction occurred between the h_2PDMS and the EDOT monomer. The Young's modulus, tensile stress, and the strain of the polymer film at the rupture are 1.17 ± 0.10 MPa, 22.4 ± 2.1%, and 0.24 ± 0.03 MPa, respectively.

The PEDOT-PDMS co-polymer was coated onto the prepared high-voltage $NaLiFePO_4F$ electrode to protect the electrode from hydrofluoric (HF) acid attack and prevent the loss of active material. The resulting PEDOT-PDMS coated $NaLiFePO_4F$ electrode showed a specific capacity of 88.1 mAh g^{-1} at 0.5 C after 500 cycles, and good cycling stability, with about 100% retention of the initial discharge capacity. As for the $NaLiFePO_4F$ control electrode, its specific capacity recorded was 59.5 mAh g^{-1} only under the same conditions, which is 78% retention of the initial discharge capacity. The coated electrode shows high chemical diffusion coefficient of Li^+ (1.89×10^{-9} and 1.20×10^{-9} cm^2 s^{-1} during charging and discharging) compared to $NaLiFePO_4F$ control electrode (7.17×10^{-10} and 5.29×10^{-10} cm^2 s^{-1} during charging and discharging).

Furthermore, PEDOT-PDMS was employed as a protection coating layer on the surface of commercially available Si nanoparticles to provide conducting pathways and suppress the volume change in cycling. The coated Si was found to show superior performance as anode of Li-ion battery with a capacity of 1512 mAh g^{-1} obtained after 1000 cycles, which is 69.8% retention of the highest specific capacity around the 160th cycle (~2166 mAh g^{-1}) at 0.5 C. As for the Si control electrode, its specific capacity only was 605 mAh g^{-1} after the 500th, which is 29% retention of the highest/initial discharge capacity. Also, the coated Si electrode shows higher Li-ion diffusion coefficient (2.47×10^{-11} cm^2 s^{-1}) and lower internal resistance than that of the Si control electrode (5.07×10^{-13} cm^2 s^{-1}). The in-situ TEM results directly confirm that the polymer coating layer provides conducting pathways and buffers the stress induced by the lithiation, leading to less retardation effect and less self-limiting lithiation. Hence, the conducting-flexible polymer has a positive impact on the electrochemical performances of Si nanoparticles anode.

List of Publications Out of This Thesis

[1] Wang J W, Chen G H, Song S H., Na-ion conducting gel polymer membrane for flexible supercapacitor application [J]. Electrochimica Acta, 2020, 330：135322.

[2] Wang J W, Bai Z W, Song S H, Chen G H. Conductive and flexible coating of cathode made of $NaLiFePO_4F$ as active material for high-performance Li-ion batteries. (manuscript under preparation)

[3] Wang J W, Song S H, Chen G H. Conductive and flexible coating of Si nanoparticles for the anode in Li-ion batteries. (manuscript under preparation)

Acknowledgements

First and foremost, I would like to express my sincere gratitude to my supervisors Prof. Guohua Chen, from the Hong Kong Polytechnic University, and Prof. Shenhua Song, from Harbin Institute of Technology (Shenzhen), for their great patience, valuable guidance, and continuous support during my joint PhD. study.

I also would like to express my gratitude to my group members (Dr. Yang Liu, Dr. Xianying Qin, Dr. Fei Zhang, Dr. Yanan Zhu, Dr. Zhaowen Bai, Dr. Junye Cheng, Dr. Somyadip Majumder, Dr. Qiang Liu, Ms Zeqi Zhou, Miss Yutong Liu, Mr. Yinggang Zhu, Mr. Lei Huang) for their valuable advice and kind help in my research. Besides, my great thanks go to Mr. Benny CK LEUNG for his technical support in conducting my experiments.

Last but not least, I am deeply grateful to my fiancé, Dr. Zejia Zhao, and my family members for their love, and whole hearted support.

Table of Contents

List of Figures

List of Tables

List of Abbreviations

Abbreviation	Full name
DEC	Diethyl carbonate
DFEC	Doubly fluorinated EC
Diglyme	Diethylene glycol dimethyl ether
DMC	Dimethyl-carbonate
DME	Dimethoxyeyhane
EC	Ethylene carbonate
EMC	Ethylmethyl carbonate
ES	Ethylenesulphite
FEC	Fluoroethylene carbonate
PC	Propylene carbonate
Triglyme	Triethylene glycol dimethyl ether
VC	Vinylene carbonate

Chapter 1 Introduction

1.1 Background

Energy is one of the most challenging problems that people are facing nowadays. Renewable energy is important in the future. With the development of smartphones, electric vehicles, portable electronic devices, and other electronics products, the present supply of energy storage systems cannot meet the increasing demand. Thus, it is essential to develop effective renewable energy storage technologies, for example, batteries and supercapacitors (Bhide et al., 2014; Phattharasupakun et al., 2018; Zhang et al., 2018). They can achieve an effective, and reliable transmission and distribution of electrical energy (Dunn et al., 2011). They are becoming the major flagship technologies offering a meaningful solution to the electric grid and electric vehicles (Saha et al., 2014).

A lithium-ion battery (LIB) is mainly composed of two types of electrodes that show different chemically stable potentials and that are insulated through a separator, and electrolyte facilitating the Li-ion conduction, showing in Figure 1.1 (Baskoro et al., 2019). The cathode is usually a Li-intercalation mixture made of transition metal oxides, and the anode is made of graphite in most commercial products (Flandrois and Simon, 1999; Ellis et al., 2010). Through inserting or extracting of Li^+ from the active materials, the redox reactions can occur on the cathode. (Zhao et al., 2015). To date, although the extensive applications of Li-ion batteries have been seen in the power system for electric vehicles, their development has only made incremental progress because of the limitations of electrodes, the challenges of suitable electrolytes development and the issues of interfacial phenomena between electrodes and electrolyte (Armand and Tarascon, 2008; Goodenough, 2012). Large numbers of innovation efforts is still necessary to improve the energy density, safety and cost for EVs-CY 2020 (Xiao and Sun, 2018). To maximize the efficiency of electrode materials, researchers have investigated the use of advanced materials and modification of existing materials such as silicon and lithium as an anode. While these directions always end up with the concern of the surface of materials where the majority of side reactions resulted from nonequilibrium diffusion reactions occur (Islam and Fisher, 2014).

The isostructural fluorophosphates compound $NaLiFePO_4F$ is a promising cathode candidate. It shows high potential on account of the inductivity of PO_4^{3-} group and the F^- with electron-withdrawing character. In addition, it shows high capacitance and low-cost. Unfortunately, $NaLiFePO_4F$ is significantly sensitive to hydrofluoric (HF) acid. Its electronic conductivity also should be improved. As for the promising anode candidates, Si has been considered as one for Li-ion batteries with high energy on account of the high theoretical capacity (4200 mAh g^{-1}), a low charge voltage plateau (0.2-0.3 V *vs*. Li/Li^+), and good environmental compatibility. However, Si shows a significant volume expansion of about 420% during the lithiation because of their intake of large amounts of lithium. This can lead to poor electronic and ionic conductivity, and thus capacity fading quickly.

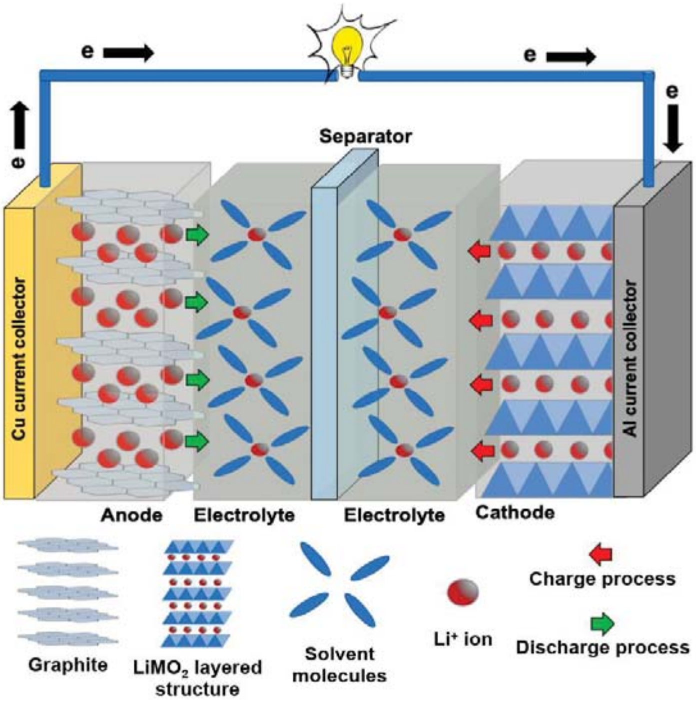

Figure 1.1 Schematic of a conventional Li-ion battery (Reprinted with permission from (Baskoro et al., 2019), Copyright (2019) American Chemical Society.)

The electric double-layer capacitors (EDLCs) also have been considered as one of the attractive energy storage devices on account of the fast charging and discharging performance, high coulombic efficiency, and long service life. Since their first introduction in 2001, lithium-ion conducting capacitors have achieved great progress. They have been fabricated by using activated carbon (Cao and Zheng, 2012), carbon nanotubes (Cheng et al., 2018), graphene (Gao et al., 2020), as well as $Li_4Ti_5O_{12}$ (Ye et al., 2015), Fe_3O_4 (Huang et al., 2019), SnS_2 (Hao et al., 2019) and Li_3VO_4 (Shen et al., 2017) battery-type electrodes with a liquid electrolyte. Some commercial lithium-ion capacitors have been developed for the brake energy recovery system from subway operation in China (Zhang et al., 2018). Although the lithium-ion capacitors will play a significant role in energy storage in the future, the growing demand for lithium, however, may eventually result in the shortage of this metal (Xu et al., 2018). Hence, to fulfil the demand for the next generation of sustainable energy usage, sodium offers a logical alternative due to its abundance in the earth crust and close relation to lithium. Sodium has similar physical and chemical performances to lithium (Chen et al., 2018; Tarascon et al., 2018). Investigation on sodium-ion capacitors started in 2012 (Chen et al., 2012; Yin et al., 2012; Han et al., 2019). When searching for new electrode materials, researchers realized that the study of sodium-ion conducting electrolytes is also crucial because both the interface between electrode and electrolyte and the stability of electrolyte play some key roles in improving the performances of devices (Zhao et al., 2018).

Electrodes and electrolyte are two key components of both batteries and supercapacitors. Interestingly, polymers have been widely used in the making of electrolytes and electrodes. For example, since (Feuillade and Perche, 1975) found out that polymers can be plasticized with an aprotic solution, many polymer hosts including poly (ethylene oxide) (PEO), polyvinyl alcohol (PVA), chitosan (CS), poly (3-caprolactone) (PCL), poly (methyl methacrylate) (PMMA), poly (vinylidene fluoride) (PVDF), and their copolymers are used to prepare polymer electrolytes from solid electrolytes to gel electrolytes that can serve as electrolyte and separator (Thakur et al., 2012). These polymer-based electrolytes have been paid more and more research attention on account of their high safety and good thermal property.

In addition, some conductive polymer materials, such as polypyrrole (PPy), polyaniline (PANi), poly(3,4-ethylenedioxythiophene) (PEDOT) and poly (3,4-

ethylene-dioxythiophene)- poly(styrenesulfonate) (PEDOT-PSS), have been served as electrode materials for supercapacitors (Ghosh and Inganäs, 1999; Snook et al., 2011). Furthermore, these conducting polymers are also used as protective coating materials on electrode materials to improve their electrical or ionic conductivity and suppress surface side reactions (Xiao and Sun, 2018). In addition, some flexible polymers such as poly(dimethylsiloxane) (PDMS) and poly(ethyl α-cyanoacrylate) have been designed as an artificial protection layer on electrodes to accommodate volume expansion and absorb the stress of electrodes during charging and discharging process (Zhu et al., 2017).

Therefore, it is necessary for researchers to explore polymer materials used in supercapacitors and batteries to facilitate further progress in electrode and electrolyte materials development.

1.2 Research Objectives

Herein, this thesis mainly focuses on exploring the effects of polymers on enhancing the electrochemical performances of electrolytes and electrodes used for EDLCs and Li-ion batteries. The objectives are as follows:

(1) To improve electrochemical performances of EDLCs by preparing biodegradable polymer electrolytes;

(2) To enhance the capacity and cycling stability of high-voltage $NaLiFePO_4F$ as a cathode by using a new conductive and flexible polymer coating on its surface;

(3) To prolong the cycling performance of high-capacity Si anode by using the new polymer coating of Si nanoparticles.

Chapter 2 Literature Review

2.1 Introduction

Polymer materials have been a key constitute of electrical energy storage (EES) typically batteries and supercapacitors. As the demand for performances of the next-generation EES increases, functional polymer materials that are designed to have the desired physical and chemical properties, will be required to satisfy the demands in the areas of electrolyte and electrode materials. The prior arts in these fields will be concisely reviewed in this chapter.

2.2 Electrolyte Materials for Supercapacitors and Batteries

2.2.1 Electrolyte basics

The electrolyte is one of the key constitutes of batteries and supercapacitors. To prepare an electrolyte that can be used in both supercapacitors and batteries, the electrolyte basics are introduced firstly.

Supercapacitors are classified into three kinds on the basis of the charge storage mechanism, including EDLCs, pseudocapacitors, and hybrid supercapacitors (see Figure 2.1) (Pal et al., 2019). In the case of EDLCs, the negative electrode could absorb the positive ions from the electrolyte, and the negative ions are absorbed on the positively charged electrode. Thus, energy storage occurs at the electrolyte-electrode interface via nonfaradaic charge accumulation, which is because of the formation of the electrical double layer. The EDLCs show excellent cyclic stability and low specific energy density ($\leqslant 10$ wh kg^{-1}). As for pseudocapacitors, energy storage occurs via Faradic reaction in the electrode such as metal oxides and conducting polymers. Hence, the cyclic stability is not as perfect as that of EDLCs, yet the specific capacity is higher. The hybrid supercapacitors combine the charge storage mechanism both of EDLCs and pseudocapacitors. The charge storage occurs not only through the formation of electric double-layer but also through Faradic reaction in the electrode. As a result, battery-type hybrid capacitors show the largest specific energy density. It is noticed that the specific energy density is directly related to the specific capacitance and work voltage of the devices. Hence, many researchers are focusing on the exploitation of electrode materials for high specific capacitance and electrolyte materials for high voltage.

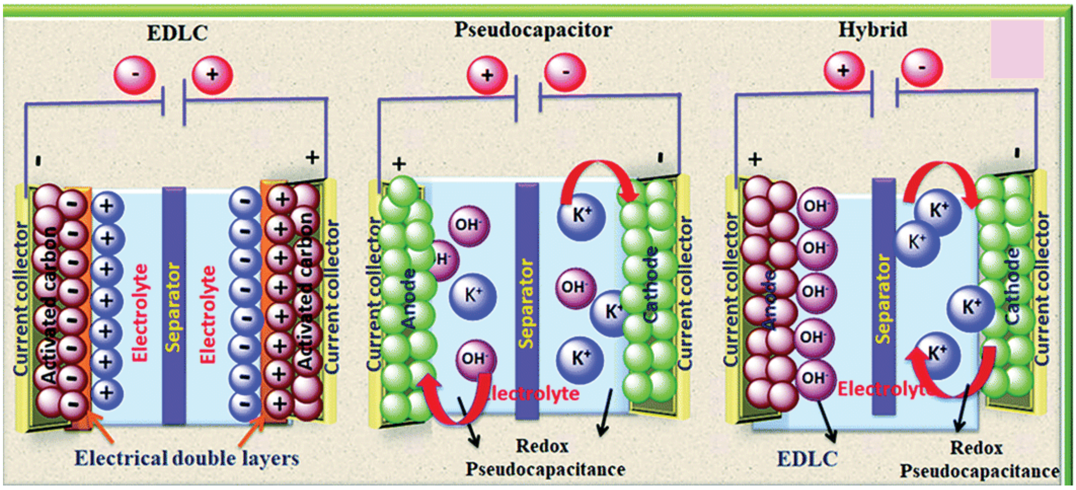

Figure 2.1 Schematics of the EDLC, pseudocapacitor and hybrid supercapacitor (Reproduced with permission from Royal Society of Chemistry) (Pal et al., 2019)

The conventional electrolytes of the supercapacitors are listed in Table 2.1. Obviously, different kinds of electrolytes have been investigated, mainly including aqueous and organic electrolyte, ionic liquid electrolyte, ceramic electrolyte, and polymer electrolyte (solid, gel and composite electrolyte). Their properties are shown in Figure 2.2. All of these five types of electrolytes can be applied in supercapacitors. Every type of electrolyte show its natural characteristics. For example, although aqueous-based electrolytes, such as acid-based H_2SO_4, alkaline-based KOH, and neutral-based KCl, have high ionic conductivity and can be easily handled, they show narrow voltage windows (~0-1.3 V) on account of the decomposition of water. Moreover, the organic electrolyte, ionic liquids electrolyte, ceramic electrolyte and the polymer electrolyte are also usually used in secondary batteries. Organic electrolytes are dominating the commercial market due to their wide operating voltage window (~0.01-2.8 V for capacitors, ~0.01-5.0 V for batteries). However, some disadvantages such as high cost, flammability, toxicity, and volatility should be considered. Ionic liquids electrolytes exhibit high thermal, chemical durability and electrochemical stability, but their high cost and high viscosity limit their practical application (Tarascon and Armand, 2011). High viscosity could lead to the large internal series resistance of devices. Ceramic electrolytes show high ionic conductivity and excellent mechanical performance, but the poor chemical and electrochemical stability cause an unavoidable side reaction between electrodes and electrolyte (Wang et al., 2018). Polymer-based electrolytes show different performance due to their states such as solid state and gel state. Generally, they show some advantages such as a wide voltage window and high safety. Also, they show some drawbacks typically including poor mechanical properties and low ionic conductivity.

Table 2.1 The conventional electrolytes for supercapacitors

Supercapacitors	Electrolyte	Reference
Double-layer capacitors	$PVA/LiClO_4/TiO_2$	(Lim et al., 2014)
	PVA/NH_4NO_3	(Kadir and Arof, 2011)
	PVA/NH_4I	(Aziz et al., 2020)
	PVA/KOH	(Ma et al., 2014)
	PVA/H_2SO_4	(Karaman and Bozkurt, 2018)
	PVA/H_3PO_4	(Hashim et al., 2005)
Pseudo capacitors	$H_2SO_4/Na_2MoO_4/KI$	(Xu et al., 2017)
	$KOH/K_3Fe(CN)_6$	(Su et al., 2009)
	Na_2SO_4/KBr	(Tang et al., 2017)
	PVA/H_2SO_4	(Xu et al., 2015)
	PVA/KOH	(Yan et al., 2020)
	PVA/LiCl	(Wang et al., 2012)
Hybrid supercapacitors	1-buthyl-3-methyl-imidazolium ionic liquids (BMIMX, X=BF_4^-, PF_6^-)	(Balducci et al., 2004)
	Na_2SO_4 electrolyte	(El-Kady et al., 2015)
	*X*OH(*X*=Li, Na, K)	(Ma et al., 2015)
	$LiPF_6$ in EC/EMC/DMC	(Naoi et al., 2010)
	PVA/KOH	(Yuan et al., 2006)

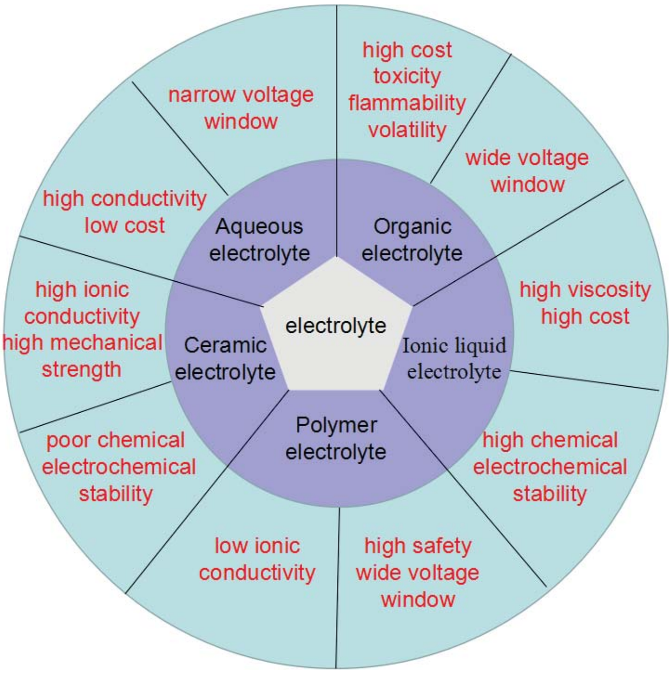

Figure 2.2 Classification and properties of various electrolytes

For the typical batteries, the conventional electrolytes are listed in Table 2.2. Obviously, organic electrolyte, ionic liquid electrolyte, and ceramic electrolyte, and polymer electrolyte (solid, gel and composite electrolyte) are widely used in batteries. Polymer electrolytes are responsible for containing and shuttling the charge carriers such as Li^+, Na^+, Mg^{2+}, etc. between anode and cathode. In addition, they are the substitute of the separator to isolate the electrodes, avoiding short circuit. They are majorly composed of polymer host providing the high mechanical integrity, electrolytic salt providing the sources of charge carriers and other additives such as plasticizers and inorganic oxides. If a polymer electrolyte is used for the application in electrical energy storage devices, it must satisfy several requirements as listed in Table 2.3. Clearly, meeting all the requirements in Table 2.3 should be a formidable challenge. However, it is necessary to optimize the above requirements because they are general and not given with respect to the specific optimal. A polymer electrolyte optimization is primarily conducted through varying constitutes, polymer hosts, salts and additives, and their respective ratios (Kumar and Hashmi, 2010; Chen et al., 2015; Singh and Singh, 2015; Giffin et al., 2017). Moreover, it can be optimized by changing its microscopic structure (Kim et al., 2005; Xi et al., 2006; Idris et al., 2012; Kalami et al., 2019).

Polymer electrolytes have been deployed in the progress of various batteries with high energy density (Muldoon et al., 2015).

Table 2.2 The conventional electrolytes for batteries

Batteries	Electrolyte	Reference
Li-ion batteries	Organic electrolytes, (Li(ClO_4^-, BF_4^-, PF_6^-, Tf^-, $TFSI^-$) in solvent (EC, PC, DEC, DMC, DME)	(Fan et al., 2018)
	Polymer electrolytes (PVDF-HFP/PVA/LiTFSI/MMT)	(Ma et al., 2016)
	Ceramic electrolytes ($Li_{6.4}Ga_{0.2}La_{2.75}Y_{0.25}Zr_2O_{12}$)	(Luo et al., 2019)
	Ionic liquid-based electrolyte	(Francis et al., 2020)
Li-S batteries	Organic electrolytes, (Li(ClO_4^-, BF_4^-, PF_6^-, Tf^-, $TFSI^-$) in solvent (EC, PC, DEC, DMC, or DME) with additives such as VC, butyl sultone, and $LiNO_3$)	(Fan et al., 2018)
	Polymer electrolytes (PVDF-HFP/PMMA/MMT)	(Zhang et al., 2014)
	Ionic liquid-based electrolyte ($PP13TFSI/DOL/DME/LiTFSI/LiNO_3$)	(Wang et al., 2016)
	$MoS_2/Li_2S\text{-}P_2S_5$ glass-ceramic electrolyte	(Xu et al., 2017)
Na-ion batteries	Organic electrolytes, Na(ClO_4^-, BF_4^-, PF_6^-, Tf^-, $TFSI^-$) in solvent (EC, PC, DMC, DEC, EMC, DME, Diglyme, Triglyme) with additives (FEC, VC, ES, DFEC)	(Ponrouch et al., 2015)
	Ionic liquid-based electrolyte (NaFSI in Pyr13FSI;NaTFSI in Pyr14TFSI)	(Ding et al., 2013; Noor et al., 2013)
Na-ion batteries	Polymer electrolytes (solid, gel, composite)	(Ponrouch et al., 2015; Zhao et al., 2018)
	Ceramic electrolytes, ($Na_{10}GeP_2S_{12}$)	(Tsuji et al., 2018)

Table 2.3 The requirements of a polymer electrolyte for applications in EES

	Key properties	Reference
1	Chemical stability	(Quartarone and Mustarelli, 2011)
2	Mechanical stability	(Quartarone and Mustarelli, 2011)
3	Thermal stability	(Quartarone and Mustarelli, 2011)
4	High ionic conductivity	(Quartarone and Mustarelli, 2011)
5	Low toxicity	(Aziz et al., 2018)
6	Low cost	(Aziz et al., 2018)

2.2.2 Criteria for polymer and electrolytic salt in polymer electrolytes

There are several important factors that could impact the interactions between the polymer and metal ion. For polymer hosts, it includes the functional groups and the distance between them, compositions, branching degree, and molecular weight. For salts, they include cationic nature and charge, and anionic nature (Rivas et al., 2003). Accordingly, preparing a polymer electrolyte with good performances, it is important to choose the kinds of both polymer hosts and electrolytic salts.

Typically, the choice of polymer largely lies in the following criteria (Table 2.4). Basically, polymers have good film-forming and have polar groups for providing the ability to coordinate cation. In addition, polymers show low hindrance to bond rotation and low glass transition temperature for satisfactory high ionic conductivity.

Table 2.4 Typical criteria of a polymer host prepared for polymer electrolytes

	Criteria	Reference
1	low hindrance to bond rotation and the existence of polar groups	Aziz, 2013)
2	high molecular weight and ease of forming a thin film	Rivas et al., 2003)
3	high dielectric constant and low glass transition temperature	(Cui et al., 2017)

The basic information of several widely used polymers that serve as host polymers are listed in Table 2.5 (Aziz et al., 2018). Following the discovery of PEO host polymer, various polymer materials such as PMMA, poly(vinylidene fluoride - hexafluoropropylene) (PVDF-HFP), polyacrylonitrile (PAN), and PVA have been attempted for the promising host material of polymer electrolyte membranes (Aziz et al., 2018). Among them, only PVA is biodegradable.

Table 2.5 The common host polymers in polymer electrolyte

Name	Polar groups	Key properties	Reference
PEO	Ether (-O-)	High solvating power for electrolyte salts Excellent compatibility with electrode Poor mechanical strength	(Zhu et al., 2019)
PMMA	Carbonyl (C=O)	Good affinity to liquid electrolyte Poor mechanical strength	(Zhu et al., 2019) (Cheng et al., 2015)
PVDF-HFP	Fluorine (-F)	High dielectric permittivity Poor compatibility with liquid electrolyte	(Zhu et al., 2019)
PAN	Cyano (C≡N)	Amorphous polymer Outstanding physical and chemical properties Severe passivation upon contact with Li metal anodes	(Zhu et al., 2019) (Baskoro et al., 2019)
PVA	Hydroxyl (-OH)	Abundant Biodegradable Good affinity to liquid electrolyte	(Zhu et al., 2019) (Aziz et al., 2018)

As for the electrolytic salts, the choice largely depends on the following criteria in Table 2.6. For the sake of achieving high ionic conductivity, the electrolytic salt has large-sized anion and low dissociation energy in solvent. Furthermore, the excellent chemical stability is critical to electrolytic salt, which finally has a positive influence on the whole properties of electrolytes. Non-toxicity and safety should also be considered. Actually, many resulting properties including advantages and disadvantages often mainly depend on the anion other than cation.

Table 2.6 The criteria of an electrolytic salt used for polymer electrolytes

	Criteria	Reference
1	Large-sized anion and low dissociation energy in the solvent	(Cheng et al., 2018)
2	Chemical stability vs. oxidation and reduction	(Ponrouch et al., 2015)
3	Non-toxicity and safety	(Ponrouch et al., 2015)

Table 2.7 summarizes the mostly used sodium salts with physical-chemical properties for Na-ion conducting polymer electrolytes (Ponrouch et al., 2015). The anions in sodium salts have been applied in the area of electrolytes. ClO_4^- anion is the most commonly used one for sodium salt, but it is forbidden to a certain extent for some practical cell application due to its strong oxidation power. BF_4^- anion has a strong interaction with cation, leading to less available charge carriers. PF_6^- anion is the most commonly used one for lithium salt due to its high safety even at high temperature, but it can yield PF_5, POF_3, and HF under the existence of moisture. As for Tf^- and $TFSI^-$ anions, both of them show the large size that is easy to create mobile ions, and they are non-toxic, thermally stable. Unfortunately, they corrode the aluminium current collector (Krause et al., 1997). All problems of the above anions also can be observed in lithium-ion conducting electrolytes (Hong et al., 2013). Generally, lithium salts have lower melting points than that of the sodium salts, making them relatively poor thermal stability.

Table 2.7 Basic performances of the typically applied sodium salts

(Ponrouch et al., 2015).

Salt	Anion structure	M_w (g mol^{-1})	T_m (°C) (Li-salt)
$NaClO_4$	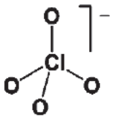	122.4	468 (236)
$NaBF_4$	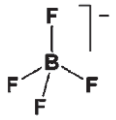	109.8	384 (293)
$NaPF_6$	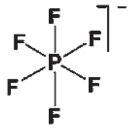	167.9	300 (200)
NaTf	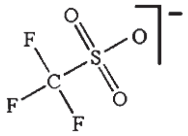	172.1	248 (>300)
NaTFSI	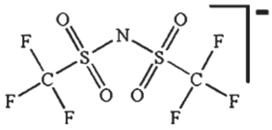	303.1	257 (234)
NaFSI	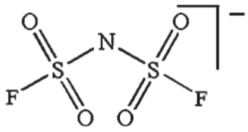	203.3	118 (130)

For the dissolution of both polymer host and metal salts, a good solvent is required to serve as the medium for ions movement. It should show large dielectric constant (ε>15) for facilitating the dissociation of electrolytic salts and limiting ion pairing (Ponrouch et al., 2015), good chemical and electrochemical stability (Cheng et al., 2018).

2.2.3 Classifications of polymer electrolytes

Polymer electrolyte films have been considered promising electrolyte candidates in the development of EESs with massive research efforts made. They have been typically categorized into solid polymer electrolytes (SPEs), gel polymer electrolytes (GPEs), and composite polymer electrolytes (CPEs) (Di Noto et al., 2011).

A solid polymer electrolyte (SPE) is created through dissolving inorganic salt in the polymer as an ionic conducting solid electrolyte (Edman et al., 2000). In the case of the SPEs, the interactions between cation and functional groups are electrostatic forces and the formation of coordinating bonds (Rivas et al., 2003; Kumar and Srivastava, 2015). The schematic illustration of the ionic transport mechanism in SPE are shown in Figure 2.3. The ions can be transferred via the segmental transport because of the weak coordinate of ions to sites along polymer chains, i.e., from one coordinated position to another, under a condition of electric field. Hence, the conduction in solid polymer electrolyte depends on the amount of mobile ions and temperature. In addition, the amorphous region of the polymer host can accelerate ions transfer, i.e., the lower the degree of crystallinity, the higher ionic conductivity in SPEs. PEO is one of the popular polymer hosts because of the admirable stability, good mechanical performances, low crystallinity and ability to dissolve various types of electrolytic salts. However, the ionic conductivity is low (10^{-5}-10^{-7} S cm^{-1}) at ambient temperature. Thus, PEO-based solid electrolytes operating at 60-80 °C can increase ionic conductivity (Ponrouch et al., 2015). Conductivity in several PEO-based SPE with different kinds of sodium salts has been studied (Wang et al., 2019). Some anions such as FSI and TFSI in sodium salts can facilitate Na^+ conduction, because these large-sized anions could interact with chain segments, decreasing the crystallinity and improving the amount of mobile Na^+ ions (Boschin and Johansson, 2015).

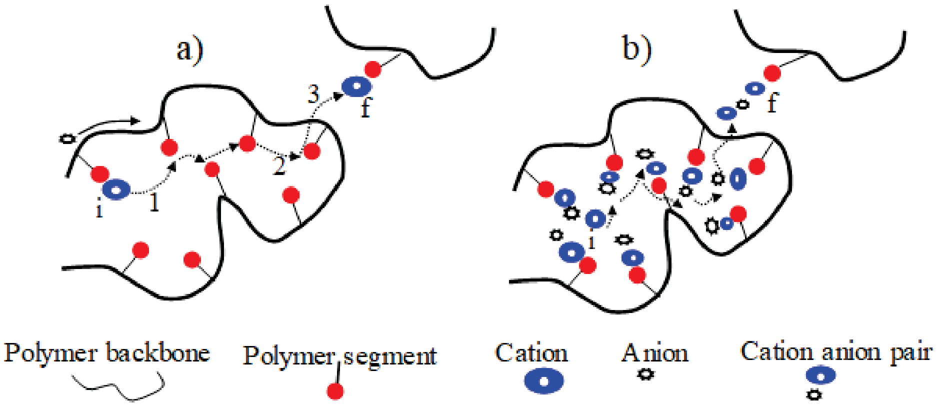

Figure 2.3 Schematic representations of ion conducting mechanism in SPE: (a) with low salt content and (b) with high salt content (Reproduced with permission from Springer Nature and Copyright Clearance Center) (Kumar and Srivastava, 2015)

Unlike SPEs, gel polymer electrolyte (GPE) exhibits a quite attractive ionic conductivity (10^{-3} S cm^{-1}) even at ambient temperature (Kumar and Hashmi, 2010). This is because GPEs is formed by mixing a certain amount of organic solvents or plasticizer. The incorporated organic solvent and plasticizer decrease the amount of active sites of polymer chains and thus reduce their intermolecular and intramolecular force, forming a widely connected network that provides fast ion-conducting pathways, and then facilitates ions transportation and finally enhances ionic conductivity (Honary and Orafai, 2002). The influence of plasticizer on the ion transportation is shown in Figure 2.4 (Patel et al., 2010). One can see that the portion of the amorphous phase in polymer host is smaller in the left of the figure, leading to the lower ionic conductivity. In contrast, the plasticized polymer electrolyte shows a larger amount of amorphous regions (the right one of Figure 2.4), resulting in the higher ionic conductivity.

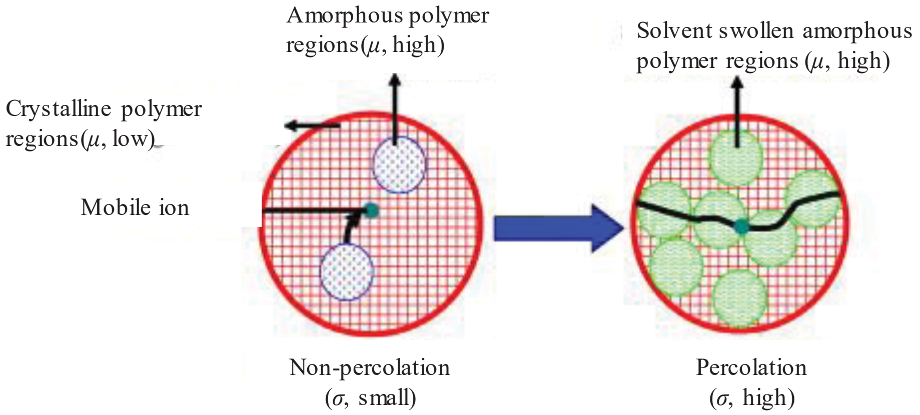

Figure 2.4 Transformation from non-percolation to percolation in gel electrolytes (Reproduced with permission from Elsevier and Copyright Clearance Center) (Patel et al., 2010)

For gel polymer electrolyte, some kinds of ions could transport under the external electric field so the metal ion transference number could be small (Wang et al., 2019). For example, Table 2.8 shows the ionic conductivity and transference number in various Na ion conduction GPEs. Also, it can be seen that PVDF is a popular polymer matrix because of its high electrochemical stability. Its derivative PVDF-HFP opens a new market for gel polymer electrolytes. PVDF-HFP is semi-crystalline and has high flexibility because of the addition of hexafluoropropylene (HFP) unit (Kumar and Hashmi, 2010; Kumar et al., 2011; Gao et al., 2015; Yang et al., 2015; Isa et al., 2017). In addition, PMMA and PAN have been used as sodium ions conduction gel polymer hosts, which also have good capability of conducting ions even at ambient temperature (Kumar and Hashmi, 2010; Vignarooban et al., 2017).

Although gel polymer electrolytes exhibit some advantages of a liquid electrolyte such as high room-temperature conductivity, and solid electrolyte such as high safety, they still show some disadvantages such as the release of liquid solvent, poor mechanical strength and undesired high reactivity with the metal electrode (Stephan et al., 2009; Liao et al., 2010; Saikia et al., 2011).

Table 2.8 Some electrochemical properties of different gel electrolytes

(Wang et al., 2019)

GPEs	σ, S cm^{-1}	Transference number	Reference
PVDF-HFP/$NaClO_4$/ Glass fiber/PC	4.6×10^{-3}	-	(Gao et al., 2015)
PVDF-HFP+$NaCF_3SO_3$-EC-PC+SiO_2	4.1×10^{-3}	0.43	(Kumar et al., 2011)
PVDF-HFP/EC/$NaClO_4$	6×10^{-4}	0.3	(Yang et al., 2015)
PVDF-HFP+EMItriflate+$NaCF_3SO_3$	5.74×10^{-3}	0.23	(Kumar and Hashmi, 2010)
PVDF-HFP+$NaCF_3SO_3$+ EC-PC	2.5×10^{-3}	0.62	(Isa et al., 2017)
PMMAPC/EC+SiO_2/ $NaClO_4$	3.4×10^{-3}	0.23	(Kumar and Hashmi, 2010)
PAN+EC/PC/$NaClO_4$	4.5×10^{-3}	-	(Vignarooban et al., 2017)

The third kind of polymer electrolyte is named as composite polymer electrolytes (CPEs). The appearance of CPE is because that the ion-pairs and ion triplets in polymer electrolyte could reduce its ionic conductivity. This depends on the weak dielectric constant of the polymer (Mohapatra et al., 2009). In order to solve this issue and enhance the quality of polymer electrolytes, many approaches have been explored. Inorganic passive or active ceramic fillers with high dielectric constant, such as SiO_2, TiO_2, ZrO_2, Al_2O_3, γ-$LiAlO_2$, $BaTiO_3$, $PbTiO_3$, $LiNbO_3$, and NASICON-type as well as garnet-type, clay or carbon nanotubes are dispersed into the polymer matrix, forming new hybrid composite materials to make valuable use of the ceramic filler and polymer (Chen et al., 2015; Lin et al., 2015; Lin et al., 2017). This composite material is considered as a heterogeneously disordered matrix (Soulintzis et al., 2009).

Compared with the other two types of polymer electrolytes, the ion conduction phenomenon is complex in CPEs, which could be analyzed through PEO-based composite electrolyte (see Figure 2.5) (Wang and Alexandridis, 2016). It can be seen that the incorporated ceramic fillers could interact with the ether oxygen from both the polymer segments and anions from metal salts through the oxygen vacancies on the surface of fillers. Hence, the ion transport can be accelerated within polymer matrix due to the following three reasons:

Firstly, the interact between ceramic fillers and polymer segments could suppress polymer crystallization and enhance the amorphous region of the polymer (Croce et al., 1998; Chen-Yang et al., 2002). Another reason is that the interaction between fillers together with Lewis acid-base natural character and the salts would immobilize the anions and thus break down the ion pair, releasing more mobile cations and increasing interfacial ionic conductivity (Wieczorek et al., 1996). The third reason is that the ions can move in the incorporated active ceramic nanoparticles and through the polymer-ceramic interface, proving even faster-conducting pathways over polymer host (Liu et al., 2017). The composite polymer electrolytes could achieve high ionic conductivity, excellent mechanical performances, and satisfied chemical and thermal properties through simply controlling the amount, size, shape and functional group of incorporated fillers (Cheng et al., 2015).

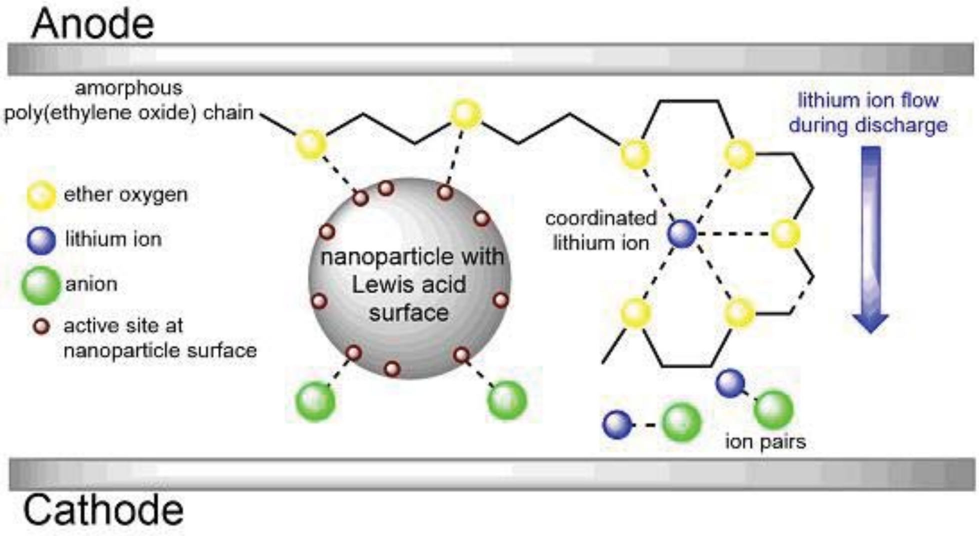

Figure 2.5 Schematic illustration of the interact among polymer, alkali salt and the ceramic nanoparticle (Wang and Alexandridis, 2016)

2.2.4 The performance improvement of gel polymer electrolytes

Gel polymer electrolytes render a high ionic conductivity and good flexibility, making them one of the most attractive candidates for the application of flexible devices. It is worth noting that the demand for flexible power supply is becoming increasingly high because of the wearable and portable devices found in various fields including medical, military and outdoor sports (Pu et al., 2016). The role of GPEs in these devices generally is: (1) to separate anode and cathode; (2) to serve as an electronic insulator; (3) to allow the transport of desired ions (Cheng et al., 2018). When they are employed for such applications, several requirements need to be satisfied simultaneously, including satisfied ionic conductivity and high Li^+ transference number, excellent chemical and thermal stability performances, satisfied interfacial contact with anode and cathode, wide electrochemical stability window, and strong mechanical stability and more flexibility.

However, some conventional gel polymer electrolytes show poor mechanical performance and thermal stability (Moskwiak et al., 2006). For GPEs applications, varieties of strategies such as adding inorganic/organic fillers or plasticizers, creating single ion conduction, and introducing redox-active mediators, have been explored.

Plasticized polymer electrolytes are typically produced by adding ionic liquid (Ravi et al., 2016), propylene carbonate (PC) organic solvent (Das and Ghosh, 2015), organic solvent ethylene carbonate (EC) (Mishra et al., 2019), dimethylcarbonate (DMC) (Selulos, 2012), or swelling the resulting polymer electrolyte membranes in PC/EC (Verma et al., 2020). Among them, ionic liquid has some desirable properties, including high ionic conductivity, and good electrochemical stability. It can be used as a plasticizer for forming GPEs with desirable electrochemical properties (Moreno et al., 2014).

Another effective strategy of enhancing the properties of GPEs is to create homogeneous porous frameworks in polymer hosts by cross-linking of polymers, adding and subsequently removing of pore-forming agents, facilitating ions transportation and storing sufficient organic solvents (Oh et al., 2015). Furthermore, the porous structure can also be designed based on the electrolytic salt complex (Rohan et al., 2015). For example, a porous GPE membrane composed of poly (vinylidenefluoride) and polystyrene-poly(ethylene oxide)-polystyrene (PS-PEO-PS) tri-block copolymer composites were made using glycerin as the non-solvent (Xiao et al., 2019). The porous membrane was obtained after evaporation of glycerin at high temperature. The GPEs with the porous membranes as matrices exhibit high ionic conductivity in the order of 10^{-3} S cm^{-1} after uptaking 201% liquid electrolyte in the mass of their own weight at room-temperature. Li/$LiFePO_4$ batteries fabricated with the porous GPEs exhibit good cycling performance and rate property (Xiao et al., 2019). Similarly, a porous cross-linked PVDF-HFP based electrolyte film was made by mixing ZnO nanoparticles as pore-forming additive (Gu et al., 2018), showing an attractive ionic conductivity in the order of 10^{-3} S cm^{-1} and tensile strength of 10.7 MPa.

To solve concentration polarization of electrolytic salts and to increase lithium ion transference number, researchers explored single Li-ion conducting GPEs by limiting or eliminating the transport of anions. For example, poly(ethyleneoxide) -b-polystyrenesulfonyl lithium- (trifluoromethylsulfonyl)imide diblock copolymers (PEO-PSLiTFSI) were synthesized (Inceoglu et al., 2014). The anion is totally limited by the polymer, and thus all of the current is produced by Li^+. Although the mobile Li^+

ions can be trapped in the glassy polystyrene-rich microphase at low temperature, the Li^+ ions released from the clusters at increasing temperature would significantly increase the ionic conductivity (Inceoglu et al., 2014). Similarly, some electrolytic salts with a low degree of charge comnination are used in GPEs to weaken the electrostatic interaction of cations/anions and produce large number of free Li^+ ions. For instance, boron atom within the electrolytic salts, polymeric lithium tartaric acid borate (PLTB) (Wang et al., 2013), lithium oxalate polyacrylic acid borate (Zhu et al., 2013), lithium bis(oxalato) borate (Aravindan and Vickraman, 2007), lithium poly(1,2,3,4-butanetetracarboxylicacid borate) (Zhang et al., 2014) and lithium polyvinyl alcohol oxalateborate (Zhu et al., 2012), can lead to the weak electrostatic interaction between Li^+ and anions that are covalently bonded to the polymer, leading to high ionic conductivity.

Recently, incorporating a small number of redox agents to the gel polymer electrolytes has been found as a feasible approach to significantly enhance the specific capacity of supercapacitors. The redox-active polymer electrolytes could be prepared by adding the additives with GPEs. The redox-active additives, such as methylene blue (MB) (Roldán et al., 2012), hydroquinone (HQ) (Roldán et al., 2011), KI (Xun et al., 2019) and $VOSO_4$ (Senthilkumar et al., 2013), could provide pseudocapacitance due to the Faradaic oxidation/reduction reaction (Chun et al., 2015). Among them, iodide ions could improve the ionic conductivity of the electrolytic solution and contribute a source of pseudocapacitance behavior. For instance, a typical redox-active polymer-based electrolyte film was made by adding $KI/VOSO_4$ to PVA/H_2SO_4 gel polymer electrolyte film for application in an EDLC based on activated carbon (Fan et al., 2014). The electrode can attract the redox ions with opposite charge in the GPE under the applied electric filed, improving the energy density of the EDLCs due to the redox reactions occurred at the electrolyte and electrode interface. The EDLC delivered a high specific capacitance (1232.8 F g^{-1}) (Fan et al., 2014).

However, it can be observed that most gel polymer electrolytes devote to the application in Li-ion batteries. Although lithium-ion capacitors may supplement today’s energy demand, the concern of high cost and limited availability would eventually result in the shortage of lithium metal in the future (Xu et al., 2018). Fortunately, the exploration of sodium metal brings some hope as the next-generation sustainable energy material.

The sodium metal offers a logical alternative to lithium due to its earth-abundance and closely related physical and chemical properties (Chen et al., 2018; Tarascon et al., 2018). On the other hand, it is of the prime consideration to investigate biodegradable and environmentally friendly gel polymer electrolytes. PVA is especially a promising representative in terms of environmental, chemical stability and mechanically durability, yet few reports are available on Na-ion conducting biodegradable polymer electrolytes. Some reported PVA-based Na-ion conducting electrolytes are listed in Table 2.9.

Table 2.9 The performances of some PVA-based Na-ion conducting electrolytes

Electrolyte	Solvent	Ionic conductivity ($S\ cm^{-1}$)	Stability window (V)	Reference
PVA/NaBr	H_2O	1.4×10^{-6}	-	(Bhargav et al., 2008)
PVA/Na_2MoO_4	H_2O	1.1×10^{-6}	-	(Abdullah et al., 2017)
PVA/Na_2SO_4/Pyr14Br Redox-active	H_2O	2.71×10^{-2}	2.0	(Geng et al., 2019)
PVA/Na_2SO_4	H_2O		1.8	(Batisse and Raymundo-Pi, 2017)
PVA/$Na_3C_6H_5O_7$/Dy_2O_3	H_2O	1.06×10^{-4}	2.68	(Ramesh Babu et al., 2018)
PVA/$NaClO_4$/ZrO_2	H_2O	4.3×10^{-3}	-	(Naik et al., 2018)
PVA/NaTf	H_2O	7.39×10^{-5}	-	(Aziz et al., 2017)

It can be observed from Table 2.9 that simple sodium salt, such as NaBr and Na_2MoO_4, could have a negative effect on the electrochemical property of electrolytes

(Ponrouch et al., 2015). The electrochemical stability window is too narrow for application. The ionic conductivities of most electrolyte films are less than 10^{-3} S cm^{-1}, yet PVA/Na_2SO_4/Pyr14Br redox-active shows high one (2.71×10^{-2} S cm^{-1}). Unfortunately, supercapacitors assembled with redox-active based electrolyte have short cycling lifespan due to the redox reaction at the interface. In addition, all the PVA-based Na-ion conducting electrolytes are prepared by using water as the solvent. As a result, the residual combined water and free water in the electrolyte membrane can deteriorate the electrochemical performances of supercapacitors or batteries. Furthermore, the contact between electrolyte film and the electrodes was found mechanically weak (Chen et al., 2019) when assembled into energy storage devices.

Therefore, considerable efforts should be expanded on the development of PVA-based Na-ion electrolyte films that could be used in secondary batteries and supercapacitors simultaneously.

2.3 Surface Behaviors and Modifications of Cathode in Li-ion Batteries

The study about interfacial behavior between electrodes and the electrolyte is very crucial, which influences the whole performance of the energy storage devices. Thus, large numbers of attempts of surface modifications have been made to adjust the physical and chemical performances of the surface.

2.3.1 Surface behaviors

Various types of surface behaviors could be observed of cathode materials during the batteries cycling, such as phase reconstruction, stress-induced cracking, electrolyte decomposition and transition metal dissolution, and formation of solid-electrolyte interphase (SEI) to decrease electrical conductivity (Liu et al., 2011; Xiao and Sun, 2018).

Surface phase reconstruction always happens in the layered cathode materials such as $LiCoO_2$, $xLi_2MnO_3\bullet(1-x)LiMeO_2$(Me = Ni, Mn, Co) (Li-rich NCM) and Ni-rich $LiNi_{0.8}Co_{0.1}Mn_{0.1}O_2$, and spinel cathode materials such as $LiMn_2O_4$ (Chen et al., 2002;

Chung and Kim, 2002; Rozier and Tarascon, 2015). Although $LiCoO_2$ is the most successful cathode material for portable electronics application in Li-ion batteries until now, its available reversible capacity is half of the theoretical capacity (Amatucci et al., 1996). This is due to because that layered structure phase transit to a quasi-spinel one during redox cycling. Similarly, spinel structure also appears in the cycled Li-rich NMC cathode, leading to a low mean voltage of whole battery due to low voltage (~2.8 V) of spinel phase (Rozier and Tarascon, 2015). In addition, it results in a loss of active material and thus fast capacity fading as the Mn^{2+} produced by Mn^{3+} existing in the spinel structure is soluble in electrolyte. As for Ni-rich cathode material, it also experiences the phase reconstruction, i.e., the distortion of the rhombohedral structure and appearance of quasi-spinel phase as the movement of Ni^{2+} into Li^+ positions caused by their similar radius (Rozier and Tarascon, 2015; Liu et al., 2018), leading to lattice volume contraction or expansion during charge and discharge, and poor cycling performance (Kim et al., 2015).

Mechanical cracking has been found both in anode and cathode materials, which leads to poor grain-to-grain connections, poor particle-to-particle connections, and poor material-to-current collector, leading to poor electrical and ionic conductivity, and the loss of active materials. On the other hand, it also can create new spots for surface phase transition, corrosion, and some side reactions, and provide fresh surfaces that are exposed to the electrolyte, finally deteriorate the batteries performances (Yan et al., 2017). As for cathode materials, the mechanical cracking stems from both materials level and electrode level. Cathode materials could form cracks at a high current density because the Li^+ ions do not have enough time to move homogeneously, leading to residual stress within particles (Deshpande et al., 2010). In this case, the cracking can be decreased with increasing particle size (Woodford et al., 2010). Yan et al. (2017) pointed out that the intragranular cracks initiate from the inner grain at high-voltage cycling of layered cathode materials, which is sharply in contrast to common theoretical models showing the cracks initiated from the particle surface or grain boundaries (Klinsmann et al., 2016). This crack was also observed in some other cathode materials after long cyclings, such as $LiFePO_4$, $LiCoO_2$, and $LiNi_{0.6}Mn_{0.2}Co_{0.2}O_2$ (Wang et al., 1999; Chen et al., 2006; Kim et al., 2015). The intragranular cracks also can be deteriorated by thermal stress and pressure occurred when the batteries work (Yan et al., 2017; Yan et al., 2018). Besides intragranular cracks, intergranular cracks during cell charge-discharge also happen from grain boundaries because of the permeation of liquid electrolyte into the gaps and the side reactions, leading to expansion and shrinkage of particles (Shim et al., 2014; Kim et al., 2015; Xiao and Sun, 2018). Besides the cracking at the active material level, high mass loading in thick electrode could lead to various charge state from surface to the bulk and thus result in the polarization of the batteries and separation from current collectors (Yan et al., 2017).

Conventional electrolytes used in Li-ion batteries generally are composed of electrolyte solvents (EC, DEC, PC, DMC, and EMC, etc.) and $LiPF_6$ salt. Although the operational voltage range of the solvents is 1.0-4.7 V (*vs.* Li/Li^+), the electrolyte is not stable actually when the operating voltage is beyond ~4.5 V on account of the catalytic effect of cathode (Egashira et al., 2001). At high operating potential, the electrolyte will decompose via oxidation, leading to the appearance of a passive cathode electrolyte interphase (CEI) layer. This CEI layer is mainly constituted of Li_2CO_3 and LiF (Shi et al., 2012), and obstructs the insertion/extraction of Li^+ ions, causing irreversible lithium loss at the first cycles and capacity fade during cycling. Han and his coworkers (2018) demonstrated that appropriate CEI can inhibit transition metal ion dissolution, but heterogeneous and non-uniform CEI could affect the level of delithiation/lithiation. This can cause volumetric contraction and expansion of the primary particles and particles cracking, and transition metals dissolution, eventually facilitating the decrease of voltage and capacity of the materials. On the other hand, even though electrolyte is assumed to be nonaqueous, more or less moisture in electrolyte or cathode can commonly be found, leading to the production of HF (firstly $LiPF_6 \rightleftharpoons LiF + PF_5$, and then $PF_5 + H_2O \rightarrow POF_3 + 2HF$) and transition metal dissolution (Aurbach, 2000).

For some cathode materials, low electrical conductivity is a major limitation to wide applications. A typical example is olive-structured $LiFePO_4$ that suffers from its insulating characteristic and sluggish kinetics of both electrons and ions (Peng et al., 2013). The poor conductivity is due to the end member phases ($LiFePO_4$ and $FePO_4$)

(Delmas et al., 2011). Another notably low electrical cathode is $Li_3V_2(PO_4)_3$ with good structural stability because of the three-dimensional framework of $(PO_4)_3^-$ (Kim et al., 2013).

Actually, one can find that these surface behaviors of cathode materials are related closely. Hence, a modification approach may be efficient to relieve the stresses and even to meet the overall challenge.

2.3.2 Conventional surface modifications

To overcome the surface behaviors mentioned above, some conventional modifications, such as elements doping or surface coating have been explored.

Usually, elements doping includes but not limited to Ti (Xiao et al., 2017), Al (Han et al., 2017), Mg (Shim et al., 2014), Zr and Sn elements (Park et al., 2010). The incorporation of Mg by depositing MgO coating on the surface of $LiCoO_2$ could occupy Li sites, leading to an inhibition of phase change. (Xiong et al., 2011) also found that the incorporation of Al by annealing $LiMn_2O_4$ coated with Al_2O_3 could diffuse into the surface lattice, inhibiting the distortion and that the residual Al_2O_3 protected Mn from electrolyte aggressing. However, these doping materials are inert for Li-ion conduction. Another way is to use the active coating materials that have high Li-ion diffusivity including $Li_4Ti_5O_{12}$(Xu et al., 2018), $Li_2Si_2O_5$(Liu et al., 2016), Li_3PO_4(Chen et al., 2017), Li_2ZrO_3(Wang et al., 2015), and LiP_2O_7(Hu et al., 2018), and so on. The active $Li_4Ti_5O_{12}$ coating on the surface of Ni-rich cathode material could significantly enhance the cycling performance and rate property because the coating material improves Li^+ ions diffusion and relieves the phase transition (Xu et al., 2018).

To suppress the cracking, an efficient way is to prepare stable structure framework of cathode materials, yet another promising way is to conduct surface modification that should have the capability to regulate the strain generated during charging and discharging. Since the cracking in cathode materials primarily results from phase change on the surface level, the modification methods discussed above could help to suppress the existence of cracking. For example, element doping (Li and Co)(Kim et al., 2015) and surface coating of particles (Al_2O_3(Kim and Cho, 2008), $AlPO_4$(Zhu et al., 2017), FeF_3(Lee et al., 2013), and ZrO_2(Lee et al., 2006)) have been used to suppress the crack formation within the particles effectively.

Generally speaking, the surface coating of metal oxides is a straightforward approach to scavenge HF. It has been stated that the metal oxides such as ZnO (Guo et al., 2009) and Al_2O_3 (Park et al., 2008) can serve as an efficient HF scavenger formed in the electrolyte.

2.3.3 Polymer coating for cathode materials

The conventional coating materials are brittle and weak in adhesion, which could lead to delamination from the particle surface and thus diminish its performance (Xiao and Sun, 2018). In addition, these coating materials are low in conductivity for ions and/or electrons, decreasing the rate performance and increasing the irreversible capacity loss of the batteries. Considering these problems, polymers may be more efficient because of their good mechanical performances, which play a positive role in surface modification of anodes materials. Of course, a great deal of cathode materials have been modified by some polymers coating (Xiao and Sun, 2018).

In recent years, polymers, especially, three of the most well-known conducting polymers, poly(3,4-ethylenedioxythiophene)(PEDOT) (Fan et al., 2015; Son et al., 2016; McDonald and Hammond, 2018), polypyrrole (PPy) (Xie et al., 2016; Yang et al., 2018) and polyaniline (PANI) (Idris et al., 2012; Wang et al., 2013; Zhu et al., 2018), have been considered as promising surface coating materials that are electrochemically and thermally stable in batteries. Li et al. (2013) systematically compared the effect of these three polymers on the sulfur cathode. They found that the capability of these three polymers decreases in the order of PEDOT > PPY > PANI in the aspect of enhancing cycling performance and rate property of the sulfur cathode.

These three polymers have a positive influence on enhancing the performances of cathode materials. Firstly, the use of conductive polymers skin on the surface of particles efficiently improves electrical conductivity, conduction pathways and ion diffusion, and electrode stability (Murugan et al., 2008). Secondly, conductive polymer coating also plays a positive role in suppressing component dissolution and HF erosion (Li et al., 2006; Ahn et al., 2017), and controlling the formation and growth of CEI (Wu et al., 2016). Thirdly, the conductive polymers can serve as a binder for carbon black free electrode (Das et al., 2015; Pu et al., 2016), improving the energy density of batteries. Until now, these three conducting polymers have been reported as stable coating materials for some promising cathodes, for example, $LiFePO_4$ (Yang et al., 2009; Trinh et al., 2013), $LiCoO_2$ (Her et al., 2006), $Li_3V_2(PO_4)_3$ (Kim et al., 2013), $NaLiFePO_4F$(Bai et al., 2019), $LiMn_2O_4$ (Kim et al., 2001), $LiNi_{0.5}Mn_{1.5}O_4$ (Gao et al., 2015), $LiNi_{0.8}Co_{0.1}Mn_{0.1}O_2$ (Cao et al., 2018), and $Li_{1.2}Ni_{0.2}Mn_{0.6}O_2$ (Wu et al., 2016). Notable examples cover the study by Cao et al. (2018), who explored the employ of the integration of electronic conductivity of PANI and ionic conductivity of poly(ethylene glycol) (PEG) for the surface protection of $LiNi_{0.8}Co_{0.1}Mn_{0.1}O_2$, proving electronic and Li^+ ion diffusion pathway, and protecting the surface from HF erosion, and inhibiting side reactions and metal dissolution. Consequently, these modified cathode materials exhibited high capacity, and good rate performance and cycling properties. The previous work mainly focused on studying the conductive polymers (PEDOT, PANI and PPy) used in the protective coating on the surface of electrode materials.

2.3.4 High-voltage $NaLiFePO_4F$ cathode

The energy density of a Li-ion battery highly depends on cathode materials because of the lower practical capacity of cathode than that of anode materials (Baskoro et al., 2019). Meanwhile, the cost of Li-ion batteries also depends on cathode material, 38% within the major components in a PHEV20 battery pack (Xiao and Sun, 2018). It can be observed from the specific energy density (E) equation: $E = \int_0^Q V(\mathrm{q})\mathrm{d}q/wt$ that the specific capacity ($C = \int_0^Q \mathrm{d}q/wt$) and working voltage ($V$) are directly related to E (Goodenough and Kim, 2011). Hence, a high-voltage, high capacitance and low-cost cathode material are required for the purpose of high energy density.

The isostructural fluorophosphates compounds (A_2MPO_4F, A=Na and Li; M=Fe, Ni and Co) have attracted specific attention on account of the potential to more than one alkali atom activation in one unit (Khasanova et al., 2012). Among the compounds, low-cost $NaLiFePO_4F$ is a promising candidate because of its framework connectivity that could show high potential. This is attributed to the inductivity of PO_4^{3-} group and F^- with electron-withdrawing character (Antipov et al., 2015). In addition, the larger sized Na^+ could enhance the structural stability. Khasanova and his workers (Khasanova et al., 2012) found that the replacement of Na ions by Li ions could lead to a new Li_2FePO_4F phase which shows attractive electrochemical properties; they also demonstrated that the carbon coated $NaLiFePO_4F$ could be a attractive cathode material which has a specific capacitance of 113 mAh g^{-1} at 0.02C (1C=135 mAh g^{-1}) between the potential range of 2.0-4.5 V. $NaLiFePO_4F$ is significantly sensitive to hydrofluoric (HF) acid generated during the batteries operation. Its electronic conductivity also should be improved (Aurbach, 2000; Amaresh et al., 2014), but few studies focus on the modifications of this kind of electrode material.

2.4 Major Issues and Surface Modifications of High-Capacity Si Anode

Silicon has been widely considered as one attractive anode candidate for high-energy Li-ion batteries owe to the following reasons: (1) the high theoretical capacity (4200 mAh g^{-1}), which is on the basis of full alloying to form $Li_{22}Si_4$, more than ten times that of the graphite anode (372 mAh g^{-1} due to the formation of LiC_6) (Jung et al., 2003; McDowell et al., 2013; Zuo et al., 2017); (2) the low lithiation voltage plateau (0.2-0.3 V *vs*. Li/Li^+), avoiding unexpected lithium plating and lithium dendrite, and thus improving safety (Chan et al., 2008; Zhang, 2011); (3) abundance on the earth (the second abundant element, 28% by mass)(Liu et al., 2012; Wu and Cui, 2012); (4) good environmental compatibility, low toxicity, and good chemical stability (Feng et al., 2018). Unfortunately, several drawbacks limit its wide industrial applications, as will be discussed subsequently. Even so, researchers have made tremendous efforts since the 1990s (Ma et al., 2007; Zuo et al., 2017).

2.4.1 Major challenges about Si anode

Many research groups have investigated the mechanism of lithiation of Si anode (Ryu et al., 2004; Chan et al., 2008). Crystalline Si experiences from a single-crystalline to amorphous at the initial diacharge and then keeps amorphous phase at ambient temperature (Li et al., 2000), which has been shown by using X-ray and nuclear magnetic resonance (Ryu et al., 2011). Unfortunately, Si shows a significant volume expansion of about 420% during the alloying process because of their intake of large numbers of Li. As a result, the first challenge of Si anode is large volume expansion/contraction that results in high internal stress including shear stress and compressive stress (Lee et al., 2001; Liu et al., 2011). This internal stress can cause the crack and pulverization of Si, Figure 2.6a, and then cause failure of the electrical connection between the Si and conducting materials, binder, and current collector, Figure 2.6b. Eventually, this sequential phenomenon can result in poor conductivity for electron and ion, leading to capacity fading.

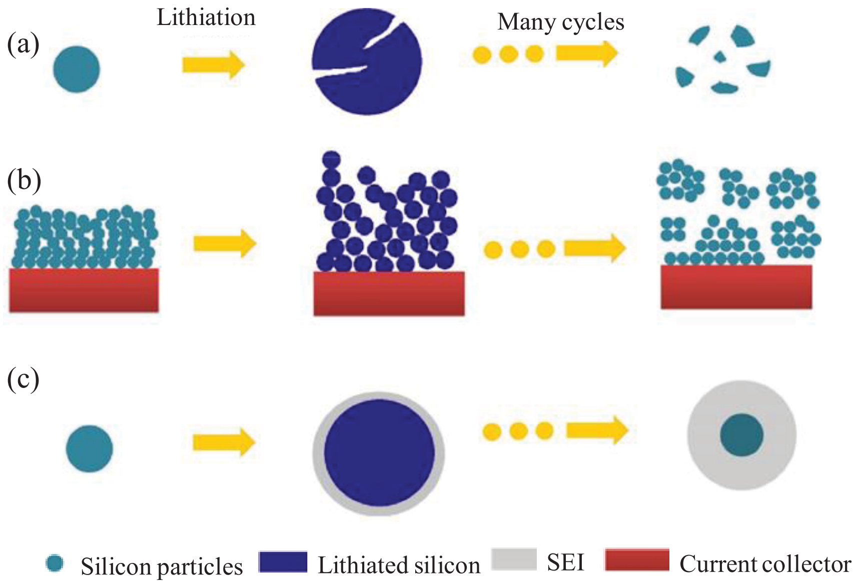

Figure 2.6 Failure mechanisms of a Si anode: a) pulverization and volume change, b) morphology change and c) SEI formation (Reproduced with permission from Elsevier and Copyright Clearance Center) (Wu and Cui, 2012)

The second challenge for silicon anode is improvement of the interface between the electrolyte and Si, which is termed as the solid electrolyte interface (Nie et al., 2013).

When the voltage of the electrode is below ~1 V (*vs.* Li/Li$^+$) organic electrolyte decomposes on the Si surface. As a result, a self-passivating SEI layer forms (see Figure 2.6c) prior to lithiation of Si because a large amount of free Li$^+$ and F$^-$ exist on the surface of Si at the initial charging. The SEI layer consists of Li_2CO_3, LiF, Li_2O and polycarbonates (Ruffo et al., 2009; Wu et al., 2012). This layer should be stable and dense to prevent further side reactions. It serves as a Li ion conductor and an electron insulator. However, the SEI layer collapses during the delithiation because of the large volume change of Li-Si alloy. The fresh electrode surface exposes to the electrolyte, causing the undesirable formation of thick SEI layer. This thick layer causes rapid degradation of Si anode because of the following reasons: (1) consumption of Li-ions and organic electrolyte; (2) poor contact between Si-based materials and current collector; (3) long diffusion pathway of Li$^+$ ions (Luo et al., 2015; Luo et al., 2017).

Another major challenge of Si anode is low electronic conductivity (10^{-3} S cm^{-1}) and Li-ion diffusion capability for practical applications. The lithium diffusion coefficient is at the range of 10^{-14} -10^{-13} cm^2 s^{-1} (Du et al., 2016). These poor intrinsic properties limit its application.

2.4.2 Conventional remediation strategies of Si anode

A great deal of efforts have been devoted to address the aforementioned challenges of Si with some promising progress achieved. Firstly, it is the structure design of Si. The development of Si nanostructures includes 0D materials (nanoparticles, hollow nanoparticles), 1D material (nanowires, nanotubes), 2D materials (Si films), and 3D Si structures (porous Si). Among the Si nanostructures, Si nanoparticle is widely used as the precursor for the preparation of Si anode. The cyclic stability highly depends on the particle size (Ryu et al., 2004; Kim et al., 2010; Liu et al., 2012). The nanosize dimension can reduce the stresses induced by volumetric change (Yoshio et al., 2006). In addition, it is relatively simple to produce Si nanoparticles. However, Si particle-based anodes show poor cyclic performance due to distortion of particles induced by repeated expansion/contraction and also attributed to the uncontrollable growth of the

SEI layer on Si surface (Ma et al., 2014).

Secondly, it is the surface coating of Si nanostructures with protective or conductive materials that has been a research focus, such as Si/C (Si/amorphous carbon, Si/carbon nanotubes, Si/graphene), Si/metal (Si/Ag, Si/Cu, Si/Fe, Si/Ni, Si/Ge, Si/Cu/Cu_3Si, Si/Fe_2Si) (Kim et al., 2005; Yu et al., 2009; Fukata et al., 2016; Luo et al., 2016), Si/metal oxide (Si/TiO_2, Si/Al_2O_3)(Lotfabad et al., 2014; Yang et al., 2017), Si/native oxides (Si/SiO_x) (McDowell et al., 2011; Sim et al., 2013; Zhang et al., 2014; Chen et al., 2015; Ma et al., 2015), and multi-layers (coating layer/Si/coating layer, Si/mechanical layer/conductive layer, Si/conductive layer/mechanical layer) (Guo et al., 2014; Liu et al., 2015; Liu et al., 2016; Luo et al., 2016). These surface coating materials can buffer its huge volume expansion, and prevent direct connection between Si and electrolyte, or provide fast transport channels for electrons or Li^+ ions, eventually maintaining the structural integrity of anode and improving cyclic stability (Li et al., 2012; Zhang et al., 2014). A typical example is that Liu and coworkers (2014) pointed out a pomegranate structure of Si-based anode. Single Si nanoparticles are sealed by a conducting carbon coating, producing large space for volume expansion and extraction of Si, and then the composite particles is sealed by using a thicker carbon coating in micro-sized pouches. The self-supporting conductive carbon layer on the surface of secondary particles limits the formation of most SEI to the outer surface rather than on the primary nanoparticles, so the SEI layer remains stable after cycling, leading to excellent cycling performance (97% capacity retention 1,000th after) and high coulombic efficiency (99.87%) (Liu et al., 2014b).

Besides the tremendous efforts focusing on the development of Si structure and its surface coating, electrolyte additives are one of the other key affecting factors on Si anode. Additives have been widely researched, such as fluoroethylene carbonate (FEC), vinylene carbonate (VC), propylene carbonate (PC), lithium bis(oxalate)borate (LiBOB), lithium difluoro(oxalate) borate (LiDFOB), and succinic anhydride (Jin et al., 2017). They have a desirable effect on stabilizing the interface of Si and electrolyte during the initial lithiation, forming a stable SEI layer and increasing the initial coulombic efficiency of Si anode. Among these additives, FEC is the most promising one that can improve the stability of SEI film (Guo et al., 2014). As a result, an initial SEI layer forms. It plays a role in limiting the degradation of EC/DEC organic solvent and thus limiting the excessive inhomogeneous SEI.

All the above-mentioned modifications show a significant impact on addressing the challenges of Si anodes. However, it is noted that many factors should be given a thought to fairly determine the promise of modified Si anode materials, such as cost of materials and preparation, electrode and its fabrication process, and effect on the environment, etc. Consequently, researchers should take much more consideration on the actual conditions when they are exploring new materials and new methods.

2.4.3 Polymers applied to Si anode modification

Conducting polymers with good chemical stability, excellent electronic conductivity and mechanical flexibility, have gained popularity among researchers in solar cell, supercapacitors, Li-S batteries, and Li-ion batteries. As discussed in Section 2.3.3, the three conductive polymers (PEDOT, PPY, and PANI) that act as protective and conductive coating, have gradually been applied to cathode materials. Accordingly, it is strongly desirable to design a very tunable and efficient approach to incorporate a uniform conductive polymers coat on the surface of Si, improving the structural stability and electrochemical properties (Luo et al., 2017).

Nowadays, these conductive polymers have been broadly implemented in Si anode research. Chew et al. (2007) reported a novel Si nanoparticles/PPY composite that was prepared by using chemical polymerization. The cycling stability of this electrode (specific capacity retained ~30%) was highly increased compared to that of the pure Si particles (specific capacity retained ~ 5%). A similar work has been investigated by Du et al., (2014), who developed a direct method for the fabrication of a protective layer (PPY) on the porous-Si hollow spheres (PHSi). PPY@PHSi retained 88% of its first capacitance (2500 mAh g^{-1}) over 250 cycles, due to the porous hollow structure for buffering the huge volume change, and the formation of stable SEI layer outside of coated Si.

The conductive polymers can partially act as a conductive binder, being an alternative to conventional conductive additive and binder. For example, Wu et al. (2013) explored a successful Si nanoparticles/PANI framework, which was polymerized in situ of aniline monomer. Such a hierarchical hydrogel framework provides a continuous electrically conductive PANI network, and a porous space for accommodating volume expansion of Si, and provides a protective layer to accelerate the formation of stable SEI. Also, the prepared viscous gel is bladed onto copper foil current collector directly without binder additive. With this anode, the half-cell could undergo 5000 cycles with only 10% capacity fading (6.0 A g^{-1}).

Another typical conductive polymer poly(3,4-ethylenedioxythiophene) and poly styrene sulfonate acid (PEDOT:PSS) has high electronic conductivity and is commercially available as aqueous dispersion (Lang et al., 2009). However, it exhibits low stretchability (< 10% strain) and poor stability in wet environments (Lu et al., 2019). For Si nanoparticles, PEDOT:PSS as both binder and conductive agent has been reported by Higgins and coworkers (2016). The Si/PEDOT:PSS was achieved by using in situ secondary doping with small amounts of formic acid. The Si particles were homogeneously coated by PEDOT:PSS. This system showed a first lithiation capacitance of 3685 mAh g^{-1} and a first cycle efficiency of ~78% at high areal loading level (1 mg cm^{-2}).

In the case of Si material modification, the previous work also mainly focused on studying the three conductive polymers (PEDOT, PANI and PPy). It is known that the binder used in electrodes should have the smallest swelling in the electrolyte, be stable in the potential ranges, be flexible, and conduct Li^+ ions for Li-ion batteries. However, these conducting polymers serving as conductive additive have poor capability of conducting Li^+ ions. In addition, their flexibility is not enough to suppress the huge volume change of Si particles at high current density for long cycles. Hence, it is important to investigate a polymer from the view of high electrical conductivity and ionic conductivity, as well as good flexibility, which can be used to modify both the high-voltage $NaLiFePO_4F$ cathode material and high-capacity Si anode material.

2.5 Summary

From the literature survey, one can see that polymers have been broadly applied in supercapacitors and batteries. In these two types of devices, electrolyte and electrode are the most significant components. Gel polymer electrolytes are one of the most attractive candidates for the application of flexible devices owe to the high ionic conductivity and good flexibility. On the other hand, a great deal of studies have been conducted on the polymer materials especially conductive polymers employed in the modification of electrode materials, with significant achievements made. The conductive polymers can control stress-induced cracking, transition metal dissolution of common cathode materials, and improve their electrical conductivity. Meanwhile, the conductive polymers have the potential benefits to the electrical conductivity of Si anode and facilitate the formation of a stable SEI layer on the outside of coating. As a result, the conductive polymer coating can stabilize the structure and improve electrochemical properties of the electrode materials. However, there are still some issues that are needed to be further addressed.

(1) Although previous studies have investigated PVA based Na-ion conducting electrolytes, some of them have been reported to show poor electrochemical stability probably because of simple sodium salts employed and H_2O solvent. Hence, this research focuses on preparing PVA based Na-ion electrolytes together with high ionic conductivity and good electrochemical stability, improving electrochemical performances of EDLCs made of the membranes as a separator and electrolyte.

(2) The previous work mainly focused on studying the conductive polymers (PEDOT, PANI and PPy) used in the protective coating on the surface of cathode and Si anode in terms of their high electrical conductivity, little attention has been paid on investigation of polymers from the view of high electrical conductivity and ionic conductivity, as well as a good flexibility. Hence, this work also focuses on synthesis and application of a new polymer with electronic and ionic conductivity as well as desired flexibility.

Chapter 3 Na-ion Conducting Gel Polymer Membrane for Flexible Supercapacitor Application

3.1 Introduction

The demand for flexible power supply is becoming increasingly high because of the wearable and portable devices found in various fields including medical, military and outdoor sports (Pu et al., 2016). As for GPEs, it renders a high ionic conductivity (σ) and excellent flexibility, making them one more attractive candidate for the application of flexible devices. PVA-based gel polymer electrolytes, such as proton-conducting electrolytes (Gao and Lian, 2014), Li-ion (Wang et al., 2012) and Na-ion conducting electrolytes (Batisse and Raymundo-Pi, 2017), have been investigated by several research groups. Until now, all the reported PVA-based Na-ion conducting electrolytes were prepared using water solvent, and sodium salts employed in most of them were too simple, resulting in poor electrochemical stability (Ponrouch et al., 2015). Furthermore, the contact between electrolyte film and the electrodes was found mechanically weak (Chen et al., 2019) when assembled into energy storage devices.

In order to prepare gel PVA based biodegradable electrolyte for fabricating EDLCs, together with high ionic conductivity and good electrochemical stability, NaTf (sodium triflate or sodium trifluoromethanesulfonate) may serve as a better sodium salt because of the interaction between the hydroxyl group of PVA and the sulfonate group of NaTf. The trifluoro group would also be potentially beneficial for the stability of the electrolyte during operation. Moreover, NaTf can be highly dissolved in PVA, is thermally stable and non-toxic. Its interaction with PVA is a kind of weakly electrostatic coordination that renders high ionic conductivity for electrolytes (Dhumal and Gejji, 2006). When this NaTf containing PVA is prepared using NMP solvent and is plasticized using ionic liquid (EMITf, 1-ethyl-3 methylimidazo liumtrifluoro methanesulfonate), the electrolyte so made would have high chemical stability and ionic conductivity, as indeed seen subsequently. It is worth to note that this chapter has been published by the author in 2020 (Wang et al., 2020).

3.2 Experimental Procedures

3.2.1 Materials

For preparing gel polymer electrolyte membranes, PVA power (Sigma, M_W =125,000 g mol^{-1}), NaTf (Aladdin, 98%), and ionic liquid EMITf (IoLiTec, 99%) was served as polymer host, metal salt, and plasticizer, respectively. The activated carbon (AC) active material (supercapacitor grade, specific surface area ~1800 m^2 g^{-1}), PVDF binder (HSV900), and carbon black conductive agent (Super P) provided by Kejingstar Technology, Shenzhen, China for the preparation of EDLCs electrodes.

3.2.2 Preparation and characterization of gel polymer electrolyte

To identify the relation between the crystallinity as well as the ionic conductivity of the electrolyte films and the concentrations of the doped NaTf and EMITf, the polymer electrolyte membranes were prepared as described previously (Wang et al., 2018), using the casting method after fast stirring (1000 rpm) of the mixed solution at 80 ºC. In fabricating GPE membranes, different quantities of EMITf were dissolved completely in the optimal NaTf-complexed PVA system, determined through X-ray diffraction (XRD) with Cu-Kα radiation (λ = 1.5406 Å) (D/max 2500PC, Rigaku, Japan), scanning electron microscopy (SEM) coupled with energy dispersive X-ray spectroscopy (Hitachi S-4700 SEM-EDS, Japan) and ionic conductivity analyses.

The surface morphologies, structural characteristics and thermal stability of polymer electrolyte membranes were evaluated using SEM, XRD, and thermal analyzer (STA 449F3 Jupiter, Germany), respectively. The electrochemical stability of the membranes was evaluated using an electrochemical workstation (Model: CHI760D, CH Instruments, China). Impedance analyzer (PSM 1735, Newton, UK) was used to measure the ionic conductivity. The as-obtained symmetric cells were used for these three evaluations, consisting of a pair of stainless steel foils as electrodes sandwiched by an electrolyte film. All the measurements and characterizations were conducted at room temperature (23-25 ºC). In addition, the Na^+ transport number of the electrolyte films was evaluated by using the Bruce-Vincent equation (Evans et al., 1987). The Na/electrolyte membrane/Na cell was polarized by applying a DC potential difference of 10 mV. The cell resistance values before and after polarization were collected by applying AC impedance spectroscopy.

3.2.3 Assembling and testing of EDLC

To evaluate the electrochemical properties of the prepared electrolyte films, they are employed in the fabrication of EDLCs. The active carbon (AC) electrode is prepared by the following procedure: AC, poly(vinylidene fluoride) (PVDF) and carbon black are mixed in NMP (the mass ratio of 80:10:10). The mixture is stirred until obtaining a homogenous paste and then doctor bladed on the Al, followed by drying at 110 °C and roll pressing. The EDLC was fabricated using the spinning-casting method to improve the contact of electrodes with polymer electrolyte. The PVA-NaTf+EMITf solution was spun on the prepared electrode at a high speed (1400 rpm) for 20 s to form a thin film (~5-6 μm) and heated to evaporate the NMP solvent at 60 ºC for about 10 min to 80% of its full extent. The experimental procedure can be seen in more detail in Figure 3.1. The amount of NMP evaporated was determined by weighing the sample before and after heating. The remanent solution (PVA-NaTf+EMITf) was then cast onto the surface of electrolyte membrane-electrode and dried in the oven at 70 ºC for 24 h. This non-fully dried electrolyte membrane (containing ~10 wt.% solvent, determined by weighing) was joined with another piece of electrode to form a symmetrical EDLC. With this method, one could prepare a number of EDLCs simultaneously (Figure 3.1).

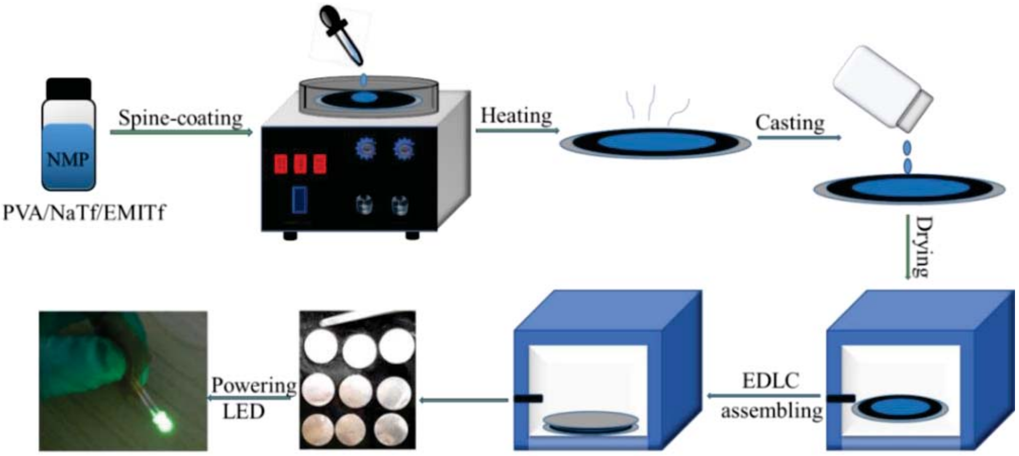

Figure 3.1 Schematic illustration showing the fabrication and application of EDLCs

The liquid electrolyte, 1 mol L^{-1} NaTf in EC and PC (v/v 1/1), was employed to fabricate CR2032-type cells with activated carbon as electrodes in a glove box filled with Ar. The volume of the liquid electrolyte is 60 μL. The glass fiber is used as separator. The measurements of CV of EDLCs were performed at room temperature (23-25 ºC) with different scan rates from 0 to 1.6 V and 0 to 2.0 V. Galvanostatic charge-discharge (GCD) was conducted at a constant current density of 313 mA g^{-1} using Neware battery testing device. Finally, the EDLCs were employed to power an LED to demonstrate the possibility of their practical application.

3.3 Results and Discussion

3.3.1 Materials characterization

To identify the optimal salt (NaTf) and ionic liquid (EMITf) contents doped in the PVA solution, the PVA film mixed with various contents of NaTf or EMITf were made using the casting method. The viscosity of the solution decreases during the rapid mixing, so that the big ions, such as Tf^- and EMI^+, are easy to be tethered by the polymer matrix and then entangled by the polymer chains, causing a decrease in the crystallinity of PVA (Zhao et al., 2017). XRD patterns of PVA films mixed with various contents of NaTf and EMITf are shown in Figure 3.2.

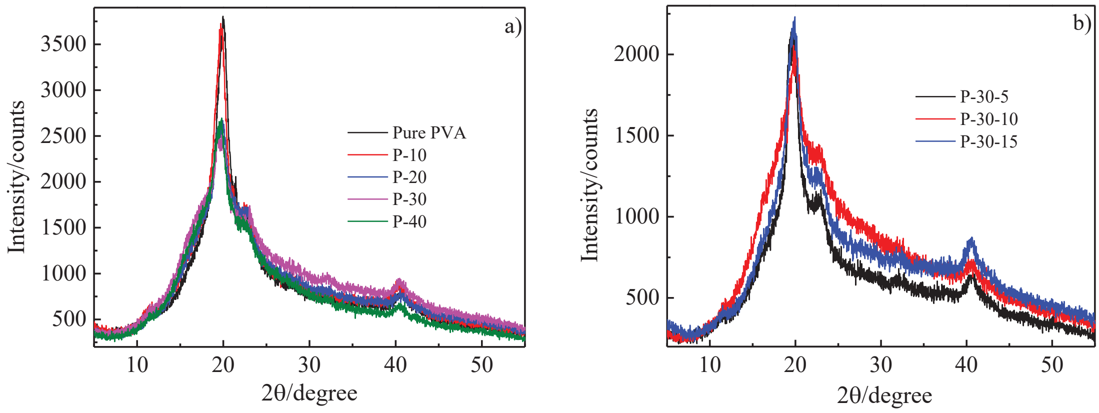

Figure 3.2 XRD patterns of (a) PVA-*x*NaTf(*x* = 0, 10, 20, 30, and 40 wt.%, denoted as Pure PVA, P-10, P-20, P-30, and P-40) and (b)PVA-30wt.% NaTf + *y*EMITf(*y*= 5, 10, and 15 wt.%, denoted as P-30-5, P-30-10, and P-30-15) membranes

The change of crystallinity is shown in Figure 3.2a in terms of X-ray diffraction. The incorporation of NaTf in a concentration range of 10 to 30 wt.% enables the diffraction peak to widen and decrease in intensity, indicating the decrease of crystallinity of PVA. However, a further increase in NaTf beyond 30wt.% leads to an increase in the intensity and a decrease in the width of the peak, indicating the increase in crystallinity. Therefore, the best composition should be P-30.

In order to obtain gel electrolyte membranes, the EMITf ionic liquid was added into the P-30 mixture with continual fast stirring (1000 rpm) at 80 ºC. As shown in Figure 3.2b, the peak intensity decreases further due to the introduction of EMITf and the best composition in terms of crystallinity is the P-30-10 mixture. The lower crystallinity can supply larger free volume, thereby leading to more segment motion and higher carrier mobility that are very crucial for the electrolyte membrane to achieve high ionic conductivity.

The morphologies of prepared electrolyte films were observed using SEM. As shown in Figure 3.3, the electrolyte membranes maintain a uniform and soft surface even after being plasticized by ionic liquid and exhibit perfect structural integrity because they are self-standing. However, many particles are apparently visible on the surface of electrolyte membranes containing 20 wt.% EMITf. These particles demonstrate the existence of NaTf as confirmed by EDS (see Figure 3.3f), where the peaks of carbon, oxygen, fluorine, sodium and sulphur are observed. The excess ionic liquid could lead to ion aggregates, being attributed to the combination of Na$^+$ and Tf$^-$, and not EMI$^+$ and Tf$^-$ since the concentration of EMITf is low (Sim et al., 2014). Accordingly, the optimal electrolyte composition would be the P-30-10 mixture.

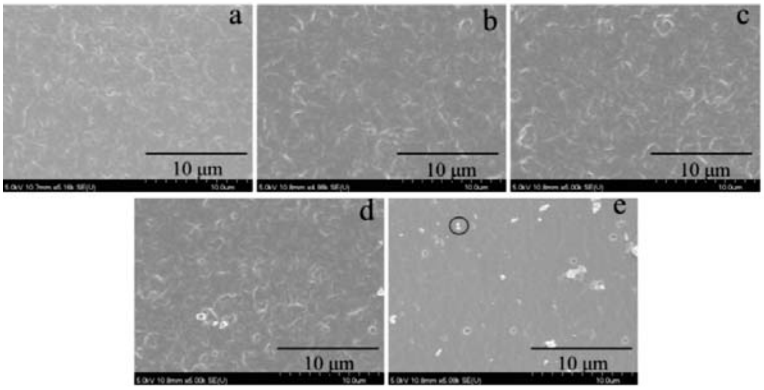

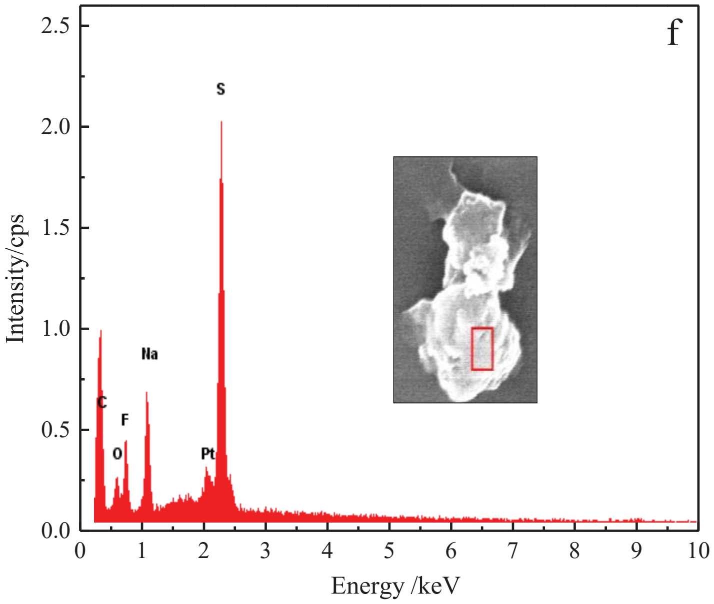

Figure 3.3 SEM images of (a-e) PVA-30 wt.% NaTf + *y*EMITf (*y* =0, 5, 10, 15 and 20 wt.%) under 5.00k magnification; (f) EDS analysis of the particle in (e)

To evaluate the thermal property of the electrolyte membrane, the thermogravimetric analysis (TGA) and differential scanning calorimetry (DSC) was employed with the results shown in Figure 3.4. Obviously, at around 80ºC, the P-30-10 membrane exhibits a ~2% mass loss, which is attributed to the loss of moisture and NMP. It also shows a weight loss at around 180 ºC because of the melting and the first decomposition stage of PVA (Mishra and Rao, 1999). A weight loss at around 240 ºC due to the decomposition of NaTf is observed (Ponrouch et al., 2015). Furthermore, the weight loss after 300 ºC may arise from volatilization of EMITf and decomposition of PVA (Shamsipur et al., 2010). Hence, the P-30-10 sample exhibits relative stability before150 ºC. This indicates that this electrolyte membrane can be applied in capacitors where high temperature is a concern (Lin et al., 2016). Besides the desirable thermal stability, the electrolyte membrane can also be completely curled without any breakage (see Figure 3.5). This gives an additional advantage of mechanical stability. Consequently, the optimum PVA-based gel polymer electrolyte membrane shows a great potential for the fabrication of flexible sodium-ion capacitors as both electrolyte and separator.

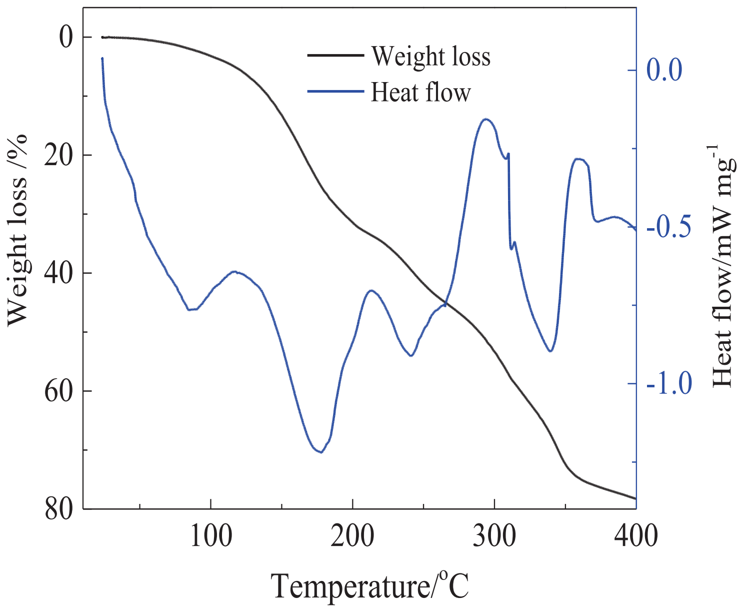

Figure 3.4 TGA and DSC plots of PVA-30 wt% NaTf + 10 wt.% EMITf membrane

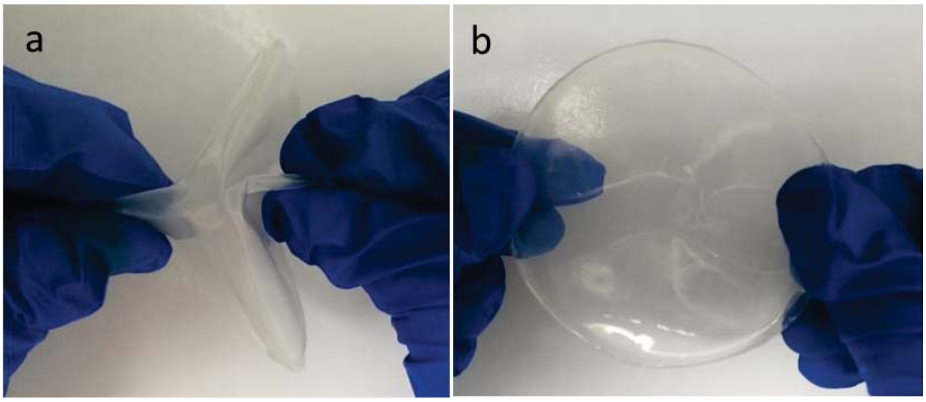

Figure 3.5 The electrolyte films (a) in bending and (b) after bending

The electrochemical properties are also critical for the application of an electrolyte film, for example, electrochemical stability, ionic transference number, and ionic conductivity. The electrochemical stability is analyzed by using cyclic voltammograms (see Figure 3.6). The P-30 without the addition of EMITf shows a good electrochemical stability up 4.15 V. When 5% EMITf is added to the P-30, and the resulting P-30-5 electrolyte membrane shows a better electrochemical stability up to ~4.70 V. This stability window is maintained even after 10% EMITf is added, implying an excellent tolerance to polarization and a great potential application for high cell-potential-difference devices. Nevertheless, further addition of EMITf to P-30 leads to some extra redox peaks, as seen from the P-30-15 CV test results. These redox peaks probably arise from the precipitated sodium salt particles due to the excessive addition of ionic liquid, being consistent with those noted from Figure 3.3e.

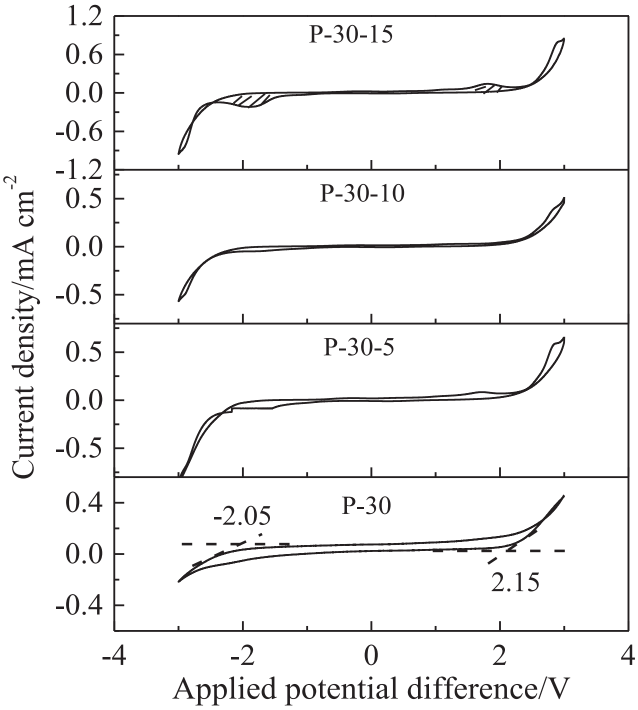

Figure 3.6 CV curves of SS/PVA-30 wt.%NaTf + *y*EMITf/SS cell (*y* = 0, 5, 10, and 15 wt.%, denoted as P-30, P-30-5, P-30-10, and P-30-15)

Ion transport depends on the cations (Na^+ and EMI^+) and anion (Tf^-). The Na^+ transport number of the electrolyte films (t_{Na+}) is given by the Bruce-Vincent equation (Evans et al., 1987):

$$t_{\mathrm{Na}^+} = \frac{I_{ss}(V - I_0 R_0)}{I_0(V - I_{ss} R_{ss})} \tag{3.1}$$

Where I_0 and I_{ss} are the initial-state and steady current; R_0 and R_{ss} are the Na/P-30-10/Na cell resistance values before and after polarization, respectively; and V is the applied potential difference. These values can be obtained from Figure 3.7. The Na^+ transport number for the P-30-10 electrolyte film is gained as ~0.59 at room temperature. Hence, Na^+ should transfer faster than the other two ions of much larger sizes and make more contribution to ionic conduction because large-sized ions can be easily pinned within the polymer matrix although the concentration of Tf^- is higher (Zhao et al., 2017; Makhlooghiazad et al., 2018).

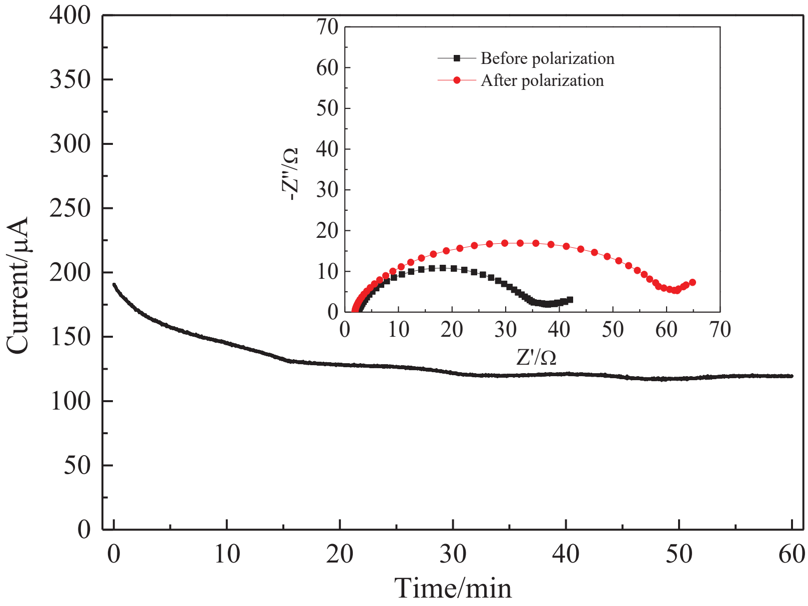

Figure 3.7 DC polarization curve of Na/P-30-10/Na cell at an applied potential difference of 10 mV and the inset shows the EIS curves before and after polarization of the cell

The Nyquist impedance analyses (Figure 3.8) were further carried out to confirm the contribution of NaTf salt and EMITf ionic liquid to ionic conductivity (σ) (S cm^{-1}) which can be calculated through

$$\sigma = t/(R_\mathrm{b}\, A) \tag{3.2}$$

where t represents thickness of a electrolyte membrane, being about 0.008 cm; A represents the electrode-film contact area; and R_b is resistance of electrolyte membrane (R_b/Ω), which is obtained from the intercept of semicircle at high frequency on real axis. As shown in Figure 3.8a, when less than 40% NaTf is added to the PVA sample, the resulting electrolyte membranes (denoted as P-10, P-20 and P-30) show a decrease of R_b, which is due to the decrease in crystallinity and the increase in mobile ions. However, when the content of NaTf is up to 40%, the value of R_b increases due to the increase in ion aggregation. Hence, the P-30 sample has the highest ionic conductivity for the unplasticized systems. Similarly, the P-30-10 sample has higher ionic conductivity (~3.8×10^{-3} S cm^{-1}) than the others. When a proper amount of EMITf (less than about 10 wt.%) is added to the P-30 mixture, the amorphous region of the electrolyte membrane increases and thus enhances the mobility of the ions. However, further addition of EMITf would result in an increase in ion aggregation. This is agree with XRD results showing the lowest degree of crystallinity for this electrolyte. The transport of mobile ions within the polymer substrate depends on amorphous domains which can promote polymer segmental motions and then enhance the mobility of mobile ions (Zeng et al., 2016). Therefore, the high ionic conductivity of the P-30-10 sample should be due to its low crystallinity and the large concentration of mobile ions.

Furthermore, it is found that the ionic conductivities obtained from the PVA electrolyte films based on sodium, magnesium and lithium salts are of a similar order of magnitude. Overall, the present value compares well with reported values (Mindemark et al., 2017; Wang et al., 2018; Wang et al., 2018). Accordingly, P-30-10 electrolyte membrane should be suitable for application in capacitors.

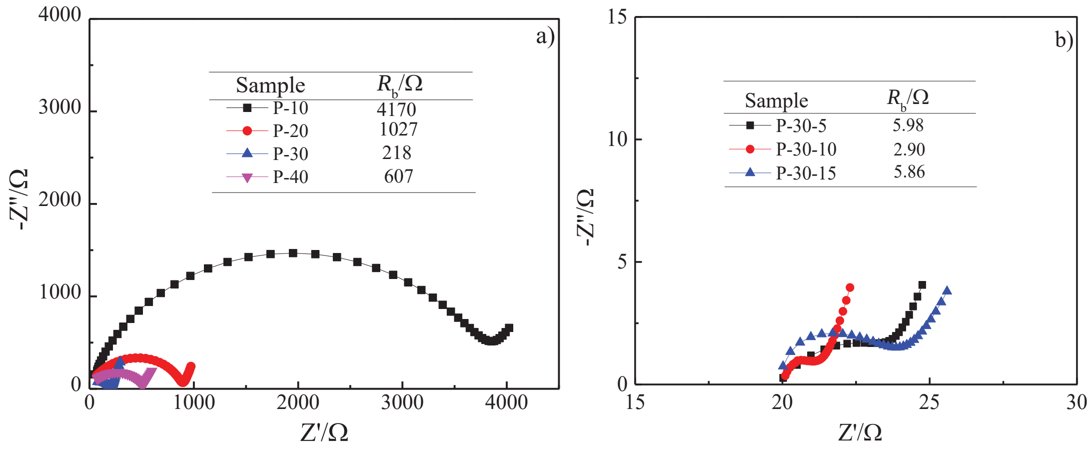

Figure 3.8 (a) Nyquist impedance plots of the PVA-*x*NaTf with a table of R_b as inset (*x* =10, 20, 30, and 40 wt.%, denoted as P-10, P-20, P-30, and P-40) and(b) PVA-30 wt.% NaTf + *y*EMITf with a table of R_b as inset (*y*= 5, 10and 15 wt.%), recorded at room temperature

3.3.2 Performance of the EDLCs

The performance of this sodium-ion conducting gel polymer electrolyte membrane was investigated by means of acting as “electrolyte and separator” in EDLCs (activated carbon (AC) as electrodes.

Figure 3.9a and 3.9b display the cyclic voltammograms (CVs) of capacitors with the gel polymer electrolyte membrane (P-30-10) (C//GPE//C) and with the liquid electrolyte (C//LE//C) at different scan rates (0-1.6V), respectively. Obviously, both of them exhibit a nearly symmetrical and rectangular shape at low scan rates, indicating that they have a desirable capacitor performance and a low resistance so that the mobile sodium ions can transfer and then generate electric double-layer near the interface of electrode-electrolyte. Nevertheless, gradually the plots lose rectangle feature with increasing scan rates. In addition, for the C//GPE//C capacitors, the areas of CV curves are slightly larger than those of the C//LE//C capacitor at low scan rates, and the difference becomes insignificant at different high scan rates of 9 and 13 mV s^{-1} for these two types of capacitors (see Table 3.1).

In order to identify the performance of capacitors at a larger potential range (0-2.0 V), these two types of capacitor were also analyzed using CV measurements. The results are depicted in Figure 3.9c for the C//GPE//C) capacitor and Figure 3.9d for the (C//LE//C) capacitor. Obviously, C//GPE//C shows slightly higher specific capacitances, due to its bigger areas of CV curves, than those of the C//LE//C capacitor at different scan rates (see Table 3.1). This means that the as-obtained gel polymer electrolyte membrane is well comparable with the liquid electrolyte.

Table 3.1 Absolute area of CV curves of C//GPE//C and C//LE//C EDLCs at different scan rates (0-1.6 V and 0-2.0 V)

EDLCs	Cell potential difference/V	Absolute area of CV at different scan rates			
		1 mVs^{-1}	5 mVs^{-1}	9 mVs^{-1}	13 mVs^{-1}
C//GPE//C	0-1.6	0.650	2.292	3.427	4.267
C//LE//C	0-1.6	0.542	1.750	3.410	4.265
C//GPE//C	0-2.0	1.050	3.124	4.725	5.813
C//LE//C	0-2.0	0.669	2.846	4.294	5.475

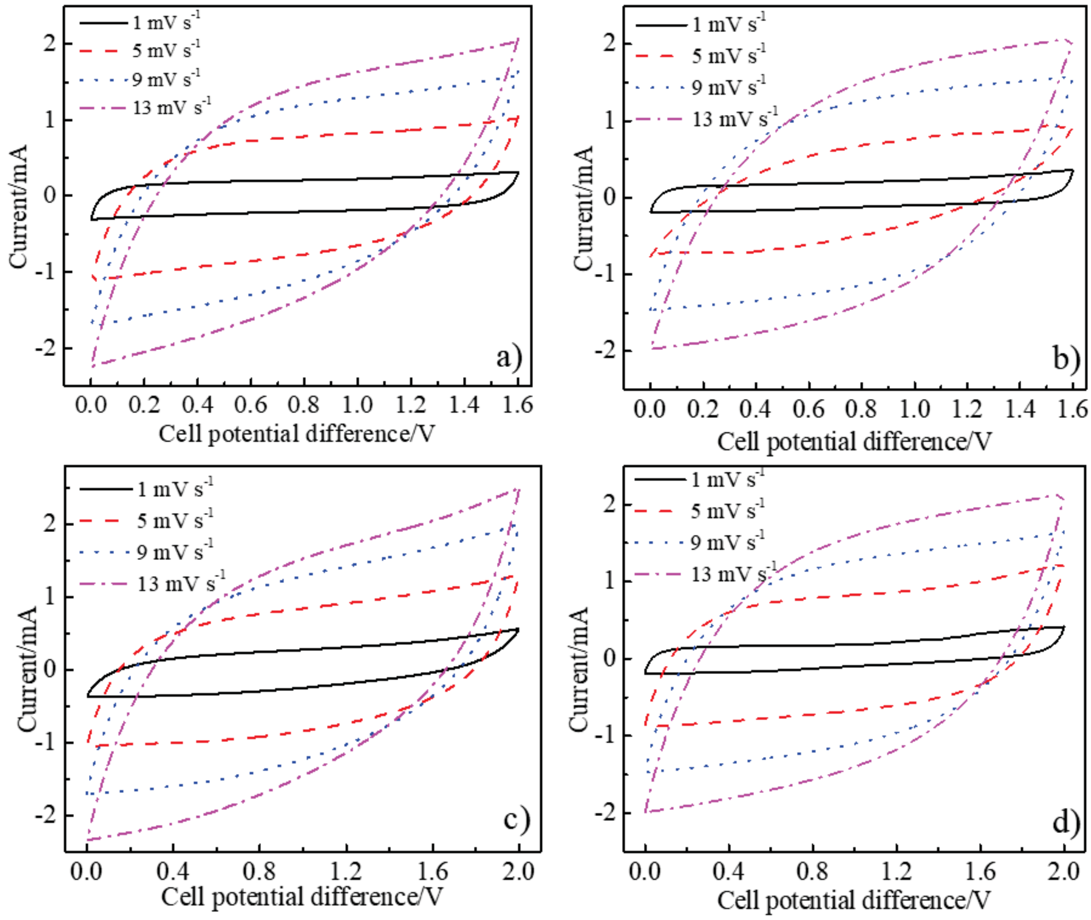

Figure 3.9 Cyclic voltammograms of EDLC fabricated with (a, c) P-30-10 electrolyte membrane and with (b, d) liquid electrolyte, determined at different scan rates in the cell potential ranges of (a, b) 0-1.6V and (c, d) 0-2.0 V, respectively

The galvanostatic charge-discharge (GCD) measurements of the C//GPE//C and C//LE//C capacitors were carried out at room temperature (23-25 ºC) to further demonstrate the reliability of this polymer electrolyte system.

Figure 3.10a and 3.10b exhibit the GCD plots of these two kinds of EDLC for the 1st, the 50th and the 100th cycles recorded in the potential of 0-1.6 and 0-2.0 V, respectively. It can be observed from Figure 3.10a, a nearly linear profile is obtained in terms of all the charging and discharging plots, further indicating a comparable capacitive property of these EDLCs, being in agreement with the CV results. Moreover, all the curves show nearly symmetrical triangles, implying that these EDLCs possess a high coulombic efficiency, which is given by

$$\eta = \frac{t_D}{t_C} \times 100\% \tag{3.3}$$

where t_C and t_D represent the times for charging and discharging in units of s.

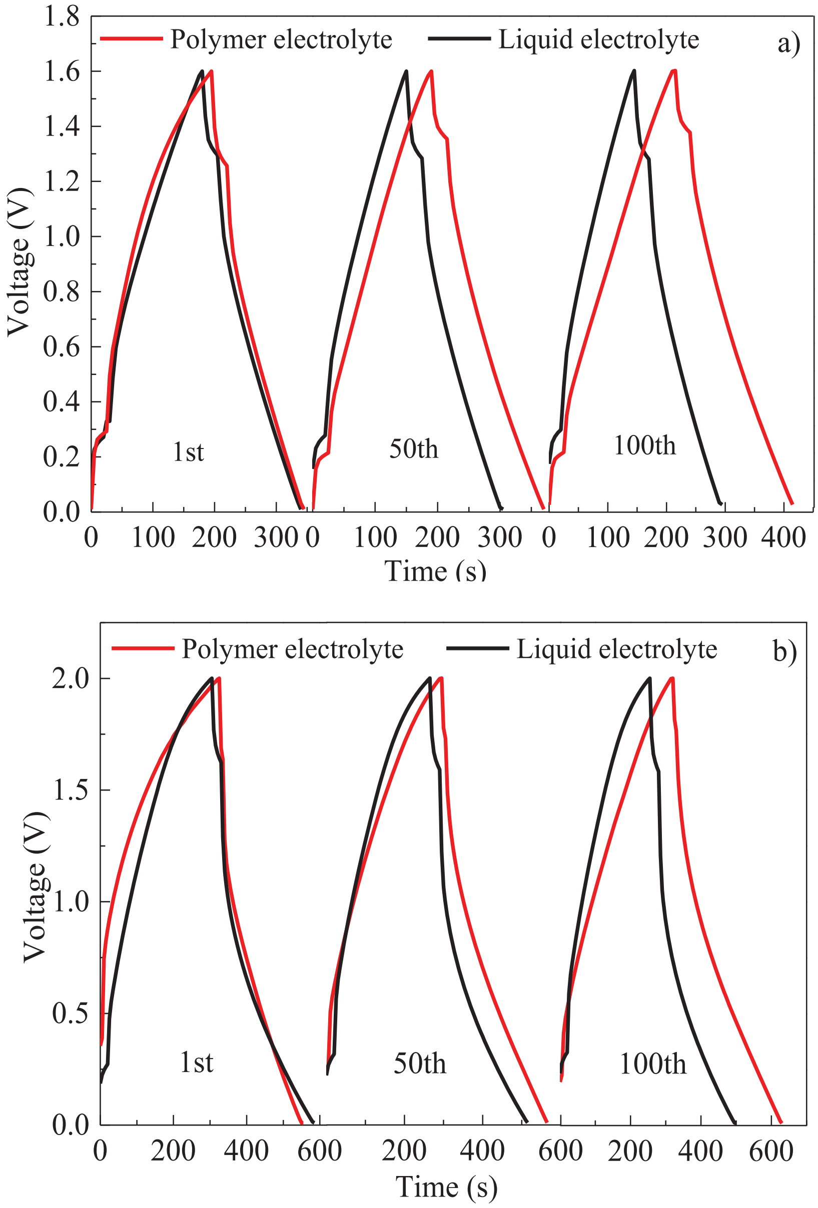

Figure 3.10 The galvanostatic charge-discharge curves of EDLCs fabricated with P-30-10 electrolyte and liquid electrolyte, respectively, at 1st, 50th and100th cycles in the cell potential ranges of (a) 0-1.6V and (b) 0-2.0 V

As shown in Figure 3.10a, a sudden drop in cell potential difference, i.e. the kink at around 1.3 V, is almost identical for both C//GPE//C and C//LE//C capacitors at the initial cycling, but it decreases with the increasing cycle for the capacitor with the polymer electrolyte while the drop of cell potential difference shows no change for the capacitor with the liquid electrolyte. This indicates that the C//GPE//C device has less energy loss during cycling. This cell-potential-difference drop is caused by the ohmic loss. This is because of several internal resistances of devices, i.e., the resistance induced by electrodes, electrolyte, electrolyte/electrodes and electrodes/current collector interfaces. In addition, it can be seen that charging for the polymer electrolyte is slower than that for the liquid electrolyte as time goes because the ionic conductivity of former is smaller than that of the latter.

To further identify the cycling performance of C//GPE//C and C//LE//C capacitors, the room-temperature coulombic efficiency and capacity as a function of the cycling number are depicted in Fig. 11a and 11b under the cell potential differences of 1.6 V and 2.0 V, respectively. The value of specific capacitance (C_s/F g^{-1}) of the single electrode is obtained by

$$C_s = 4I/(m\frac{dV}{dt}) \tag{3.4}$$

where I is current in the unit of A, m (g) represents the weight of active materials in electrodes, and dV/dt (V/s) is slope of the linear part of the discharge curve. In Figure 11a, the specific capacitance of the C//GPE//C capacitor increases with increasing cycling to ~170 cycles and then slightly decreases until a nearly steady value over 1000 charge-discharge cycles. By comparison, it keeps a decreasing trend up to 1000 charge-discharge cycles for the C//LE//C capacitor. This may be due to the difference of internal resistance between these two types of EDLCs. For both capacitors, the first value of C_s is around 100 F g^{-1}, but it increases slightly to 103.7 F g^{-1} for the C//GPE//C capacitor and 63.5 F g^{-1} for the C//LE//C capacitor in the 1000th cycle. In addition, they both show an almost 100% coulombic efficiency after several cycles until 1000 cycles. The lower coulombic efficiencies in the initial charging-discharging cycle may be attributed to the irreversible side reactions, which is common for some capacitors (Fic et al., 2015; Laheäär et al., 2015).The cycling performances for these EDLCs were evaluated by charging to 2.0 V, and the results are given in Figure 11b. Compared with above results shown in Figure 11a (charged to 1.6 V), a similar variation trend in specific capacitance/coulombic efficiency is observed, but the C//GPE//C capacitor shows a higher coulombic efficiency than the C//LE//C capacitor. For the C//LE//C capacitor, the value of C_s is 146.1 F g^{-1} in the first cycle and 85.0 F g^{-1} after 1000 cycles, and thus its capacity retention is only 41.8%. In contrast, for the C//GPE//C capacitor, the capacity retention is nearly 100% (125.4 F g^{-1} at the 1st cycle and 127.8 F g^{-1} after 1000 cycles). For both kinds of EDLCs, the corresponding energy density (E_{cell}) and power density (P_{cell}) can be calculated by (Yang et al., 2015; Phattharasupakun et al., 2018):

$$E_{\text{cell}} = \frac{C_s(\Delta V)^2}{8} \times \frac{1000}{3600} \tag{3.5}$$

$$P_{\text{cell}} = E_{\text{cell}}/(\frac{\Delta t}{3600}) \tag{3.6}$$

where ΔV is the cell potential difference excluding the cell potential drop in the unit of V and Δt (s) is discharge time. The calculated results are listed in Table 3.2. Clearly, the EDLC fabricated with the polymer electrolyte membrane provides a steady energy density and power density even after 1000 cycles at the charging voltages of both 1.6 V and 2.0 V, further indicating that the spinning-casting method is suitable for the fabrication of EDLCs and that the P-30-10 electrolyte membrane is an attractive one for applications of energy storage. However, the EDLC fabricated with the liquid electrolyte loses about half of the energy density after 1000 charge-discharge cycles, further showing the unstable internal resistance within the C//LE//C device. The relatively poor performance of EDLCs fabricated with the liquid electrolyte may be due to the sodium salt composed of large-sized anions and sodium cations. The liquid electrolyte is easy to diffuse into the electrode, forming ion aggregation and resulting in a jam and accumulation in electrode materials at an electric field. This may lead to a larger internal resistance for EDLCs along with a smaller effective specific surface area for active carbon electrodes. By contrast, the large-sized ion aggregation in polymer electrolyte could be trapped in polymer matrix. The as-fabricated EDLC with the present polymer electrolyte has been used to successfully power an LED. This further demonstrates the ideal electrochemical properties of the EDLC.

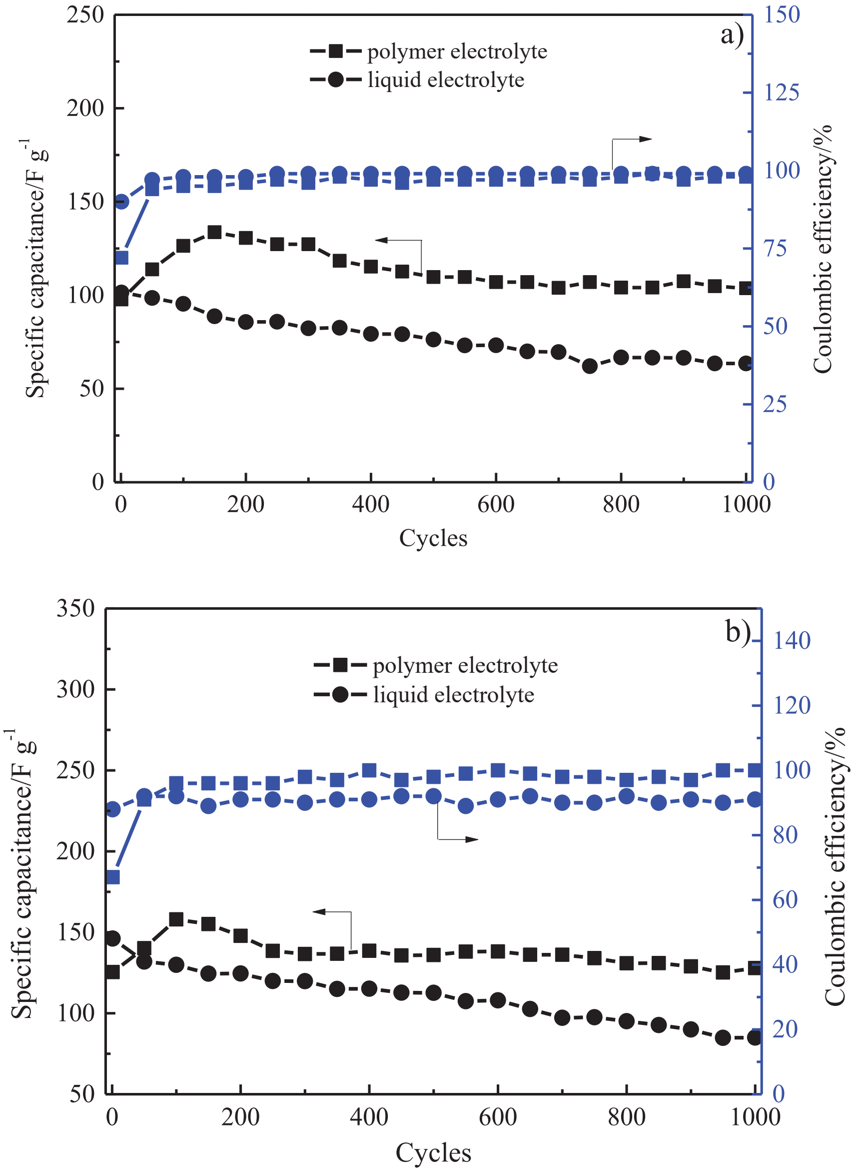

Figure 3.11 The variations of specific capacitance and coulombic efficiency with cycling for EDLCs fabricated with P-30-10 electrolyte and liquid electrolyte in the cell potential ranges of (a) 0-1.6 V and (b) 0-2.0 V

Table 3.2 Energy density (W h kg^{-1}) and power density W kg^{-1}) of C//GPE//C and C//LE//C at different cell potential differences and redox cycles

EDLC	Cell potential difference/V	$E_{cell}/1^{st}$	$E_{cell}/1000^{th}$	$P_{cell}/1^{st}$	$P_{cell}/1000^{th}$
C//GPE//C	0-1.6	6.5	7.2	161.4	167.2
C//LE//C	0-1.6	7.3	4.4	170.0	166.7
C//GPE//C	0-2.0	12.4	13.8	198.4	207
C//LE//C	0-2.0	15.9	8.1	208	194.4

3.4 Summary

Poly(vinyl alcohol) (PVA) polymer, a biodegradable one, can be utilized to fabricate gel electrolyte for EDLCs using sodium ions as the main conducting charges. The proper selection of sodium salt and solvent is essential for its performance.

(1) Sodium triflate (NaTf) has been shown as a good choice of sodium salt and NMP as the solvent of PVA. It is found that the composition of PVA-30% NaTf+10% EMITf (P-30-10) exhibits an excellent room-temperature ionic conductivity of ~3.8×10^{-3} S cm^{-1}, good electrochemical stability up to ~4.70 V, as well as thermal stability below 150 °C.

(2) The EDLCs fabricated with P-30-10 film using a spinning-casting method exhibits excellent electrochemical performance as compared with that fabricated with the liquid electrolyte. It gives both high cyclic stability and high coulombic efficiency (~100%) up to 1000 charge-discharge cycles at various potential ranges (0-1.6 and 0-2.0 V), respectively.

Chapter 4 Conductive and Flexible Coating of Cathode Made of $NaLiFePO_4F$ as Active Material in Li-Ion Batteries

4.1 Introduction

Nowadays, the Li-ion batteries have become a type of the most attractive novel energy storage systems for powering electric devices because of the intrinsic advantages, for example, high energy density, high efficiency, and no memory effect (Taracson and Armand, 2001; Liu et al., 2015; Xiao and Sun, 2018; Liu et al., 2019). The expectations are high, as the increasing energy demand for the electric vehicles (500 km drive range with one charge) (Xu et al., 2017). The costs of Li-ion battery-packs (below 100 euros per kilowatt-hour by 2020) (Schmidt et al., 2017), and the safety (e.g., by replacing the flammable liquid organic electrolytes) (Bresser et al., 2018) is still waiting for further optimization. Hence, although the application of Li-ion batteries has been commercially available within electric vehicles, the demand for the developments of devices with good performance, high safety and low cost is still great (Dunn et al., 2011). The isostructural fluorophosphates compounds (A_2MPO_4F, A represents Na and Li; M represents Fe, Co and Ni) have attracted particular attention. Among the compounds, low-cost $NaLiFePO_4F$ is a promising candidate because of its framework connectivity that could show high potential. This is attributed to the inductivity of PO_4^{3-} functional group and F^- with electron-withdrawing character (Antipov et al., 2015). However, the material has low electronic conductivity and is significantly sensitive to HF. Few studies focus on the high-voltage and low-cost $NaLiFePO_4F$ cathode material. Bai found that the capacity of $NaLiFePO_4F$ cathode material under the larger current (0.5C) was low, but the capacity was improved after the conducting PPy coating (Bai, 2019). Conductive polymers have been broadly used for the modifications of electrode active materials in batteries. Among them, PEDOT synthesized from EDOT monomer shows a better capability to improve cycling and rate performances of electrodes. Meanwhile, poly(dimethylsiloxane) (PDMS) has also attracted much attention. It has been used as a stable interfacial layer for Li-metal batteries showing good performances owe to mechanical flexibility and chemical stability (Zhu et al., 2017). PDMS molecules can form a helix structure because of the corresponding rotations around the highly flexible Si-O bonds, leading to good mechanical properties (Klonos et al., 2015). It should be noted that nanopores in the PDMS film could be created by HF etching and they provide more pathways for Li^+ transport (Zhu et al., 2017). In this part of the study, in order to optimal the efficiency of $NaLiFePO_4F$ cathode materials (i.e. improving electronic conductivity and ionic conductivity), a new polymer of PEDOT-PDMS with good conductivity and flexibility was synthesized. The reaction occurs between ethylenedioxythiophene (EDOT) conductive skeleton and flexible hydride terminated poly(dimethylsiloxane) (h_2PDMS) with the help of Karstedt catalyst.

The PDMS matrix has the capability of absorbing HF. In addition, the HF is derived from the reaction between PF_5 and water, when electrolyte migrate into the electrode, the PF_6^- anions are easily interact with the conjugate structure in PEDOT-PDMS, leading to less amount of PF_5 in the electrode and then less HF. Hence, the conformal coating of PEDOT-PDMS on the prepared electrodes containing $NaLiFePO_4F$ active material would not only be beneficial to electronic conductivity but also protect $NaLiFePO_4F$ from HF corrosion, maximizing the performance of $NaLiFePO_4F$ cathode material. Indeed, the prepared $NaLiFePO_4F$ electrode@PEDOT-PDMS electrode exhibits high capacity and good cycle stability as reported subsequently.

4.2 Experimental Section

4.2.1 Materials

Hydride terminated poly(dimethylsiloxane) (h_2PDMS, $M_W = 580$ g mol^{-1}), NMP (anhydrous, 99.5%), and toluene (anhydrous, 99.8%) were bought from Sigma-Aldrich. 3,4-Ethylenedioxythiophene (EDOT, >98.0%) was purchased from TCI. Karstedt catalyst solution was purchased from Aladdin. $NaLiFePO_4F$ was provided by a lab mate in our research group (Bai, 2019). PVDF (HSV900) binder and Super P conducting additive were provided by Kejingstar Technology, Shenzhen, China.

4.2.2 Preparation of PEDOT-PDMS and its characterization

First, h_2PDMS (410 μL) and EDOT (80 μL) were dissolved in toluene, denoting as Solution A. Second, 10 μL Karstedt catalyst was added into a round-bottom flask with the protection of Ar, denoting as Solution B. Then, Solution A was added into Solution B by using an injector (5 mL), and the two solutions were mixed for 4 h at 60 °C in oil bath with a magnetic stirrer. The resulting solution was connected on a reduced pressure (i.e. the flask connecting to a vacuum pump, 10-15 mmHg) to remove the unreacted monomers for 1h.

The presence of PEDOT-PDMS was confirmed from the results of Nuclear magnetic resonance (NMR, Jeol ECZ500R 500 MHz) ^{1}H spectra and Fourier transform infrared spectroscopy (FTIR, Nicolet 380). The FTIR were obtained in the range of 400-3000 cm^{-1} at the resolution of 4 cm^{-1}. The structural characteristics of PEDOT-PDMS was evaluated through X-ray diffraction (Smartlab 90kw, Rigaku) with Cu Kα radiation. The new polymer was further evaluated by using X-ray photoelectron spectra (XPS, PHI 5000 Versa Probe), providing the information of elemental composition within the sample. The spectra were collected in the range of 0-1100 eV. The mechanical properties of the film was evaluated by using Low Force Universal Testing Systems (Instron 3344). The size of the membrane is 50×8×0.78 mm (length×width×thickness). Scanning electron microscopy (SEM, TESCAN VEGA3) equipped with an energy dispersive spectroscopy was employed to examine the microstructure and elemental distribution.

4.2.3 Electrode preparation, cell assemble and battery testing

The $NaLiFePO_4F$ electrode served as the control electrode that was made without coating, i.e. 70 wt% $NaLiFePO_4F$ (0.1 g), 10 wt% PVDF (0.0143 g) as a binder, and 20 wt% super P (0.0286 g) were fully mixed with NMP (500 μL). The resulting homogeneous slurry in the mortar was cast onto Al foil (16 μm) by using the scraper (BEVS, 1806B/100) and the loading density of the electrode material was 1.5-1.7 mg cm^{-2}. Finally, it was dried for 12 h in a vacuum oven at 80 °C. $NaLiFePO_4F$

electrode@PEDOT-PDMS was prepared by applying PEDOT-PDMS solution on to the surface of each electrode made of $NaLiFePO_4F$ as active material (area= 0.785 cm^2). The resulting electrode was heated at 90 °C for 12 h under vacuum in a vacuum oven, forming the coated electrode as shown in Figure 4.1. Coin-type cells (2032) were assembled inside a glovebox filled with Ar (H_2O<0.1 ppm, O_2<0.1 ppm). A Li foil was served as the reference electrode. A Celgard 2325 micro-porous polypropylene (PP) was utilized as the separator. The electrolyte employed was a high-voltage electrolyte (LB-111, $LiPF_6$ in EC/DMC with additives.) supplied by DoDochem. The dosage of electrolyte in every coin-type cell was 50 µL.

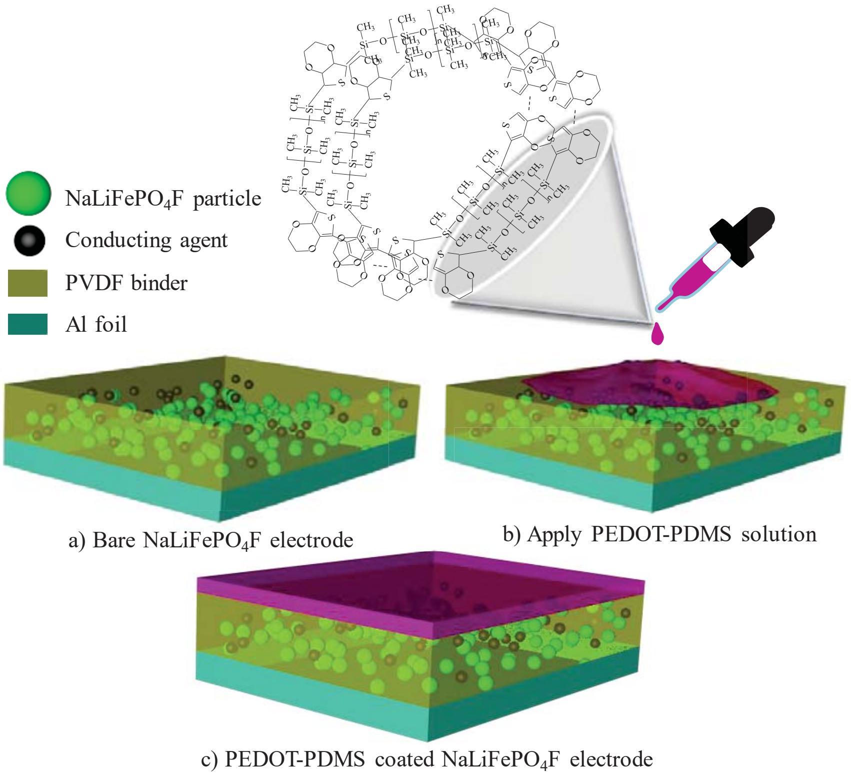

a) Bare $NaLiFePO_4F$ electrode

b) Apply PEDOT-PDMS solution

c) PEDOT-PDMS coated $NaLiFePO_4F$ electrode

Figure 4.1 Schematic illustration of the coating of electrode

Galvanostatic charge-discharge cycling were conducted by using a LAND battery testing system (CT2001A) in a potential range of 4.5-2.0 V (*vs*.Li/Li^+), at current density of 0.2C and 0.5C (1 C = 270 mAh g^{-1}) under 25 °C. The rate performance was measured at the current density from 0.2C to 3.0C and then returning to 0.2C. The electrochemical impedance spectroscopy (EIS) analysis and cyclic voltammetry (CV) measurements were carried out by using a work station (Autolab PGSTAT100). Lithium diffusivity in the charge and discharge region was calculated from the data obtained from the galvanostatic intermittent titration technique (GITT).

4.3 Results and Discussion

4.3.1 Synthesis and characterization of PEDOT-PDMS

4.3.1.1 Chemical composition and structure

The digital photos of mixed solution composed of h_2PDMS and PEDOT are shown in Figure 4.2a. The solution before the reaction is nearly transparent. However, it changed to yellowish after reaction catalyzed by Karstedt catalyst at 60 °C, indicating that some reaction has taken place. A brown film forms after drying the reacted solution and it bends without fracture (see Figure 4.2b). However, the film will break when completely folded.

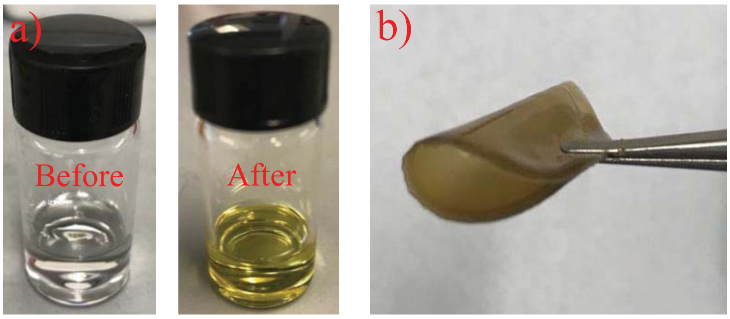

Figure 4.2 (a) The digital photos of mixed solution composed of h_2PDMS and EDOT before and after the reaction, and (b) the digital photo of PEDOT-PDMS film

The reported works have demonstrated that Si-O segments in PDMS can lead to an amorphous structure that offers a sufficient Li^+ ion mobile pathway (Kang et al., 2005; Lin et al., 2017). In addition, both more anion doping such as PF_6^- and electron-donating coupled to the thiophene ring can result in electron-conduction (Kvarnström et al., 1999; Kayser and Lipomi, 2019). Hence, in this study, the flexible and conducting polymer PEDOT-PDMS is expected to be synthesized through the hydrosilylation and dehydrocoupling reaction occurred between h_2PDMS and the EDOT monomer. The hydrosilylation reaction occurs between Si-H and C=C groups, and dehydrocoupling reaction occurs simultaneously between Si-H (C-H) and C-H in the presence of Karstedt catalyst (see Figure 4.3).

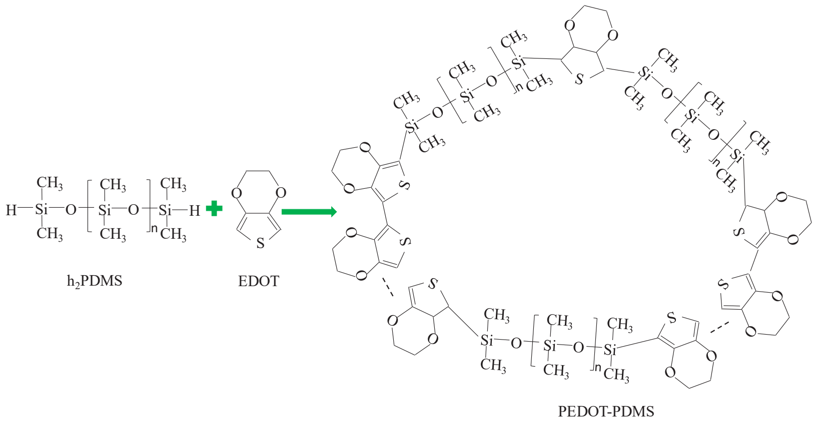

Figure 4.3 The schematic of the synthesis of the expected PEDOT-PDMS

In order to identify the reaction and the product after reacting between EDOT and h2PDMS, the NMR and FTIR are performed. The ^{1}H NMR spectra of EDOT, h2PDMS, and PEDOT-PDMS are shown in Figure 4.4. Signals 1(C=CH) and 2 (CH_2) are assigned to EDOT monomer (Wei et al., 2017). Signals 3 (Si-H) and 4 (CH_3) are assigned to h2PDMS (Risangud et al., 2015). The characteristic C=CH and Si-H signals are used to evaluate the reaction between EDOT and h2PDMS. After reaction, the C=CH signal disappears while CH_2 signal is unchanged. In addition, the Si-H signal disappears and CH_3 signal also is unchanged. A new signal 5 at around 1.55 ppm appears, which can be associated to the CH group. Hence, the PEDOT-PDMS product can be confirmed initially by using NMR.

In order to further evaluate the reaction and the product after reaction, FTIR spectra of h2PDMS and PEDOT-PDMS are measured as exhibited in Figure 4.5. The peaks around 2958 and 2900 cm^{-1} are due to stretching vibrations of CH_3 groups; the peaks at 1411 and 1260 cm^{-1} are related to deformation vibration and symmetrical vibrations of CH_3 groups; one peak at 793 cm^{-1} is due to the CH_3 rocking vibration and the Si-C stretching vibration; the peaks located at 1085 and 1030 cm^{-1} are response of the asasymmetric and symmetric stretching of Si-O-Si for PDMS, respectively (Zengin et al., 2019). Obviously, the characteristic Si-H group at 2131 and 908 cm^{-1} has disappeared, providing the evidence of the successful reaction between h2PDMS and EDOT (Klasner et al., 2009; Li et al., 2017). Some new peaks can be observed in FTIR spectroscopy of PEDOT-PDMS. The new peaks around 1470 and 2857 cm^{-1} are attributed to the C=C band and symmetric CH_2 stretching, respectively (Gordin et al., 2009; Chen et al., 2019). The characteristic of Si-C bond around 865 cm^{-1} overlaps with the CH_3 rocking vibration and the Si-C stretching vibration.

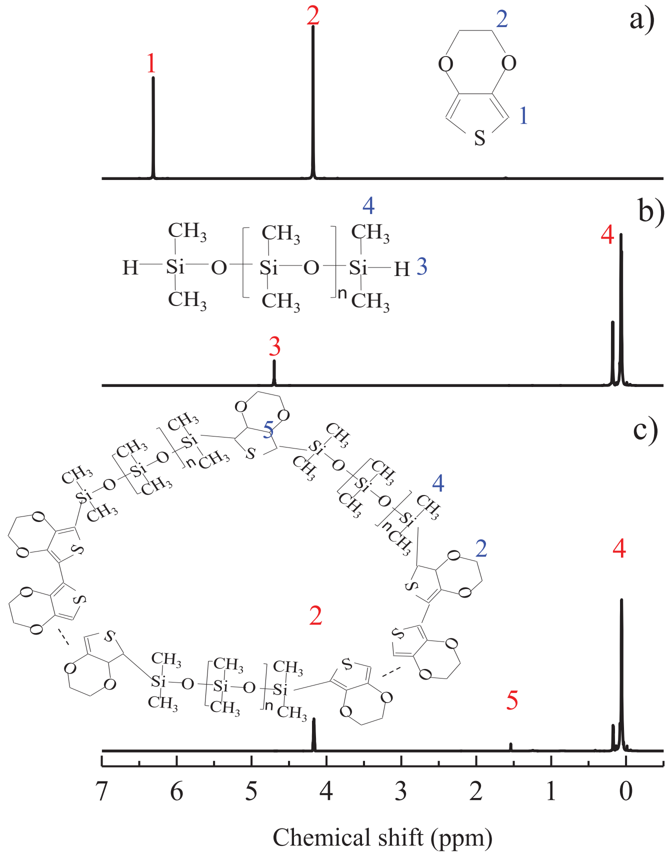

Figure 4.4 The ^{1}H NMR spectra of EDOT, h_2PDMS, and PEDOT-PDMS

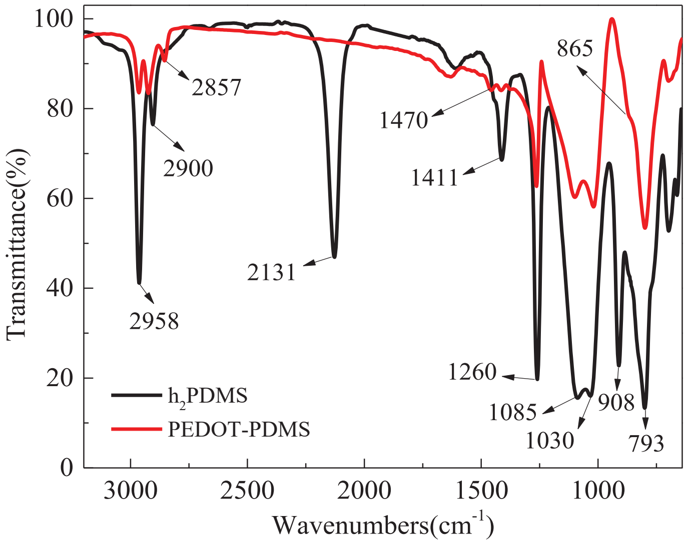

Figure 4.5 The FTIR of h_2PDMS and the expected PEDOT-PDMS

4.3.1.2 Mechanical properties

The mechanical properties of PEDOT-PDMS are investigated to test the flexibility. PEDOT-PDMS solution was cast on the Al sheet to obtain free-standing membranes according to Kayser's work (Kayser et al., 2018). Five samples are conducted and the typical stress-strain curve is shown in Figure 4.6. It can be seen that the film exhibits elastic and plastic behavior. The tensile stress and strain at rupture are 22.4±2.1% and 0.24±0.03 MPa. The Young's modulus (elastic modulus) is 1.17±0.10 MPa. Kayser and his work demonstrated that the PEDOT:PSS film shows brittle behavior with Young's modulus of 284 MPa and strain at rupture of 8.5% (Kayser et al., 2018). In addition, Noh demonstrated that the Young's modulus of PDMS sheet is 605 kPa (Noh, 2014). In comparison, the PEDOT-PDMSS film is more flexible than PEDOT:PSS film and more brittle than PDMS membrane.

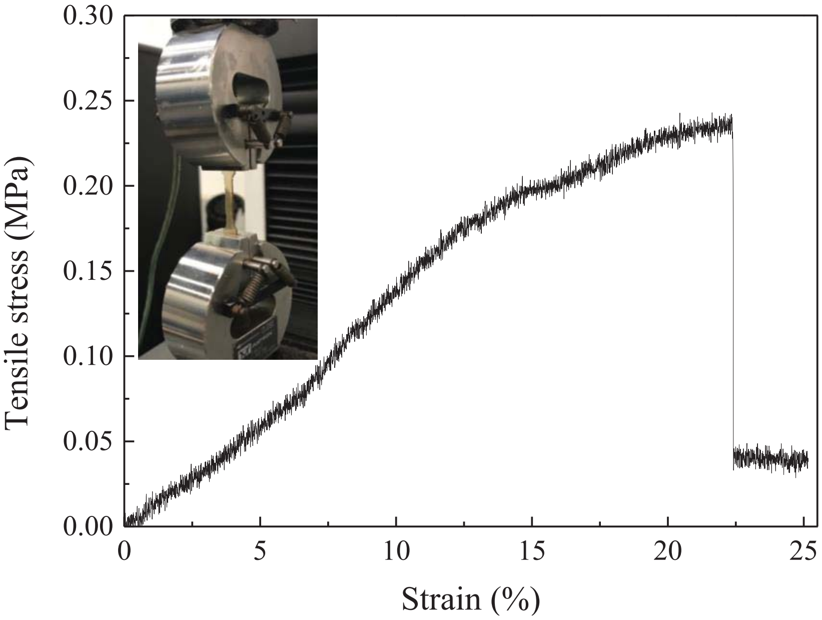

Figure 4.6 The stress-strain curve of PEDOT-PDMS film (picture taken during test)

Figure 4.7 depicts the XRD curve of PEDOT-PDMS membrane. It can be seen that no sharp peaks appear except two broad peaks. The broad peaks located in the regions of 8.5°-14.9° and 17.1°-26.2° are observed due to the amorphous nature in PEDOT-PDMS (Sharma et al., 2019). In general, the amorphous state is more ductile than crystalline (Lee and Gleason, 2015), and is able to accelerate the transference of Li-ions (Zhan et al., 2008).

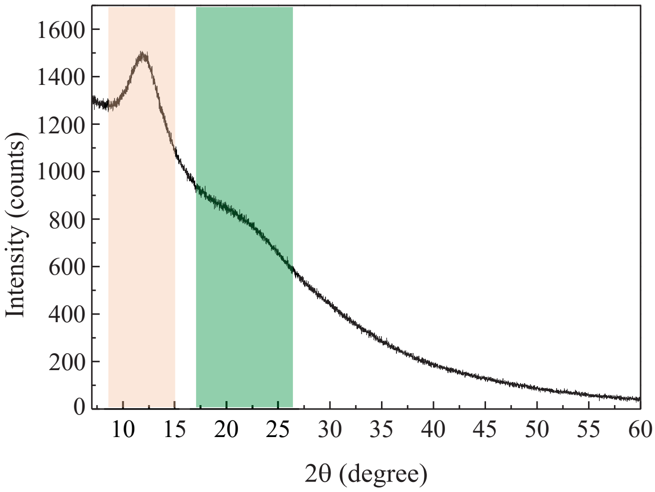

Figure 4.7 XRD pattern of PEDOT-PDMS film

4.3.1.3 Electrochemical properties

To evaluate the conducting property of the PEDOT-PDMS film, the EIS curves of the symmetrical cells are exhibited in Figure 4.8. The EIS of symmetrical cells assembled with stainless steel sheet as electrodes (Cell A) is shown in Figure. 4.8a. The EIS of symmetrical devices assembled with stainless steel sheet coated by PEDOT-PDMS film as electrodes (Cell B) is shown in Figure 4.8b. It should be noted that the first EIS was performed after fabricating cells for resting 2 min and the second cycle was performed after resting for 15 h. It can be observed from Figure 4.8a that the total resistance of bulk (R_b) and charge transfer (R_{ct}) for Cell A at the first cycle (4.0 Ω) is close to the total resistance at the second cycle (3.6 Ω) which can be obtained through the intersection of line and the X axis. However, for Cell B, the total resistance (R_b+R_{ct}) is about 85.9 Ω in the first cycle, which is much higher than that of Cell A due to the resistance of PEDOT-PDMS layer. However, it decreases to 69.1 Ω after the second cycle. The conductivity can be determined by Equation (4-1) (Lee et al., 2014):

$$\sigma = q\rho\mu \tag{4-1}$$

where q is the unit charge (1.6×10^{-19} C), ρ and μ are carrier concentration and mobility, respectively. The carrier concentration is directly related to the doping level. At first, there is no dopant in PEDOT-PDMS, and the dopants (PF_6^- and Li^+) in PEDOT-PDMS increase with cycles. Hence, the carrier concentration in PEDOT-PDMS increases with cycling, resulting in an increase in conductivity. In addition, the line in Figure 4.8b is not parallel to the Y-axis (minus imaginary Z). The obtained results indicate that the polymer (PEDOT-PDMS) could provide Li^+ transfer pathway through the amorphous phase and be able to conduct through the conjugated structure. Hence, it will be used to modify the $NaLiFePO_4F$ electrode.

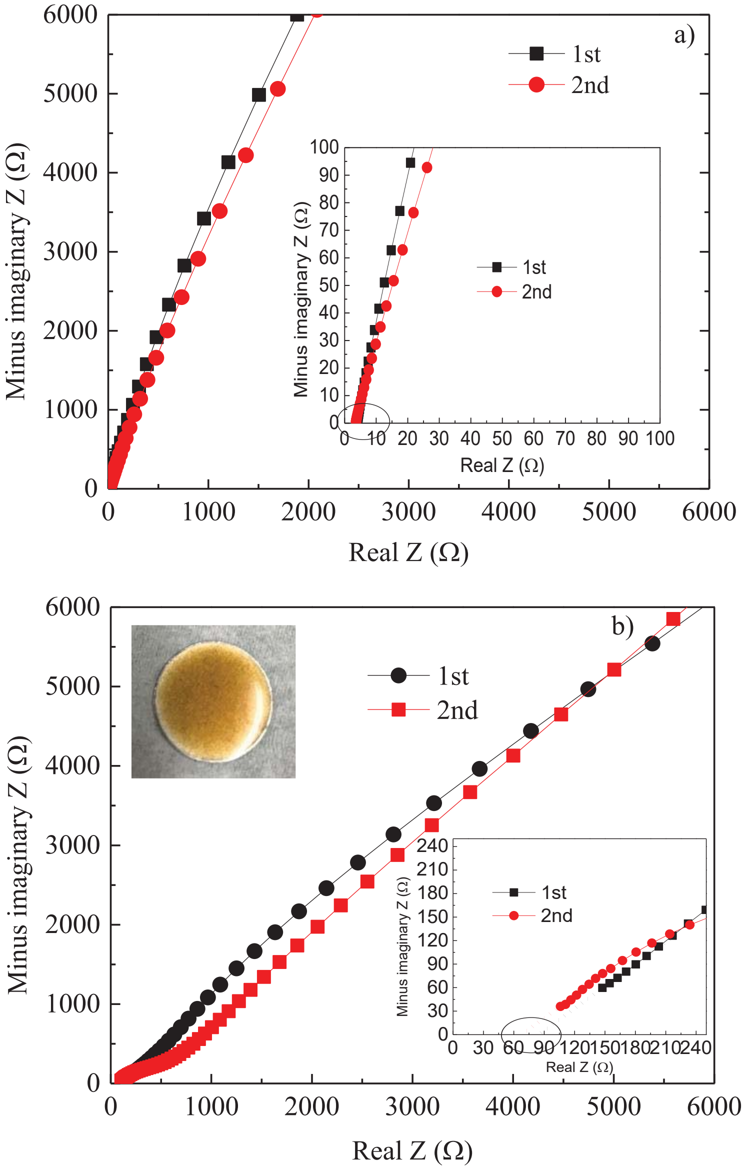

Figure 4.8 The EIS of (a) stainless steel electrode and (b) stainless steel coated by PEDOT-PDMS electrode (shown as inset) symmetrical cells between 1 and 2 cycles

The XPS of the PEDOT-PDMS and PEDOT-PDMS coated $NaLiFePO_4F$ electrode were collected to further examine the successful synthesis of PEDOT-PDMS. The result is exhibited in Figure 4.9. It can be observed from Figure 4.9 that for the PEDOT-PDMS sample (applying PEDOT-PDMS solution on the surface of Al foil) and PEDOT-PDMS coated $NaLiFePO_4F$ electrode, the representative spectra peaks of C1s, O1s, Si2s, Si2p, S2s and S2p are detected, and no other peaks appear such as representative spectra peaks of Na, Fe, P and F within the $NaLiFePO_4F$ electrode. The peak at 100.4 eV is attributed to the new Si-C bonds in PEDOT-PDMS. The XPS analysis results indicate the formation of the compact PEDOT-PDMS layer on the $NaLiFePO_4F$ electrode.

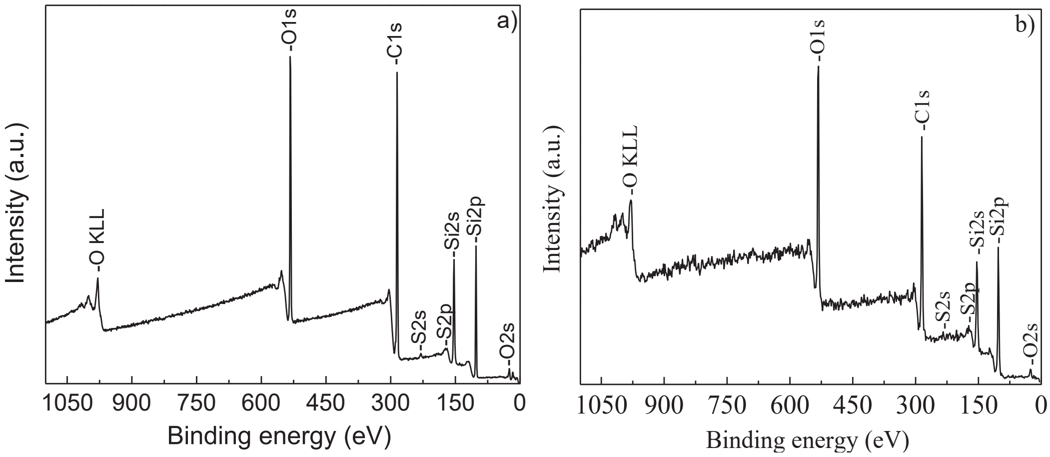

Figure 4.9 XPS of (a) PEDOT-PDMS and (b) $NaLiFePO_4F$ electrode@PEDOT-PDMS

4.3.2 Performance of the coated $NaLiFePO_4F$ electrode

4.3.2.1 Electrochemical performance

The coating can be directly observed from the SEM images between $NaLiFePO_4F$ control electrode (Figure 4.10a) and PEDOT-PDMS coated $NaLiFePO_4F$ electrode (Figure 4.10b). The thickness of PEDOT-PDMS layer and contact between PEDOT-PDMS and $NaLiFePO_4F$ electrode can be observed from cross-section image of the coated electrode (Figure 4.10c). Obviously, the surface of the coated electrode is smooth while it is rough for the bare electrode. The thickness of the coating is uneven because of the pothole of $NaLiFePO_4F$ electrode. This can be also observed from the cross-section image of the coated electrode. The section marked with the yellow line is $NaLiFePO_4F$ electrode and the red line section is PEDOT-PDMS layer. The good contact and compatibility between $NaLiFePO_4F$ and coating are observed.

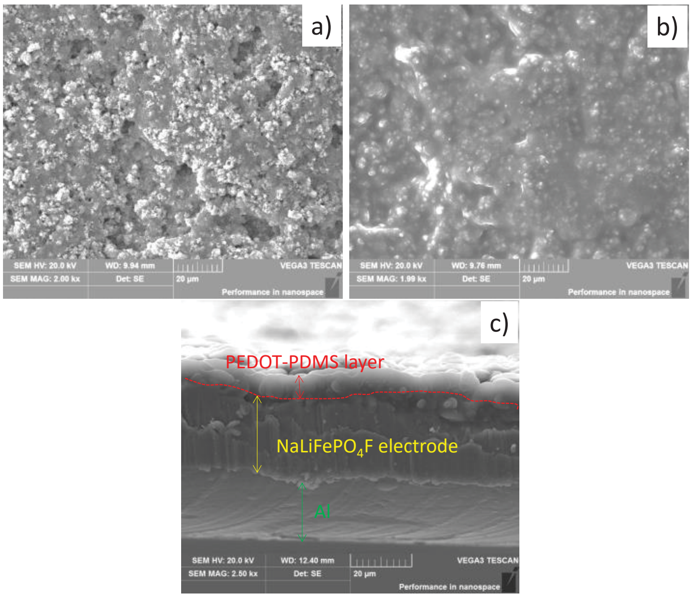

Figure 4.10 SEM of (a) NaLiFePO$_4$F control, and (b) NaLiFePO$_4$F electrode @PEDOT-PDMS and (c) its cross-section image

To characterize the electrochemical properties of PEDOT-PDMS coated NaLiFePO$_4$F electrode, the cells with Li foil as a reference electrode were examined in the voltage range of 2.0-4.5 V in a temperature-controlled room (22-25 °C), and NaLiFePO$_4$F electrode served as a control. In order to cover the NaLiFePO$_4$F electrode completely, the smallest thickness of PEDOT-PDMS layer could be 1 μm because the surface of NaLiFePO$_4$F electrode is rough. The thickness of polymer layer with 3, 5, and 6 μm also are designed. The specific capacitance of the batteries are obtained on the basis of the NaLiFePO$_4$F mass.

The PEDOT-PDMS coating can enhance the charge transfer at the interface of electrodes and liquid electrolyte, which can be confirmed by the EIS of NaLiFePO$_4$F electrode with different thickness of PEDOT-PDMS coating (Figure 4.11a and 4.11b). The charge transfer resistance (R_{ct}) for NaLiFePO$_4$F control, NaLiFePO$_4$F coated with coating of 1 and 3 μm are around 180, 163 and 140 Ω, respectively. In contrast, the NaLiFePO$_4$F coated by thick coating (5 and 6 μm) exhibit larger charge transfer resistance because the charge diffusion path in the coating during the electrochemical reaction is longer. Hence, it shows a lower initial capacity, a longer capacity increase, and poor cycle stability at 0.2 C, obtaining a capacity retention rate of only 82.1% after

200 cycles, as shown in Figure 4.11c. The large charge transfer resistance could lead to the polarization including the internal resistance drop and the concentration polarization, and then result in the poor charge/discharge efficiency and finally the loss of active material and capacity decay. Obviously, the specific capacities show an increasing trend for all the cells initially. This is because that the huge difference theoretical capacity of $NaLiFePO_4F$ (135 mAh g^{-1}) and Li_2FePO_4F (270 mAh g^{-1}) (Khasanova et al., 2012). During the charging and discharging process, the larger size Na^+ ions are gradually exchanged by smaller size Li^+ ions, forming new active material Li_2FePO_4F and therefore leading to an increase in theoretical capacity. Moreover, it is more difficult for the larger size Na^+ to be taken out from active material and through the PEDOT-PDMS layer, leading to a slow increase of capacity (Khasanova et al., 2012; Cui et al., 2016). Also, the thick coating could delay electrode activation, so it is longer for the cells fabricated with an electrode with the thick coating to reach a stable capacitance. It can also be observed from Figure 4.11c that an increase in specific capacity exhibits for the $NaLiFePO_4F$ electrodes coated by thickness of 1 and 3 μm. The discharge capacities of the $NaLiFePO_4F$ control, $NaLiFePO_4F$ coated with the coating of 1 μm and 3 μm are initially at 94.7, 102.3, and 115.5 mAh g^{-1}, respectively, but change to 91.5, 100.1, and 113.8 mAh g^{-1} after 200 cycles, corresponding to 96.6, 97.8, and 98.5% of the specific capacity retention, respectively. This indicates that the coating can protect $NaLiFePO_4F$, causing no loss of $NaLiFePO_4F$ and high capacity. Thus, the thickness of the PEDOT-PDMS layer plays a major role in improving the cycle performance of $NaLiFePO_4F$ electrode. A thickness of around 3 μm shows a relatively low charge transfer resistance.

On the other hand, in order to verify whether PEDOT-PDMS material contributes to the capacity of the whole battery, the batteries with bare PEDOT-PDMS electrode as cathode and a Li foil as the counter electrode were examined under the same conditions (the voltage of 2.0-4.5 V, at 0.2C). The bare PEDOT-PDMS electrode was prepared by applying the PEDOT-PDMS solution on the surface of Al foil directly without binder and super P. The electrode was obtained after drying at 90 °C in a oven under vacuum for 12 h. The cycle performance of the bare PEDOT-PDMS electrode is shown in Figure 4.12. The specific capacitance is very small but very stable even after 200 cycles, indicating a negligible contribution to capacity and stable chemical and electrochemical properties of PEDOT-PDMS material.

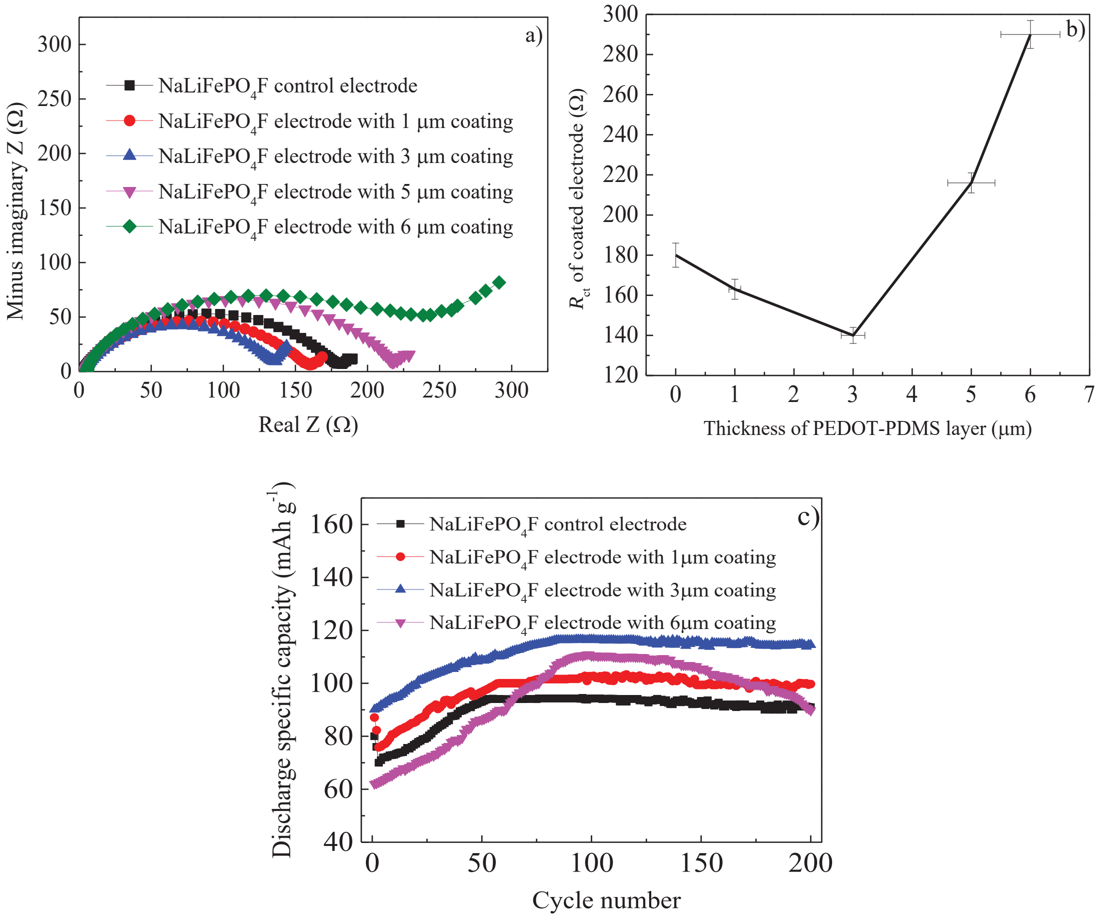

Figure 4.11 a) EIS, and b) R_{ct} and c) of Cycle performance and $NaLiFePO_4F$ electrode with different thickness PEDOT-PDMS coating

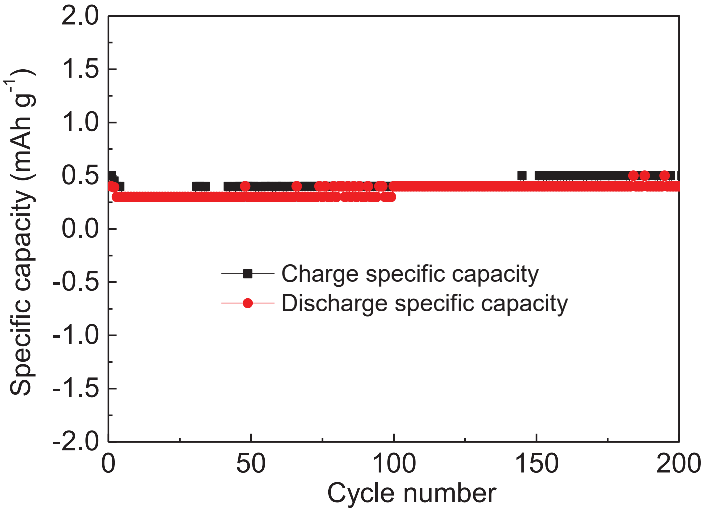

Figure 4.12 Cycle performance of the pure PEDOT-PDMS electrode

4.3.2.2 Cyclic Voltammetry analysis

The cyclic voltammetry (CV) plots of the $NaLiFePO_4F$ control and PEDOT-PDMS (3 μm) coated the $NaLiFePO_4F$ electrode in the potential region of 2.0-4.5 V (0.1 mV s^{-1}) are exhibited in Figure 4.13.

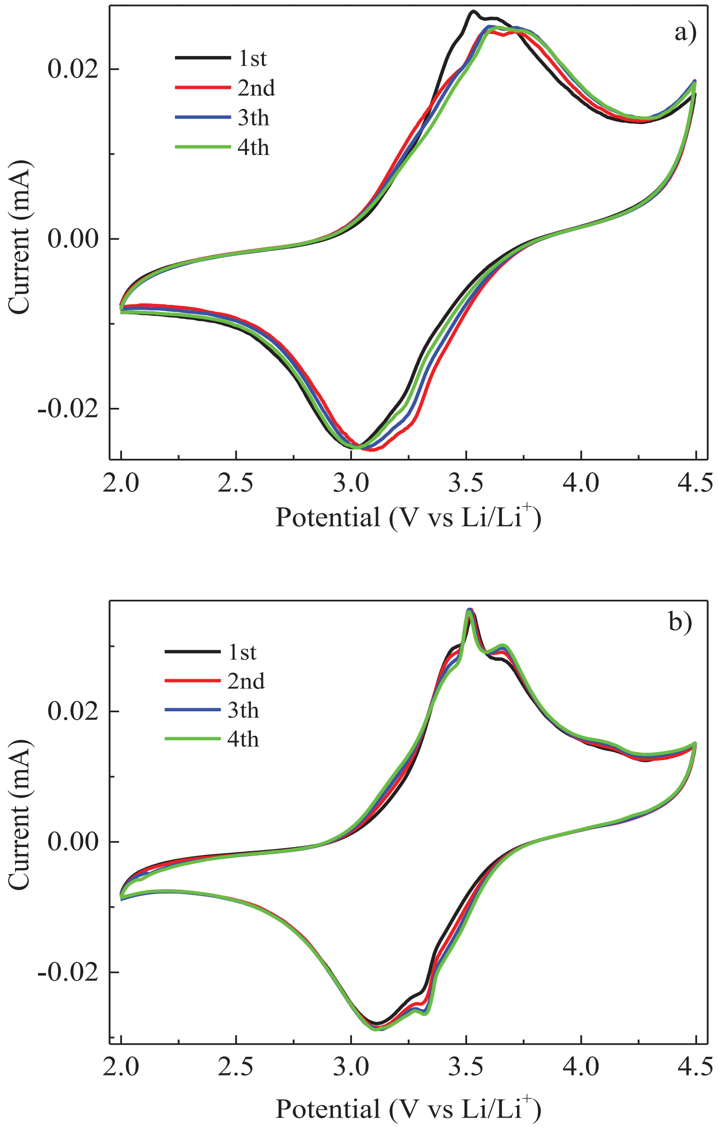

Figure 4.13 CV curves of (a) $NaLiFePO_4F$ control and (b) $NaLiFePO_4F$ electrode @PEDOT-PDMS

It can be seen from Figure 4.13 that for the $NaLiFePO_4F$ control electrode, an anodic peak at the potential of 3.53 V assigning to oxidation of Fe from Fe^{2+} to Fe^{3+} shifts to a high potential (~3.62 V) after the first cycle, which is related to the kinetic limitations of the electrode (Ahn et al., 2017). While for PEDOT-PDMS coated

$NaLiFePO_4F$ electrode, the oxidation of Fe from Fe^{2+} to Fe^{3+} anodic peak at 3.52 V at the first cycle gradually shifts to a smaller potential of 3.51 V after four cycles, indicating that the introduction of PEDOT-PDMS can cause a decrease in polarization effect and an improvement in electrochemical performance (Ma et al., 2014). Furthermore, it can be indicated from the CV curves that the redox peak currents of PEDOT-PDMS coated $NaLiFePO_4F$ electrode are higher than that of the $NaLiFePO_4F$ control electrode, indicating higher Li insertion capacity (Zhou et al., 2016). As a result, PEDOT-PDMS on the surface of the prepared $NaLiFePO_4F$ electrode is supposed to effectively facilitate the ions and electrons transport and finally enhance the reaction kinetics for the effective use of $NaLiFePO_4F$ active material, which will further be confirmed by using GITT measurement.

4.3.2.3 Cycling performance

Figure 4.14 exhibits the voltage profiles of the $NaLiFePO_4F$ control and PEDOT-PDMS coated $NaLiFePO_4F$ electrode, respectively. As shown in Figure 4.14, the initial charge and discharge capacitance of the control electrode is 76.3 and 52.2 mAh g^{-1}, respectively, and the initial coulombic efficiency is 68.4%. For the coated $NaLiFePO_4F$ electrode, the initial charge and discharge capacity is 81.7 and 66 mAh g^{-1}, and the corresponding initial coulombic efficiency is 80.8%. After the 500th cycle, the charge and discharge capacity of control electrode decrease to 59.5 and 59.2 mAh g^{-1}, while charge and discharge capacity of coated electrode increase to 88.1 and 87.3 mAh g^{-1}. In addition, compared with $NaLiFePO_4F$ control electrode, the coated electrode has a smaller polarization gap with cycling. The larger polarization of the $NaLiFePO_4F$ control electrode results from the limited Li-ion diffusion and charge migrate at the interface between electrode and electrolyte. The smaller gap of the coated electrode indicates the coated electrode shows better interfacial chemistry. The layer could enhance electron conductivity due to more PF_6^- doping with cycling (Novák et al., 1997; Kayser and Lipomi, 2019). The polarization is generated by their internal electrochemical reactions. The polarization is responsible for the cyclability of batteries.

The large polarization means large charge transfer resistance or internal resistance, which can lead to the poor charge/discharge efficiency and finally the loss of active material and capacity decay. One can also note that the control electrode shows low voltage in the initial cycle than that of the 250th and 500th, while the coated ones are reverse. The SEI can form for the $NaLiFePO_4F$ control electrode during charging and the inner resistance of the battery cannot be avoided. However, the capability of conducting of the coated electrode could be enhanced with cycling. The anodic peak shift in CV curves also confirms this. For the control electrode, the anodic peak shifts to a higher voltage with cycling, while it shifts to a lower voltage range with cycling for the coated electrode.

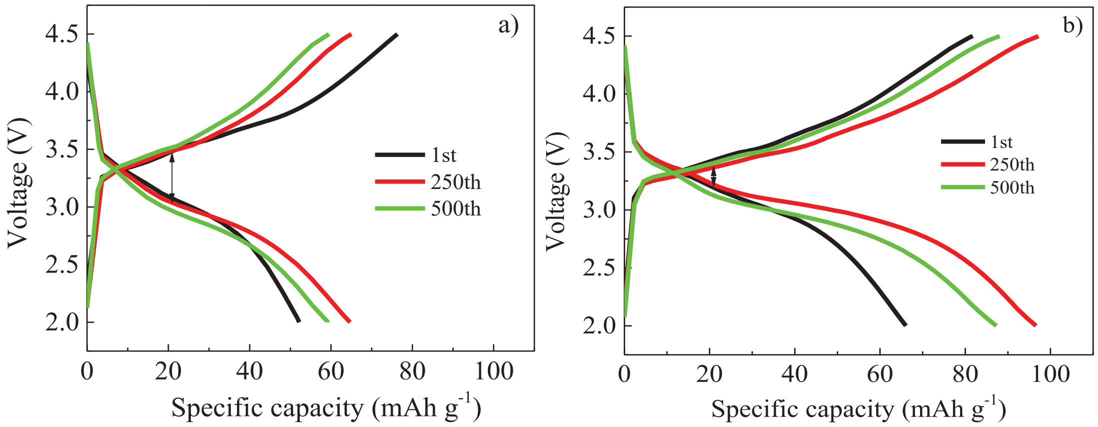

Figure 4.14 Charge-discharge curves of 1st, 250th and 500th of (a) $NaLiFePO_4F$ control and (b) $NaLiFePO_4F$ electrode @PEDOT-PDMS at 0.5C

The cycling performance of $NaLiFePO_4F$ control and PEDOT-PDMS coated $NaLiFePO_4F$ electrodes were compared after up to 500 cycles at 0.5 C as shown in Figures 4.15. Their capacities show increasing behavior with cycling in the initial cycles. The growth behavior for the control electrode is completed after 50 cycles, while this trend of PEDOT-PDMS coated $NaLiFePO_4F$ electrode lasts until around the 130th cycle, which is due to slow large-sized Na^+ and Li^+ exchange, and the gradual penetration of electrolyte into the coat. The penetration of electrolyte can provide a sufficient amount of anions such as PF_6^- for doping, and the full use of active material. Thus, compared to the control electrode the specific capacity of the coated electrode is higher all the time. The initial charge capacities of $NaLiFePO_4F$ control and PEDOT-

PDMS coated $NaLiFePO_4F$ electrodes are 76.3 and 81.7 mAh g^{-1}, respectively. The capacitances are 59.5 and 88.1 mAh g^{-1} after 500 cycles, showing 78%, 100% retention, respectively. This indicates that PEDOT-PDMS polymer layer could enhance the electrochemical stability of $NaLiFePO_4F$ electrodes, which has a close relationship with the enhancement of electron migrate at the interface of the electrolyte and electrode (Ahn et al., 2017). Besides, the polymer layer plays a major role in protecting $NaLiFePO_4F$ from HF attack during cycles as mentioned the performance of $NaLiFePO_4F$ coated cathode before cycling and after cycling, resulting in no loss of active material. The first coulombic efficiency for the coated electrode is 80.8% because of the consumption of a certain amount of lithium in SEI and the insertion of Li^+ into polymer in the first charge and discharge process (Chen et al., 2017). However, the value (80.8%) is much higher than that of the control electrode (68.4%) due to the coating protection leading to fewer side reactions.

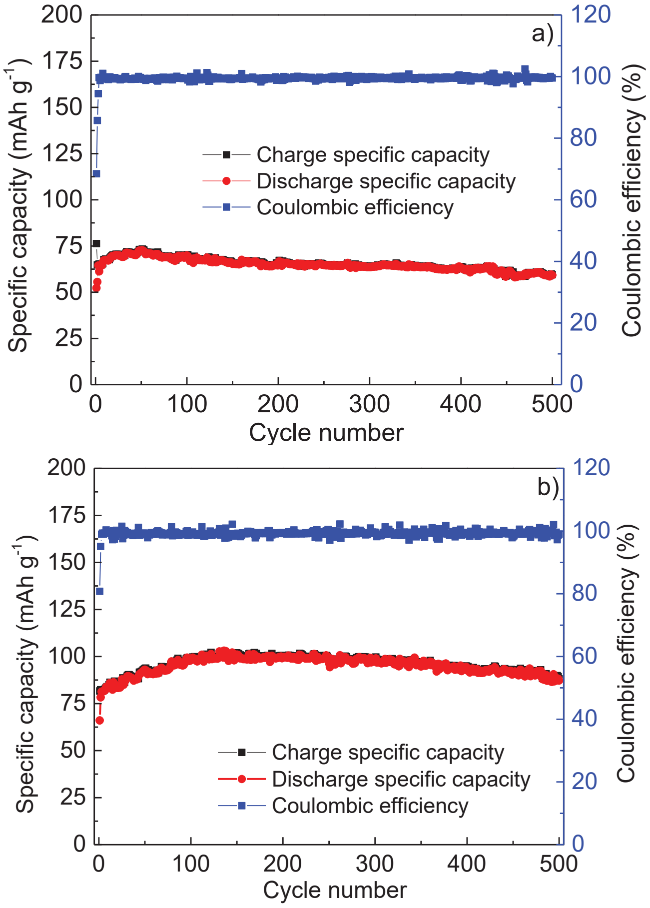

Figure 4.15 Cyclic performance of $NaLiFePO_4F$ control (a) and $NaLiFePO_4F$ electrode@PEDOT-PDMS electrodes (b) at 0.5C

4.3.2.4 Rate performance

The corresponding rate capability associated with high power applications of the control and PEDOT-PDMS coated $NaLiFePO_4F$ electrodes is shown in Figure 4.16. The batteries were activated during the first two cycles at 0.01C. The capacity of batteries fabricated with coated electrodes remains relatively high for C rates varying from 0.2 C to 3.0 C and then returning to 0.2 C. With the increase of the current density to 0.5 C, 1.0 C, 2.0 C and 3.0 C, the coated electrode achieves capacities of 84.9, 60.2, 42.3 and 24.7 mAh g^{-1}, respectively. Also, when the battery is discharged back to lower current densities again, i.e. 2.0 C, 1.0 C, 0.5C and 0.2 C, satisfactory reversible capacities are obtained, indicating the good stability at different current densities. The better rate performance of the coated electrodes suggests the assistance of PEDOT-PDMS in suppressing the loss of active material and improving electrical and ionic conductivity which will be further confirmed by the following EIS and GITT tests. Although the control electrode also delivers good stability at different current densities, the capacities are always relatively low. The capacity values of 64.3, 41.3, 28.7 and 19.6 mAh g^{-1} were obtained at 0.5 C, 1.0 C, 2.0 C, and 3.0 C.

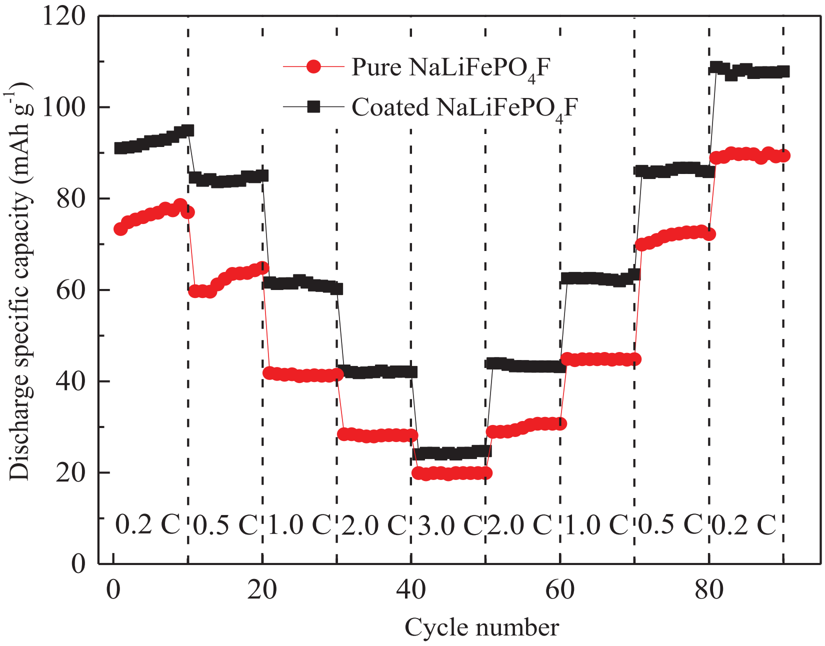

Figure 4.16 Rate performance for $NaLiFePO_4F$ control electrode and $NaLiFePO_4F$ electrode @PEDOT-PDMS in the potential range of 2.0-4.5 V

4.3.2.5 Structure characterization of the electrode

The SEM of the coated electrode before (left) and after (right) cycling 500 times are exhibited in Figure 4.17.

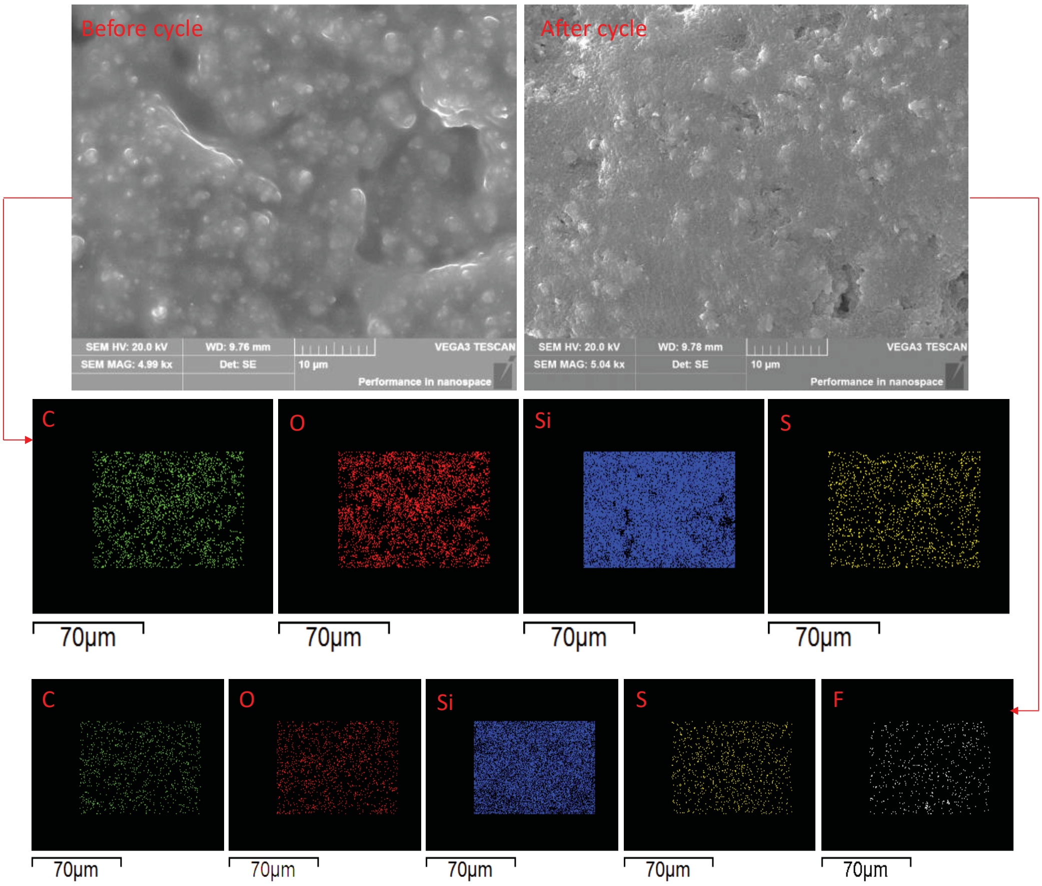

Figure 4.17 SEM images of NaLiFePO$_4$F electrode@PEDOT-PDMS cathode before cycling and after cycling with the elemental distribution mapping

It can be observed from Figure 4.17 that the PEDOT-PDMS layer shows excellent structural integrity and stability after cycling. This is because the conductive layer is stable without dissolution in the electrolyte. The surface of the PEDOT-PDMS layer becomes rough after cycling. Simultaneously, the surface elemental distribution of the coated electrode before and after cycling was evaluated by EDS mapping. In the case of the sample before cycling, the elements C, O, Si and S are distributed uniformly. Moreover, the presence of the elements in the EDS maps reveals that PEDOT-PDMS layer homogeneously formed on the surface of the NaLiFePO$_4$F electrode. As for the sample after cycling, elements C, O, Si and S also appear and the distribution still is uniform, further indicating that the PEDOT-PDMS layer remains well on the

$NaLiFePO_4F$ electrode surface after cycling. In addition, the element F is detected and no other elements such as P, Na, and Fe emerge, demonstrating that the F is derived from LiF of SEI composition instead of $LiPF_6$ electrolyte salt or $NaLiFePO_4F$ electrode. Moreover, it is known that the Na^+ ions can be replaced by Li^+ after cycling. However, there is no trace of Na in the polymer layer. The absence of Na in the maps of the coated electrode after cycling suggests the effective ion conductive performance of PEDOT-PDMS coating as Na^+ transfers through the polymer coating into the electrolyte. This observation is also supported by the XPS characterization of the coated electrode after cycling (see Figure 4.18). The elements C, O, Si, S and F appear on the surface of the coated electrode after cycling. As a result, PEDOT-PDMS could be a potential protective coating material for the electrode used in energy storage devices to improve cycle stability.

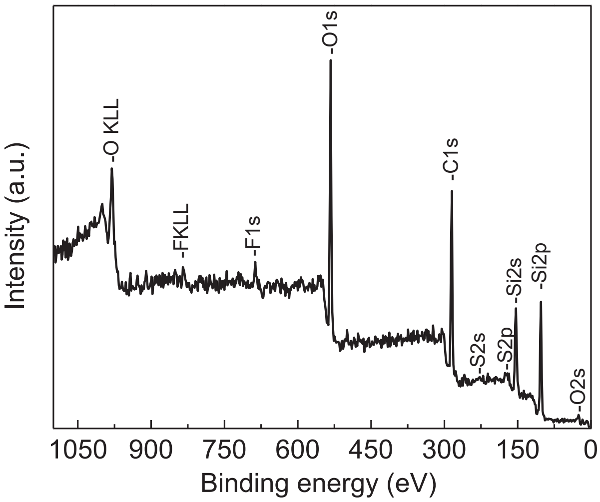

Figure 4.18 XPS of $NaLiFePO_4F$ electrode@PEDOT-PDMS after cycling

4.3.2.6 EIS analysis

The EIS test is a powerful technique for understanding the interfacial effect for surface modification (Ahn et al., 2017). To further evaluate the effect of PEDOT-PDMS on the property of $NaLiFePO_4F$, the EIS analysis of $NaLiFePO_4F$ control and coated electrodes were conducted before and after 500 cycles, with results exhibited in Figure 4.19. As shown in Figure 4.19, these two electrodes exhibit a high-frequency semicircle assigned to the charge transfer resistance (R_{ct}) and a low-frequency sloping line associated with lithium-ion diffusion. The resistance is related to the activation polarization that occurs in the electrode-electrolyte charge transfer (Heubner et al., 2016). It can be obtained from Figure 4.19 that coated $NaLiFePO_4F$ electrode has smaller R_{ct} for pristine and after 500 cycles (140 Ω and 380 Ω) than those of the control electrode (180 Ω and 590 Ω). The smaller increase in R_{ct} for the coated $NaLiFePO_4F$ electrode indicates the significant improvement in the interfacial kinetics resulted from the improved conductivity, resulting in better rate property in Figure 4.16 and smaller polarization gap in Figure 4.14.

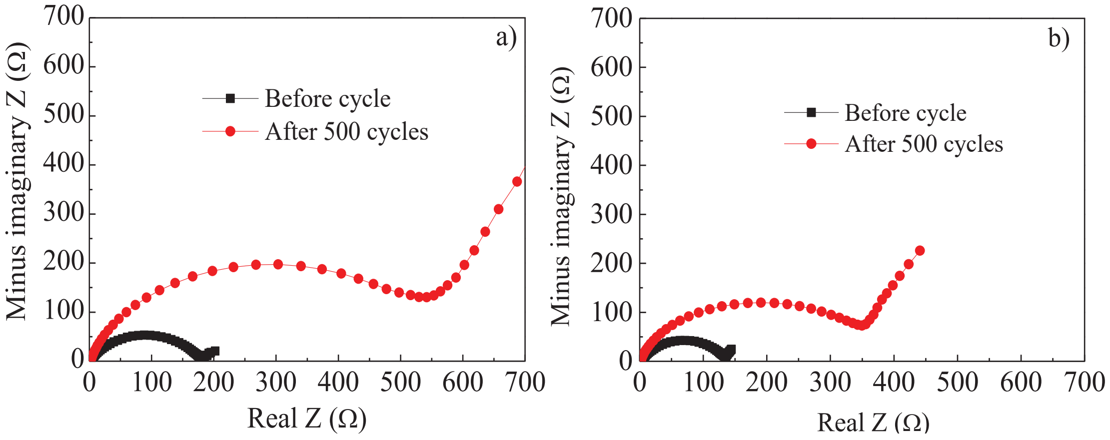

Figure 4.19 EIS of (a) $NaLiFePO_4F$ control electrode and (b) $NaLiFePO_4F$ electrode @PEDOT-PDMS

4.3.2.7 GITT analysis for chemical diffusion

The GITT is a credible approach to evaluate chemical diffusion coefficient of lithium-ion (D_{Li^+}) during cycling (Liu et al., 2014; Cui et al., 2016). It was employed to determine the D_{Li^+} of $NaLiFePO_4F$ control electrode and the PEDOT-PDMS coated $NaLiFePO_4F$ electrode. The corresponding GITT curves collected during the charge-discharge process are shown in Figure 4.20. The value of D_{Li^+} can be obtained according to the following equation (Ahn et al., 2017; Zhou et al., 2017)

$$D_{Li^+} = \frac{4L^2}{\pi\tau}\left(\frac{\Delta E_s}{\Delta E_\tau}\right)^2 \tag{4-2}$$

where L (cm) and τ(s) are the electrode thickness (2.5×10^{-3} cm) and the time (600 s) of the current pulse, respectively, and ΔE_τ and ΔE_s are the voltage change during the current pulse and rest. During the charging state, the diffusion coefficients of $NaLiFePO_4F$ control and coated electrodes are about 7.17×10^{-10} and 1.20×10^{-9} cm^2 s^{-1}; during discharging state, they are about 5.29×10^{-10} and 1.89×10^{-9} cm^2 s^{-1}. A higher diffusion coefficient, and smaller over-potential and the voltage drop of the PEDOT-PDMS coated $NaLiFePO_4F$ electrode (Figure 4.20b) and d)) indicates that the PEDOT-PDMS coating layer can improve the conductivity of the $NaLiFePO_4F$ electrode (Zhou et al., 2017).

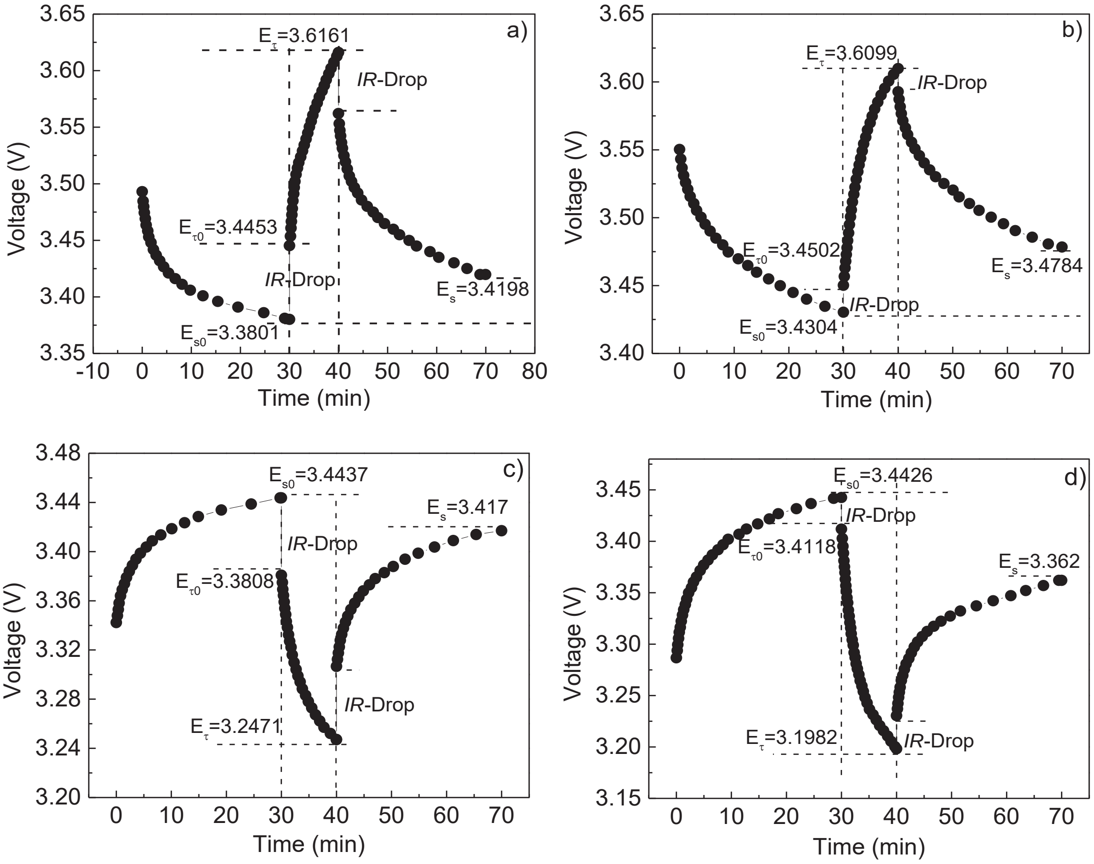

Figure 4.20 GITT curves of $NaLiFePO_4F$ control electrode and $NaLiFePO_4F$ electrode @PEDOT-PDMS (a, b) in the charge and (c, d) in the discharge region

4.4 Summary

This chapter gives the synthesis and characterizations of the new polymer (PEDOT-PDMS), and applications in modifications of electrodes materials ($NaLiFePO_4F$) used in Li-ion batteries. The obtained results are as follows:

(1) The expected conducting-flexible polymer PEDOT-PDMS can be successfully synthesized between h_2PDMS and EDOT monomer.

(2) The tensile stress and strain of the PEDOT-PDMS film at rupture are 22.4 ± 2.1% and 0.24 ± 0.03 MPa. The Young's modulus (elastic modulus) is 1.17 ± 0.10 MPa. The polymer shows the amorphous nature which provides Li^+ transfer pathway. It also could conduct through the conjugated structure.

(3) The PEDOT-PDMS coated $NaLiFePO_4F$ electrode showed high specific capacity (88.1 mAh g^{-1} after cycling 500 times at 0.5C), good cycle stability (~100% of capacity retention after cycling 500 times) and high chemical diffusion coefficient of lithium-ions (1.89×10^{-9} and 1.20×10^{-9} cm^2 s^{-1} during charging and discharging) compared to $NaLiFePO_4F$ control electrode (59.5 mAh g^{-1} after 500 cycles at 0.5C; ~78% of capacity retention after 500 cycles; 7.17×10^{-10} and 5.29×10^{-10} cm^2 s^{-1} during charging and discharging) because of three reasons. One is that the polymer coating could provide Li^+ transfer pathway at the interface between the electrode and electrolyte. Another reason is that the electron conductivity could be enhanced owing to more PF_6^- doping with cycling. The third one is that the polymer layer protects $NaLiFePO_4F$, resulting in optimal use of $NaLiFePO_4F$ active material.

(4) The coated $NaLiFePO_4F$ electrode may be a promising cathode candidate for good-performance Li-ion batteries, and the novel polymer PEDOT-PDMS could be a potential material for the electrode protection for other materials also.

Chapter 5 Conductive and Flexible Coating of Si Nanoparticles as Anode of Li-Ion Batteries

5.1 Introduction

The flexibility performance of the PEDOT-PDMS polymer cannot be fully reflected when it is used as a coating material for $NaLiFePO_4F$ electrode as reported in Chapter 4. The volume change during charging and discharging in that process is relatively small. Hence, the polymer will further be used in the modification of other electrode materials which have huge volume change during cycling.

Silicon anode material has been widely considered as one promising candidate for high-capacitance Li-ion batteries owe to its abundance in the crust (28% by weight) (Liu et al., 2012) and high specific capacitance, 4200 mAh g^{-1} based on Si mass, forming $Li_{4.4}Si$ in full lithiation state. This specific capacity is over ten times larger than that of currently commercialized graphite anode (372 mAh g^{-1}, LiC_6) (Jia et al., 2018). However, its huge volume change (300-400%) during the charge-discharge process still hinders its practical applications (Ma et al., 2015). The defect can lead to undesired cracking of electrode, loss of electric contact between Si, binder, conducting agent (super P) and current collector (Cu foil), and finally, fast fading of the capacity of batteries. Additionally, the low lithium diffusivity and conductivity of silicon also limit its electrochemical property (Chen et al., 2015).

From the previous chapter, it is also noted that the synthesized polymer PEDOT-PDMS can improve the conductivity and lithium ions diffusion of $NaLiFePO_4F$ electrode. Hence, in this Chapter, silicon nanoparticles (SiNP) will be coated by the PEDOT-PDMS polymer as a protective coating layer to improve the cycling stability of Si. The composite material is thus denoted as SiNP@PEDOT-PDMS.

5.2 Experimental Section

This research mainly focused on preparing and characterizing of SiNP@PEDOT-PDMS material and assembling and measurement of half-cell with SiNP@PEDOT-PDMS as the anode.

5.2.1 Materials

Silicon nanoparticle (99.9%, metals basis, 20-60 nm) were purchased from Aladdin. Other materials follows that introduced in Section 4.2.1 in the previous chapter.

5.2.2 Preparation of SiNP@PEDOT-PDMS and its characterization

Firstly, h_2PDMS (410 μL) and EDOT (80 μL) were dissolved in toluene with stirring. Afterwards, 0.08 g Si nanoparticle material was dispersed in the mixed solution by stirring and sonication. Then, 10 μL Karstedt catalyst solution was added into a round-bottom flask under the Ar atmosphere, and the flask was removed to air atmosphere after sealing and fixed in the oil bath. Thirdly, the EDOT, h_2PDMS and Si mixture was added into the round-bottom flask by using an injector (10 mL). The solution was stirred for 4 h with a magnetic stirrer at 60 °C maintained in an oil bath. The resulting solution was placed on a reduced pressure (i.e., the flask connecting to a vacuum pump) to remove the unreacted monomer. Finally, SiNP@PEDOT-PDMS material was obtained by heating at 100 °C for 12 h in a vacuum oven.

X-ray diffraction (Smartlab 90kw, Rigaku) was applied to evaluate the structural characteristics of Si nanoparticles before and after coating. FTIR (Nicolet 380) and XPS (PHI 5000 Versa Probe) were carried out to evaluate the formation of PEDOT-PDMS in the same manner as that reported in Chapter 4. Transmission electron microscopy (TEM, Jeol JEM-2100F) was employed to examine the microstructure to directly evaluate the presence of PEDOT-PDMS on the surface of Si nanoparticles. The SEM was applied to evaluate the morphology of the electrode after 10 cycles. Briefly, the cell is disassembled in glove box, and the electrode is washed by using EC solvent. After a while, preparing the sample for SEM in glove box. At last, the prepared sample is quickly transferred in the machine for spraying gold and then quickly put in the SEM vacuum chamber.

The in-situ electrochemical experiment is conducted on FEI STEM holder with aberration corrected Titan. The pure Si or the coated Si particles are dispersed on a gold rod of 3 μm in diameter and 1 cm in length as one electrode. At the same time, the tungsten wire with Li is served as the counter electrode, having the same size to gold rod. The two electrodes are assembled on the holder with 10-20 μm apart with the help of an optical microscope inside the glove box, after that the holder is quickly (1-2 s) transferred to the TEM column vacuumed by the pump automatically. Hence, the lithiation process happens when the LiO/Li electrode is driven to contact with Si or coated Si electrode with the help of an electrostat in the in-situ system which only supplies constant voltage, in this study supplying 2 V voltage.

5.2.3 Electrode preparation, cell assemble and battery testing

For SiNP@PEDOT-PDMS working electrode, 65 wt% (0.065g) SiNP@ PEDOT-PDMS, 15 wt% (0.015 g) sodium alginate as a binder, and 20 wt% (0.02 g) super P were fully mixed with water (600 μL) in the mortar. The resulting homogeneous slurry was cast onto Cu foil (9 μm) by using a scraper (BEVS, 1806B/100) and the loading density of the electrode material was between 0.3-0.4 mg cm^{-2}. Finally, the Cu foil with slurry was dried at 90 °C overnight in a vacuum oven. For comparison, the electrode was prepared using Si without coating with the same mass to that of the SiNP@PEDOT-PDMS electrode. Furthermore, to confirm the contribution of PEDOT-PDMS to the capacity of the whole electrode, the pure PEDOT-PDMS electrode without sodium alginate and super P was prepared by applying polymer solution on Cu foil and heating at 90 °C overnight under vacuum. The electrolyte employed was 80 μL of 1.0 M $LiPF_6$ in 89 vol% EC/DEC (1:1 w/w) with 10 vol% FEC and 1 vol% VC. 2032 cells were assembled inside the same glovebox to the one talked in Chapter 4. Li metal foil was always used as the counter electrode.

Galvanostatic charging and discharging cycles were measured by using a LAND battery testing system (CT2001A) in a potential range of 1.0-0.01 V at 0.02 C at the initial cycle, 0.05 C at the second, and 0.5 C for the later cycles. (1 C = 4200 mAh g^{-1}). EIS and CV were conducted by using an electrochemical work station (Autolab PGSTAT100). Lithium diffusivity was obtained using the GITT.

5.3 Results and Discussion

5.3.1 Material characterization

In order to confirm that the PEDOT-PDMS has been successfully formed a layer on the surface of Si nanoparticles, FTIR and TEM measurements are performed for raw Si and coated Si nanoparticles. Figure 5.1 depicts the FTIR spectroscopies of the raw Si nanoparticle, PEDOT-PDMS, and SiNP@PEDOT-PDMS. It can be observed that the pattern of SiNP@PEDOT-PDMS is similar to that of PEDOT-PDMS polymer but different from that of raw Si. Comparing with the FTIR pattern of PEDOT-PDMS, there are no new peaks in SiNP@PEDOT-PDMS sample. The interaction between PEDOT-PDMS and Si is based on the hydrogen bonding interaction, i.e., between Si-OH owe to the SiO_2 on the surface of Si particles and polymer molecules (Hu et al., 2018; Jiang et al., 2020). One peak at 793 cm^{-1} is due to CH_3 rocking vibration and the Si-C stretching vibration. The peak around 1470 cm^{-1} is attributed to the new C=C band in PEDOT-PDMS (Chen et al., 2019). The peaks at 1411 and 1260 cm^{-1} are assigned as deformation vibration and symmetrical vibrations of CH_3 groups; the peaks at 1085 and 1030 cm^{-1} are due to asymmetric and symmetric stretching of Si-O-Si, respectively (Zengin et al., 2019). Additionally, the characteristic peak of Si-H group within h_2PDMS at 2131 cm^{-1} disappears, illustrating the successful synthesis of PEDOT-PDMS coating on the surface of Si nanoparticles (Klasner et al., 2009). The peak around 695 cm^{-1} is related to in-plane deformation of C-S-C (Kvarnström et al., 1999)

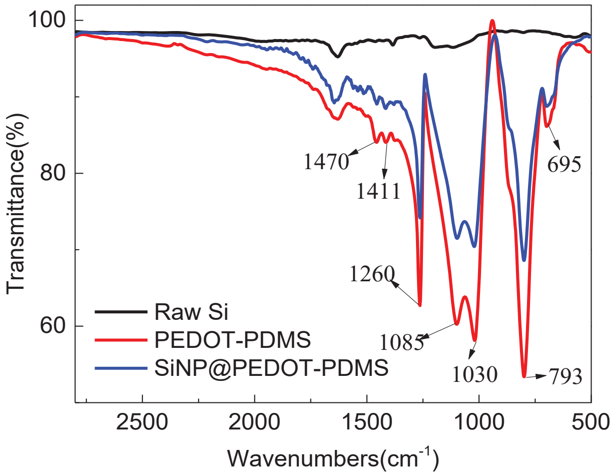

Figure 5.1 FTIR spectroscopy of raw Si, PEDOT-PDMS and SiNP@PEDOT-PDMS

TEM demonstrates the formation of the polymer coat on the surface of Si as shown in Figure 5.2. Compared with raw Si nanoparticle (Figure 5.2a), a foam-like network (arrows with yellow) formed on the surface of Si after coating by PEDOT-PDMS (Figure 5.2b), which cannot be detected in Figure 5.2a. This indicates the presence of the coat on the surface of Si, and the intimate connection between the polymer matrix and Si nanoparticles. The thickness of the coat is 3-10 nm. The insets in Figures 5.2a and 5.2b exhibit the selected area electron diffraction (SAED) images of the samples. The SAED of pure Si nanoparticles shows the Si (311), Si (220), and Si (111) planes, indicating the dominant presence of crystalline Si phase (Park et al., 2009; Liu et al., 2012). However, the SAED image of the coated Si nanoparticles displays diffuse scattering, demonstrating that the presence of coat on the surface of Si and that the coating material is amorphous (Wu et al., 2012), which is similar to that of Si coated by carbon (Tian et al., 2015).

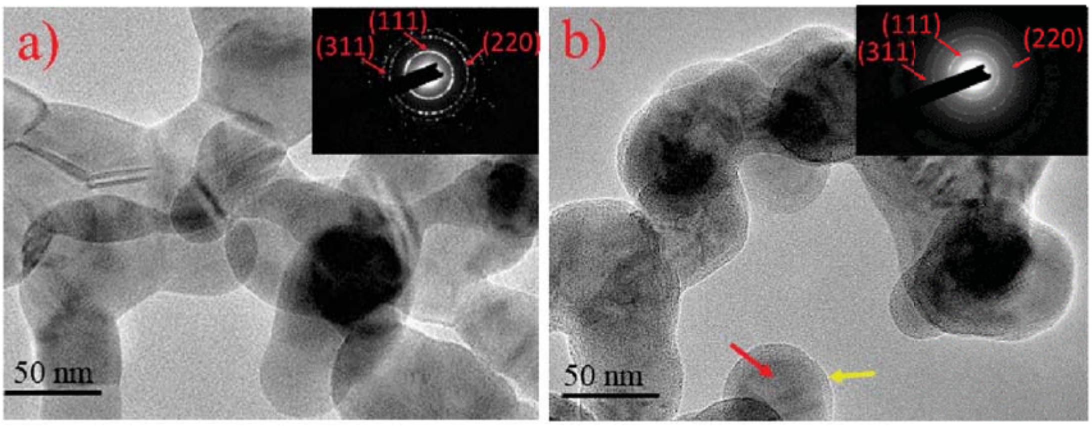

Figure 5.2 TEM and SAED images (inset) of (a) raw Si nanoparticle and (b) SiNP@PEDOT-PDMS

The crystalline structure of raw Si nanoparticles and coated Si nanoparticles is characterized by using XRD (see Figure 5.3). It can be observed from the pattern of plain Si that six obvious peaks located at 2θ of 28.4, 47.3, 56.1, 69.1, 76.3, and 88, which is indexed as the (111), (220), (311), (400), (331), and (422) crystal faces (Bridel et al., 2010; Wang et al., 2019). Moreover, no impurity peaks in the XRD patterns of SiNP@PEDOT-PDMS are detected, illustrating that PEDOT-PDMS has no effect on the crystalline structure of Si.

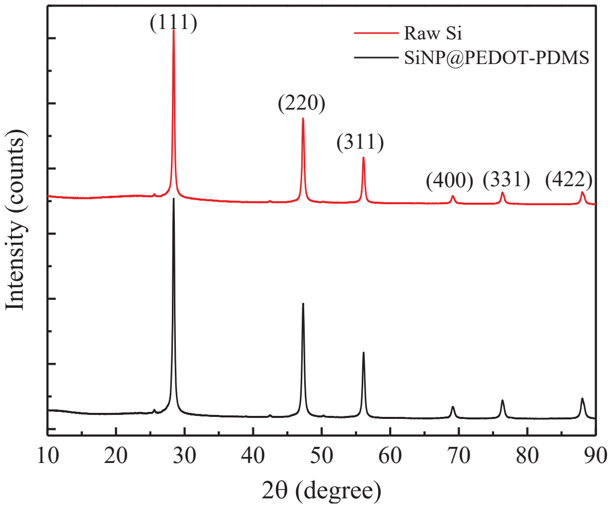

Figure 5.3 XRD of raw Si nanoparticle and SiNP@PEDOT-PDMS

5.3.2 Performance of SiNP@PEDOT-PDMS

5.3.2.1 Cyclic Voltammetry analysis

To study the electrochemical performances of SiNP@PEDOT-PDMS, as shown in Figure 5.4a, the CV was carried out (0.1 mV s^{-1}). The cycle performance of PEDOT-PDMS electrode is shown in Figure 5.4b. The potential range is between 0.01 V and 1.0 V versus Li/Li^+. It can be observed from Figure 5.4a that the CV plots of SiNP and SiNP@PEDOT-PDMS electrode show typical electrochemical behaviors, i.e., the typical lithiation and delithiation peaks, which are similar to that of graphene caged silicon nanoparticles electrode (Han et al., 2019). The SiNP@PEDOT-PDMS electrode shows a larger area of the current vs. voltage curve than that of SiNP electrode, implying a larger specific capacity of SiNP@PEDOT-PDMS electrode. The reduction peak located at 0.2 V corresponds to the transition of Si to the Li_xSi, and the oxidation peaks at 0.34 V and 0.53 V are associated to a two-phase reaction, i.e., the conversion of amorphous (α) α-Li_xSi to the α-Si (Wu et al., 2013; Han et al., 2019). The coated electrode has higher current than that of the bare electrode, implying that the coated electrode has higher capacity. Moreover, to evaluate the contribution of PEDOT-PDMS to the specific capacity of the whole batteries, the CV and electrochemical cycling performance of pure PEDOT-PDMS electrode without binder and super P was performed on half cells. The CV curve of PEDOT-PDMS electrode shows a much lower current than that of SiNP@PEDOT-PDMS, even if it is magnified five times. Moreover, the current is very stable and does not show any fluctuation. The results indicate that the contribution of PEDOT-PDMS to the capacity of the whole electrode is negligible, which also can be further supported through the cycle performance of PEDOT-PDMS electrode as shown in Figure 5.4b. The specific capacity is between 1 and 2 mAh g^{-1}, therefore it is negligible compared with that of silicon. In addition, it can also be seen that the capacity is very stable even after 1000 cycles, indicating good electrochemical stability of PEDOT-PDMS polymer during cycling.

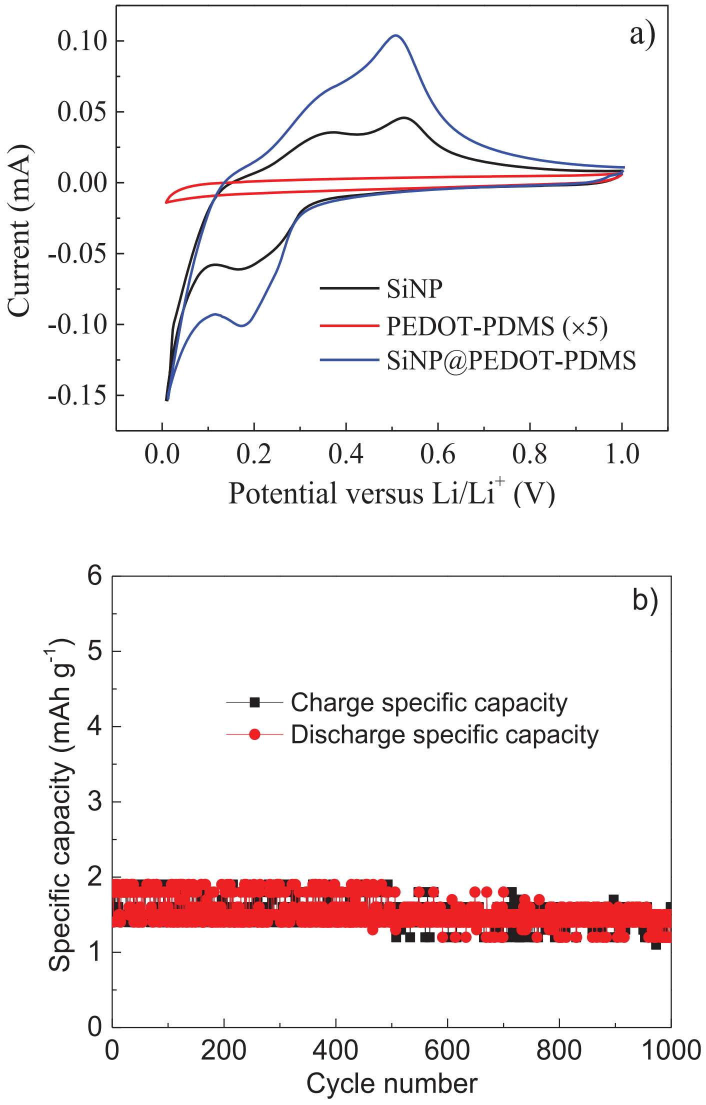

Figure 5.4 (a) CV curves of SiNP electrode, SiNP@PEDOT-PDMS and PEDOT-PDMS electrode, (b) cycle performance of pure PEDOT-PDMS electrode

5.3.2.2 Cycling performance

Figure 5.5a) displays the coulombic efficiency for both the Si nanoparticles control electrode and SiNP@PEDOT-PDMS electrode with active material mass loading between 0.3-0.4 mg cm^{-2}. The initial coulombic efficiency can indicate the stability of the SEI due to Li consumption during rupturing and reforming SEI (Liu et al., 2012). For SiNP@PEDOT-PDMS electrode, the corresponding initial coulombic efficiency is 77.44% which is higher than that of Si control electrode (~67.74%) as shown in Figures 5.5b) and 5.5c), owing to few side reaction. The coulombic efficiency of the coated electrode from the 3rd cycle increases to 99.24%, which is faster than that of the Si control electrode (increase to 98.57% after 6 cycles), indicating the quick formation of the stable SEI outside of coated electrode. However, for the coated electrode, the initial coulombic efficiency is still low due to the stable SEI built on the outside of the PEDOT-PDMS layer and the insertion of Li$^+$ into PEDOT-PDMS, consuming a certain amount of the lithium.

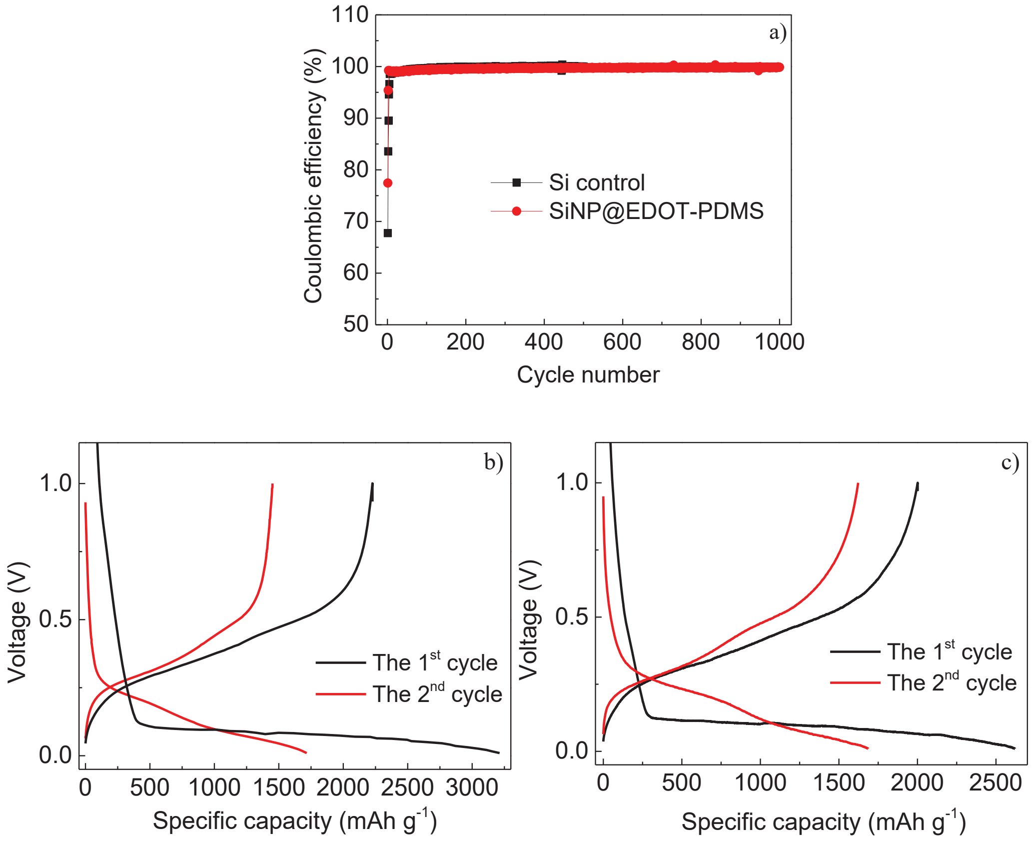

Figure 5.5 (a) Coulombic efficiency, and the 1st and 2nd charge-discharge curves of (b) Si control electrode and (c) SiNP@PEDOT-PDMS electrode at 0.5 C

As for the cycling performance, shown in Figure 5.6, the Si coated electrode shows an increase in the capacity during the initial cycles, while this behavior cannot be observed for the raw Si control electrode, which is due to the delayed wetting of electrolyte into the coated Si electrode. The cells fabricated with PANI coating on the Si particles anode exhibited similar capacity behavior during cycling (Wu et al., 2013). It also can be seen that the Si control electrode delivers a dramatic decay in charge specific capacity at 0.5 C, losing over 70% of its first specific capacitance after 500 cycles (~605 mAh g^{-1}). In comparison, the coated Si electrode shows good cyclic stability at 0.5C. A charge specific capacitance of ~1512 mAh g^{-1} is still there after cycling 1000 times, corresponding to ~69.8% capacity retention according to the highest specific capacity around the160th cycle (~2166 mAh g^{-1}).

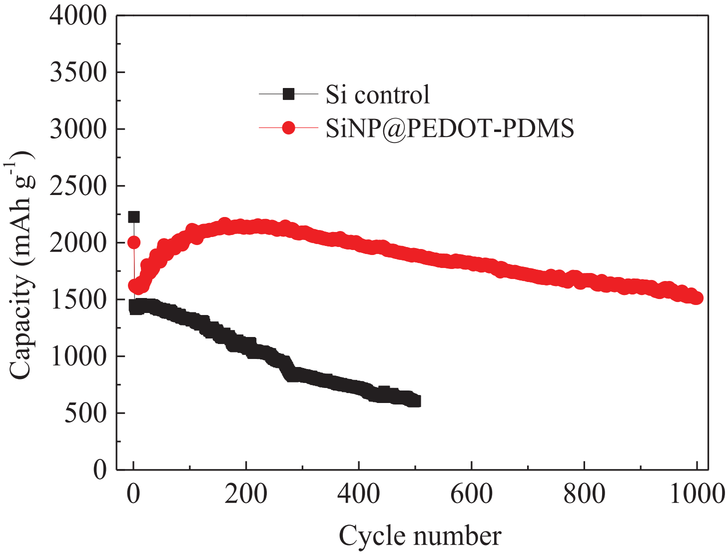

Figure 5.6 Cycle performance of Si control electrode and SiNP@PEDOT-PDMS electrode at 0.5 C

The obtained results are comparable to the results of previously reported Si particle-based anode works as listed in Table 5.1. This can ascribe to the PEDOT-PDMS polymer skin that could buffer the huge volume change of Si anode owing to the flexible PDMS matrix, leading to the formation of a more stable SEI in cycling. On the other hand, the continuously conductive PEDOT-PDMS matrix provides conducting pathways for fast electron and Li^+ transference which will be further evaluated by using EIS and GITT.

Table 5.1 Comparison of the coulomic efficiency and specific capacity of Si anode

Materials	Initial coulomic efficiency (%)	Rate (C)	Specific capacity (mAh g^{-1}) (after *x* cycles)	Capacity retention (%)	Reference
SiNP-PANI	70	1.4	550 (5000)	91	(Wu et al., 2013)
Porous Si hollow nanospheres@PPy	68	0.2	2024 (250)	78	(Du et al., 2014)
Si/C pomegranate	82	0.5	1160 (1000)	97	(Liu et al., 2014)
SiNPs cluster@Si@G	90.4	0.5	1388.4 (300)	44.8	(Wang et al., 2018)
Porous Si@C	75	0.1	1467 (370)	83	(Jia et al., 2018)
Si@3D G	76.9	0.05	1909 (100)	69.4	(Wang et al., 2019)
Si@C-Zeolite imidazolate frameworks	70	1.2	820 (1000)	28	(Gao et al., 2020)
Si@$Li_4Ti_5O_{12}$	78.8	0.1	883 (150)	64	(Liu et al., 2020)
SiNP@PEDOT-PDMS	77.4	0.5	1512(1000)	69.8	Present work

5.3.2.3 Rate performance

In the rate performance test, the cells were firstly activated for five cycles at 0.05 C and then tested at 0.2C, 0.5C, 0.8C, and 1.0C every twenty cycles. Figure 5.7 exhibits representative voltage profiles for the discharge-charge plots of SiNP@PEDOT-PDMS electrode at the potential range of 0.01-1.0 V. The capacitance of a SiNP@PEDOT-PDMS electrode varies from ~2411 mAh g^{-1} to ~1166 mAh g^{-1} at charging and discharging rate from 0.2 C to 1.0 C, which is over twice larger than that of conventional graphite electrode (1 C, 372 mAh g^{-1}). Figure 5.7 also shows the lithiation potential associating with the insertion of Li into Si at the range of 0.01-0.3 V, demonstrating the rapid passage of Li$^+$ through the PEDOT-PDMS layer to reach Si and forming the amorphous Li$_x$Si. Hence, the stable electrochemical behavior of SiNP@PEDOT-PDMS electrode is due to the smaller internal resistance of cells favored by PEDOT-PDMS.

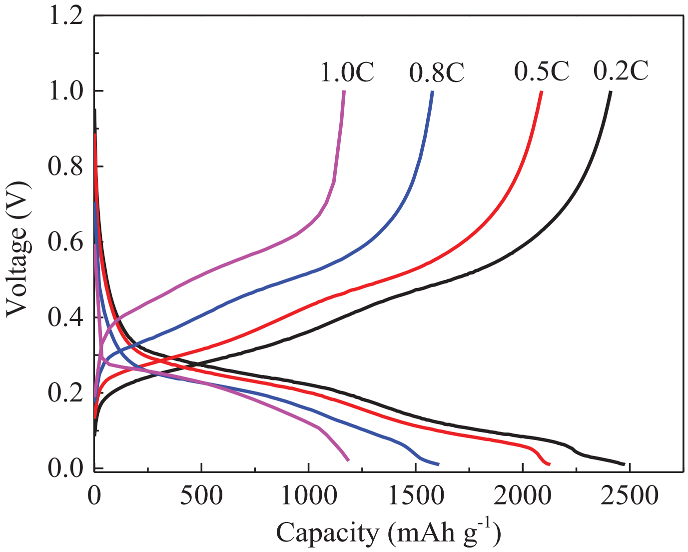

Figure 5.7 The voltage profiles of SiNP@PEDOT-PDMSelectrode at charging/discharging rate of 0.2C, 0.5C, 0.8C, and 1.0C

5.3.2.4. GITT analysis for chemical diffusion

The GITT method was used to evaluate the D_{Li^+} for Si control electrode and SiNP@PEDOT-PDMS electrode during the discharging process in the initial cycle. The battery is discharged for 10 min, following by a relaxation time of 30 min. This process is repeated until the voltage down to 0.01 V. The typical GITT plots at around 0.2 V are shown in Figure 5.8. The D_{Li^+} for Si control electrode is around 5.07×10^{-13} cm^2 s^{-1}. However, for the coated Si electrode, it is over thirty times that of Si control electrode (2.47×10^{-11} cm^2 s^{-1}). In addition, the voltage drop caused by the internal resistance for the coated electrode is smaller than that of Si control one, which benefits the electrochemical performance of the batteries. The obtained results illustrate the PEDOT-PDMS coat has the capability of improving the lithium-ion conductivity of the Si electrode, and reduce the resistance and polarization effect. This is because of the amorphous phase and the conductive structure of PEDOT-PDMS.

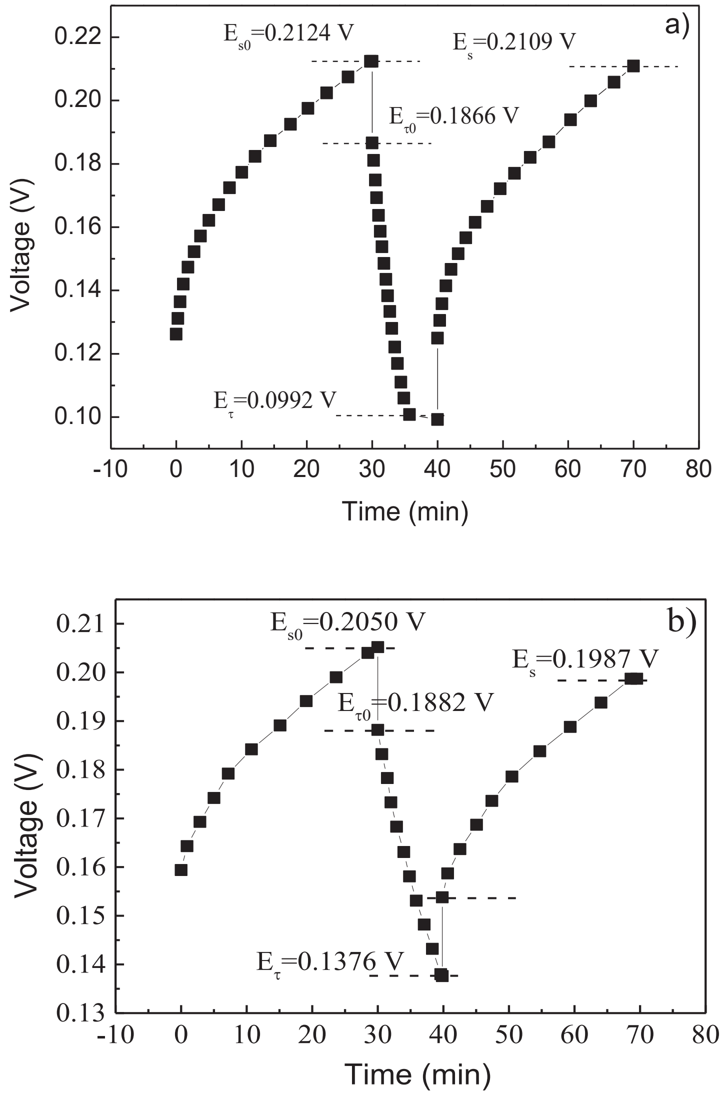

Figure 5.8 GITT curves of (a) Si control electrode and (b) SiNP@PEDOT-PDMS electrode in the discharge region

5.3.2.5 EIS analysis

The electrochemical impedance spectroscopy (EIS) was further utilized to test whether a lower charge transfer resistance is achieved for the cells assembled with SiNP@PEDOT-PDMS anode. The cell is charged and discharged at 0.5 C and the AC amplitude is 1×10^{-5} A_{RMS}. As shown in Figure 5.9, the Nyquist curves for Si control anode and SiNP@PEDOT-PDMS anode after different cycles include a semicircle at high-frequency and a low-frequency straight line. The high-frequency semicircle is associated to the combined resistance of SEI layer (R_{sei}) and charge transfer resistance (R_{ct}), as well as the contact interface resistance (R_{int}) (Wang et al., 2014; Wang et al., 2018). The straight line at low-frequency is associated to the Warburg impedance (Z_w), i.e. lithium diffusion within the electrode (Chen et al., 2015; Wang et al., 2018).

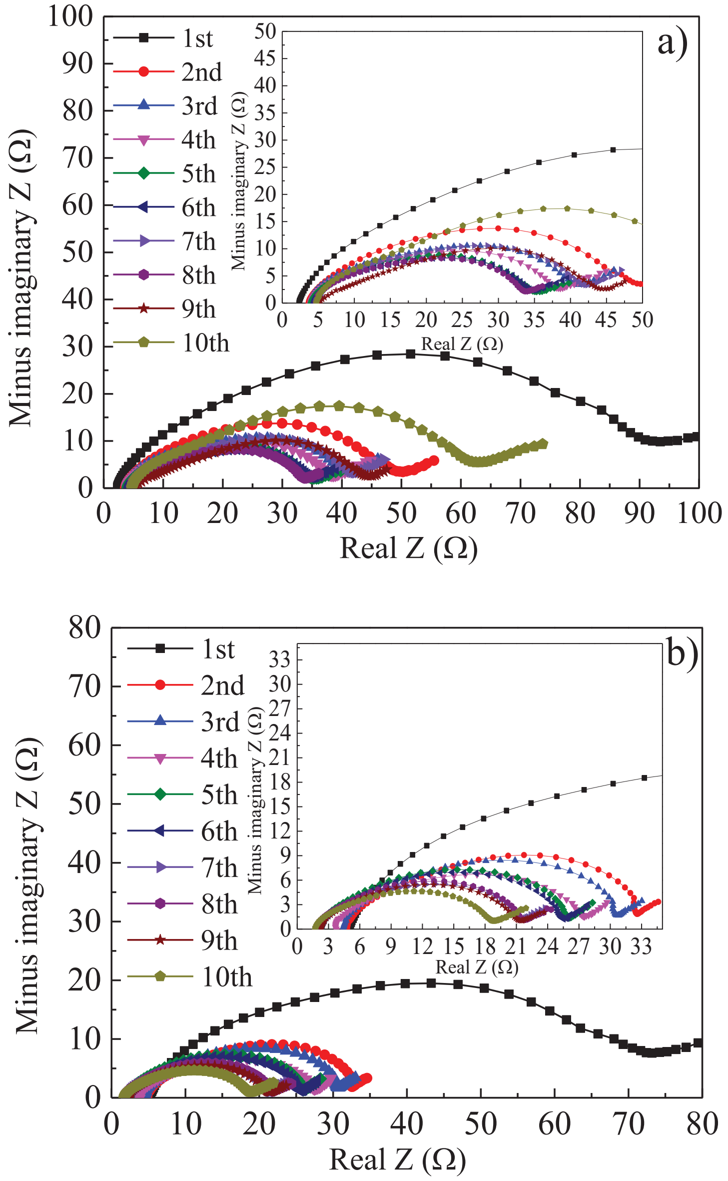

Figure 5.9 The impedance tests of cells assembled with (a) Si control electrode and (b) SiNP@PEDOT-PDMSelectrode after each cycle between 1 and 10

The following phenomena can be observed from Figure 5.9: In the case of Si control anode, the semicircles undergo a reduction process in the first seven cycles but show obvious changes for the later on cycles, reaching ~60 Ω at the 10th cycle. However, in the case of the coated electrode, the semicircle shrinks for the first few cycles, and no obvious semicircle increase was observed afterwards, keeping around 20 Ω which is much lower than that of Si control electrode.

In addition, the semicircle of Si control anode is larger than that of the coated anode after the first cycle. The phenomenon may be due to the following reasons: Firstly, after the first cycle, both of the cells fabricated with Si control anode and SiNP@PEDOT-PDMS anode have high R_{int} and R_{ct}; however, for the bare anode, the R_{sei} is larger due to naked Si. Secondly, as for the coated anode, the conductivity increases after Li^+ and PF_6^- doping (Novák et al., 1997; Wu et al., 2013; Kayser and Lipomi, 2019) and the SEI film is stable due to the capability of accommodating volume expansion, leading to smaller and more stable semicircle (Liu et al., 2014); for the Si control anode, after several cycles, the SEI film began to crack and the pulverization of Si, resulting in high resistance. Hence, the semicircle radius increases after seven cycles (Figure 5.9a) and the coulombic efficiency of Si control electrode is lower than that of coated electrode in the initial several cycles (Figure 5.5).

5.3.2.6 XPS of the electrode analysis

The XPS results, Figure 5.10a, show the elemental change of the SiNP@PEDOT-PDMS electrode before and after cycling to identify the integrity of the PEDOT-PDMS coating. It can be seen that the new F peaks of 685.7 eV originate from the LiF of SEI composition, indicating the formation of the SEI layer outside the polymer coating (Munaoka et al., 2018). In addition, the peak of S2p shifts to low binding energy (the green region in Figure 5.10b) after cycling, indicating electron-donating groups (such as PF_6^-) appear around S (see Figure 5.11). This is because π-π conjugated structure provides electrons transfer pathway and therefore the electron density increases. However, the peaks of Si2s (purple area) and Si2p (blue area) shift to high binding energy, implying electronegative groups appear around Si. Hence, the Li^+ transfers through Si-O in the amorphous phase as shown in Figure 5.11, the operation mechanism of the PEDOT-PDMS.

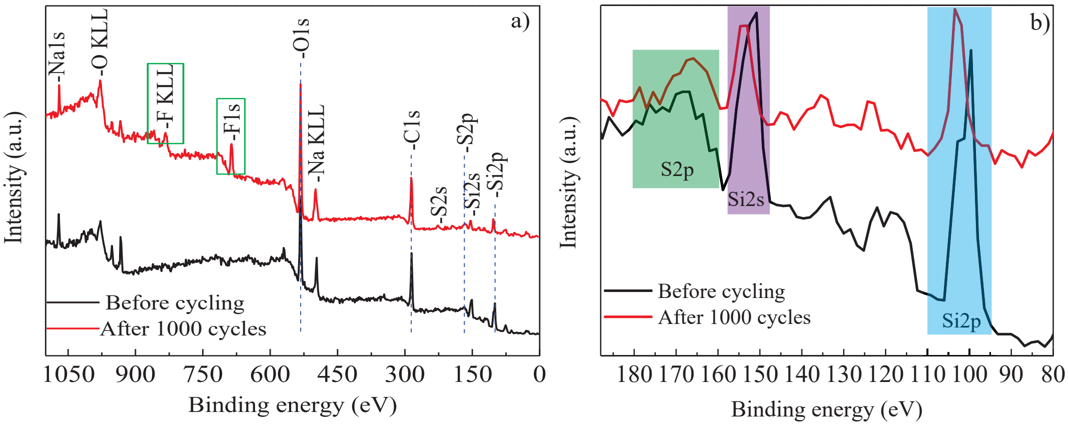

Figure 5.10 (a) XPS spectra and (b) S2p, Si2s, and Si2p of SiNP@PEDOT-PDMS electrode before and after cycling

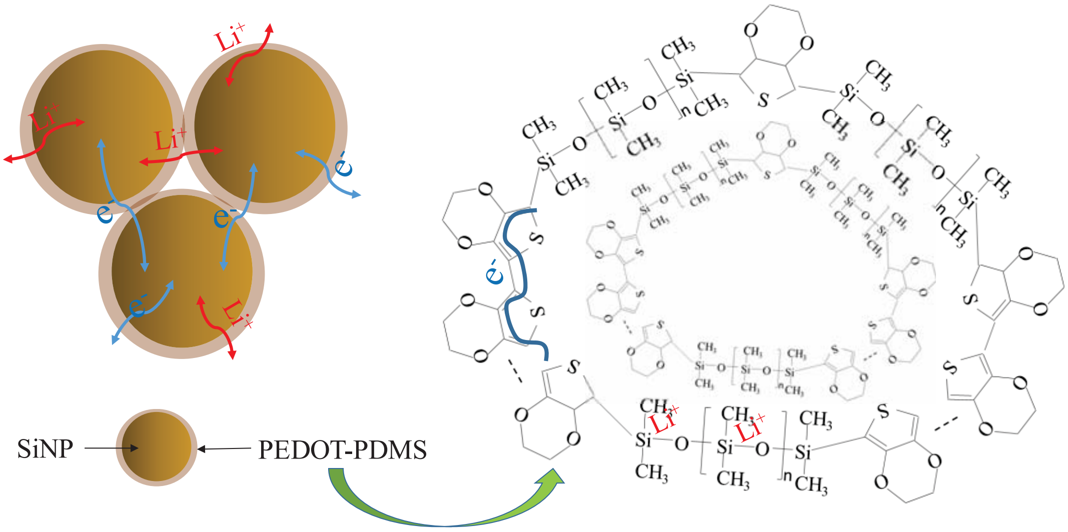

Figure 5.11 Scheme of the PEDOT-PDMS operation mechanism during cycling

5.3.2.7 SEM of the electrode analysis

In order to further confirm the difference of Si control electrode and SiNP@PEDOT-PDMS electrode after 10 cycles, the surface and the cross-section SEM images are shown in Figure 5.12. Obviously, some undesirable cracks appear on the surface and inside of the Si control electrode (see Figure 5.12a) and c)), while the SiNP@PEDOT-PDMS electrode still remains integrated without cracks on the surface and inside, which highlights the coated electrode suffers from smaller volume change during charge-discharge. On the other hand, it can be observed from the cross-section images that the unlimited growth of SEI appears for the control electrode. In comparison, the stable SEI forms for the coated electrode (see Figure 5.12d). The obtained results directly indicate that the PEDOT-PDMS coating plays a positive role in suppressing volume change and limiting SEI growth of Si electrode during charging and discharging process.

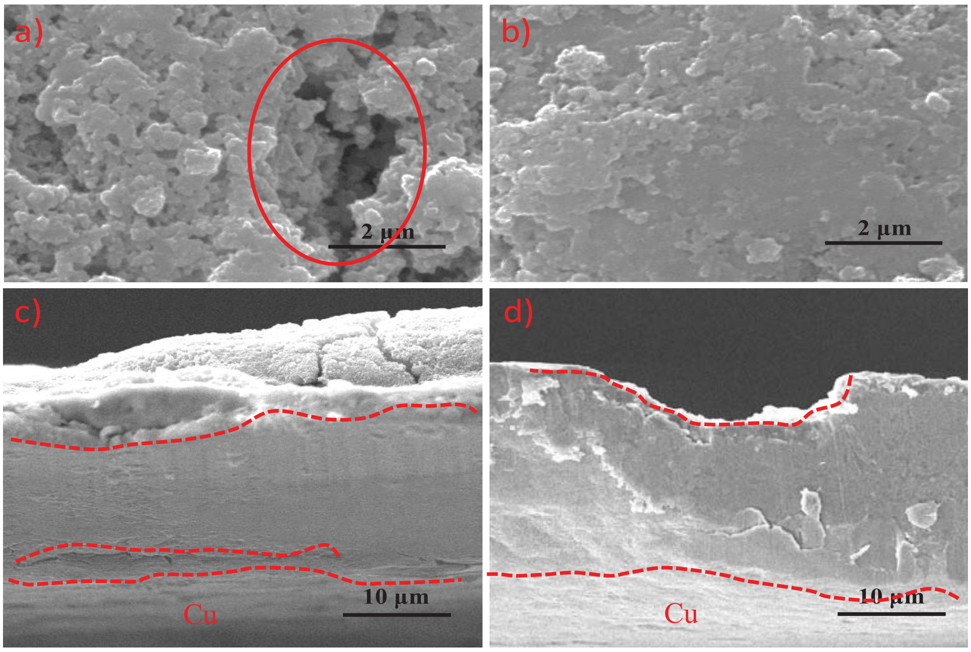

Figure 5.12 SEM images of the surface of (a) Si control electrode and (b) SiNP@PEDOT-PDMS electrode after cycling; SEM images of the cross-section of (c) Si control electrode and (d) SiNP@PEDOT-PDMS electrode after cycling

5.3.2.8 In-situ TEM analysis

The in-situ TEM is used to further directly confirm how the PEDOT-PDMS coating affects the electrochemical lithiation of Si particles. Figures 5.13a-c captured from Movie 1 show the initial lithiation process of the pure Si particle with ~95.81 nm in diameter before lithiation. Through comparing the volume change of the Si or coated Si nanoparticles (yellow arrows) that are near to the Li source, it can be fund that, after lithiation (see Figure 5.13b) for pure Si, an amorphous shell is formed on the surface of crystalline Si core because of the lithiation; After further lithiation, the diameter of Si grows to ~122.16 (see Figure 5.13c) while the crystalline Si core still can be observed, indicating the incomplete lithiation because of the retardation effect of the stress induced by the lithiation (Liu et al., 2013). In addition, the pure Si particles that are far away (~288.41 nm) from the lithium (red arrows and red circles in Figure 5.13b and c) do not show the lithiation process because of the retardation effect.

In the case of the SiNP@PEDOT-PDMS particles, the captured TEM images from Movie 2 of lithiation process are shown in Figures 5.13d-f. In comparison, the diameter of coated Si particle shows a bigger change from ~98.51 nm to ~129.10 nm, indicating more amount of Li lithiated inside the coated Si and smaller self-limiting lithiation because the coat could buffer the stress in cycling, which is consistent with the SEM results in Figure 5.12. On the other hand, the lithiation could occur for the coated Si particles that are far away (~329.10 nm) from the lithium (red arrows and red circles in Figure 5.13e and f) as the coat could buffer the stress and provide conducting pathways, which is consistent with the GITT results in Figure 5.8. Hence, the in-situ TEM results further confirm the enhanced electrochemical performance of the coated electrode.

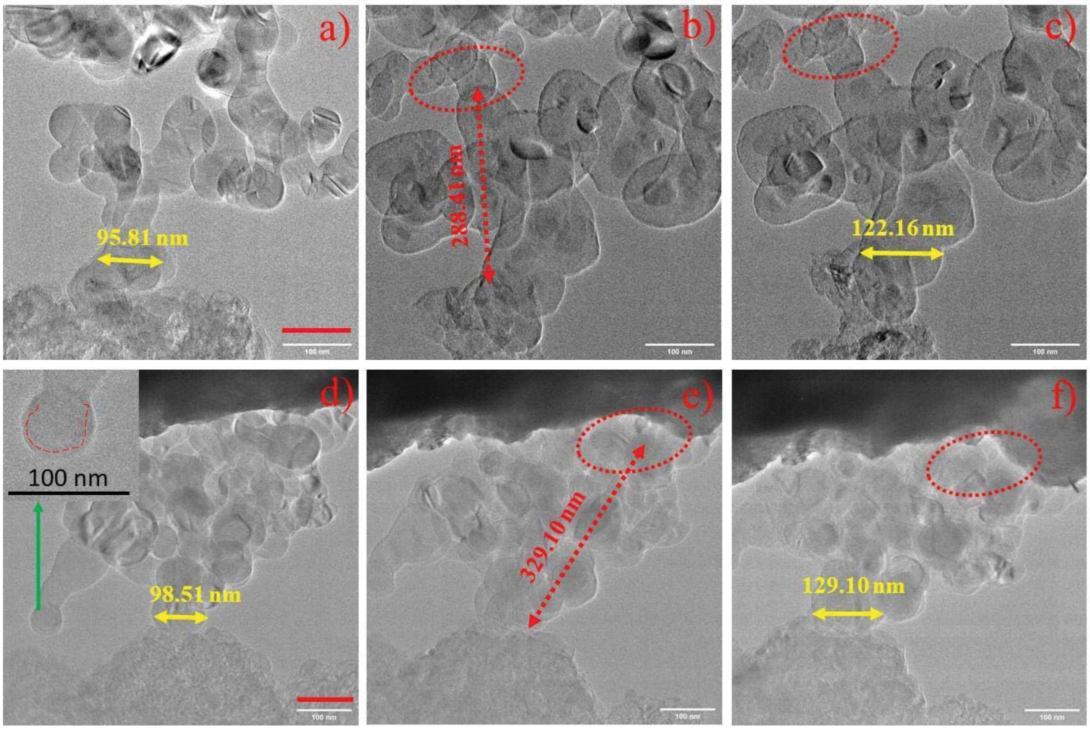

Figure 5.13 TEM images captured from Movie 1 of pure Si particle (a-c) and Movie 2 of SiNP@PEDOT-PDMS particle (d-f) during lithiation, scale bar is 100 nm, two movies are played at 7 times the real speed

5.4 Summary

This chapter introduces the preparation and characterizations of SiNP@PEDOT-PDMS electrode used in Li-ion batteries. The following results are obtained:

(1) The introduction of PEDOT-PDMS on the surface of Si nanoparticles has no effect on the crystalline structure of Si and keeps the intimate connection between polymer matrix and Si nanoparticles. This polymer coat framework could provide conducting pathways which has been discussed in Chapter 4 (Figure 4.8) and buffers the volume change as well as could facilitate a more stable SEI formation outside the polymer coat in cycling.

(2) Compared with the Si control electrode, the PEDOT-PDMS coated Si delivers relatively high specific capacitance and good cycling performance. The charge specific capacity is 1512 mAh g^{-1} after 1000 cycles at 0.5 C with a capacity retention of 69.8% of the highest specific capacitance around the160th cycle (2166 mAh g^{-1}), while the Si control electrode only shows a capacitance of 605 mAh g^{-1} after cycling 500 times with a capacity retention of 29%. The D_{Li+} for the coated Si anode during discharging process is 2.47×10^{-11} cm^2 s^{-1} which is over thirty times that of Si control one (5.07×10^{-13} cm^2 s^{-1}).

(3) The in-situ TEM results of the raw Si particles and the SiNP@PEDOT-PDMS particles indicate that the diameter of coated Si particles shows a bigger change than that of raw Si particle after lithiation, indicating more amount of Li lithiated inside the coated Si. In addition, the lithiation could occur for the coated Si particles that are far away (~329.10 nm) from the Li_2O/Li electrode, while the raw Si particles that are far away (~288.41 nm) from the Li_2O/Li electrode do not show the lithiation process.

Movie-Pure Si.avi , **Movie-Coated Si.avi**

Chapter 6 Conclusion

6.1 Contributions to Knowledge

The contributions to knowledge were made by the investigations of preparation, characterization, and application of PVA-based Na^+-ion conducting polymer electrolyte membranes, and by the synthesis of expected-conducting-flexible polymer (PEDOT-PDMS) and the application in the modifications of $NaLiFePO_4F$ and Si nanoparticle. The contributions are summarized as follows:

1. For PVA-based gel polymer electrolyte, the composition with 30% NaTf and 10% EMITf exhibits an excellent properties due to NaTf with large-sized anion, and the EDLCs assembled using spinning-casting method exhibit good electrochemical performances.
    - ➢ The polymer electrolyte shows high ionic conductivity ($\sim 3.6\times10^{-3}$ S cm^{-1}) and good thermal stability until to 150 ºC.
    - ➢ The as-fabricated EDLC exhibits high redox cyclic stability and high coulombic efficiency (~100%) up to 1000 charge-discharge cycles in the potential ranges of 0-1.6 and 0-2.0 V, respectively.
2. PEDOT-PDMS polymer could be synthesized through the hydrosilylation and dehydrocoupling reaction occurred between h_2PDMS and the EDOT monomer.
    - ➢ The tensile stress and strain of the PEDOT-PDMS membrene at rupture are $22.4\pm2.1\%$ and 0.24 ± 0.03 MPa, respectively. The Young's modulus (elastic modulus) is 1.17 ± 0.10 MPa.
    - ➢ The polymer shows the amorphous nature which provides Li^+ transfer pathway. It also could conduct through the conjugated structure.
3. PEDOT-PDMS could be used to modify $NaLiFePO_4F$ cathode and Si anode.
    - 3a. The cycle stability and specific capacity of $NaLiFePO_4F$ electrode can be improved by applying the PEDOT-PDMS solution on the surface of the electrode and forming protective layer which could enhance electron and Li^+ transfer.

- The $NaLiFePO_4F$ electrode@PEDOT-PDMS electrodes shows high specific capacity (88.1 mAh g^{-1} after cycling 500 times at 0.5 C), good cycling stability (~100% of capacity retention after 500 cycles).
- It shows high D_{Li+} (1.89×10^{-9} and 1.20×10^{-9} cm^2 s^{-1} during charging and discharging).

3b. The introduction of PEDOT-PDMS polymer coating on the surface of Si nanoparticles anode delivers relatively good cycling stability because it provides conducting pathways and buffers the stress induced by the lithiation, leading to less retardation effect and less self-limiting lithiation, as well as could facilitate a more stable SEI formation outside the polymer coat during cycling.

- The charge specific capacity of the SiNP@ PEDOT-PDMS electrode is ~1512 mAh g^{-1} at 0.5 C after cycling 1000 times together with a capacity retention of 69.8% of the highest specific capacity around the160th cycle (~2166 mAh g^{-1}).
- The Li-ion diffusion coefficient electrode during the discharging process is around 2.47×10^{-11} cm^2 s^{-1} which is more than thirty times that of Si control electrode (5.07×10^{-13} cm^2 s^{-1}).
- According to the results of in-situ TEM, the diameter of coated Si particle shows a bigger change (from ~98.51 nm to ~129.10 nm) than that of raw Si particle (from ~95.81 nm to ~122.16 nm) after lithiation, indicating more amount of Li lithiated inside the coated Si. In addition, the lithiation could occur for the coated Si particles that are far away (~329.10 nm) from the Li_2O/Li electrode, while the raw Si particles that are far away (~288.41 nm) from the Li_2O/Li electrode do not show the lithiation process.

6.2 Suggestions for Future Work

The future work is recommended according to the obtained results of this thesis research.

(1) Applying PEDOT-PDMS to coat larger sized Si particles to compare the

coating effect.

(2) The suitable PEDOT-PDMS coat thickness for the Si electrode

The thickness of polymer layer can be directly controlled by mixing different amounts of the monomer with a certain amount of Si.

References

Abdullah, O. G., Aziz, S. B., Saber, D. R., Abdullah, R. M., Hanna, R. R. and Saeed, S. R., "Characterization of polyvinyl alcohol film doped with sodium molybdate as solid polymer electrolytes," *Journal of Materials Science: Materials in Electronics,* 28(12): 8928-8936, 2017.

Ahn, J., Yoon, S., Jung, S. G., Yim, J. H. and Cho, K. Y., "A conductive thin layer on prepared positive electrodes by vapour reaction printing for high-performance lithium-ion batteries," *Journal of Materials Chemistry A,* 5(40): 21214-21222, 2017.

Amaresh, S., Karthikeyan, K., Kim, K., Nahm, K. and Lee, Y., "Alumina coating on 5 V lithium cobalt fluorophosphate cathode material for lithium secondary batteries–synthesis and electrochemical properties," *RSC Advances,* 4(44): 23107-23115, 2014.

Amatucci, G., Tarascon, J. and Klein, L., "CoO_2, the end member of the Li_xCoO_2 solid solution," *Journal of the Electrochemical Society,* 143(3): 1114-1123, 1996.

Antipov, E. V., Khasanova, N. R. and Fedotov, S. S., "Perspectives on li and transition metal fluoride phosphates as cathode materials for a new generation of li-ion batteries," *IUCrJ,* 2(1): 85-94, 2015.

Aravindan, V. and Vickraman, P., "A study on LiBOB-based nanocomposite gel polymer electrolytes (NCGPE) for lithium-ion batteries," *Ionics,* 13(4): 277-280, 2007.

Armand, M. and Tarascon, J. M., "Building better batteries," *Nature,* 451(7179): 652, 2008.

Aurbach, D., "Review of selected electrode-solution interactions which determine the performance of li and li ion batteries," *Journal of Power Sources,* 89(2): 206-218, 2000.

Aziz, S. B., "Li^+ ion conduction mechanism in poly (ε-caprolactone)-based polymer electrolyte," *Iranian Polymer Journal,* 22(12): 877-883, 2013.

Aziz, S. B., Abdullah, O. G. and Rasheed, M. A., "Structural and electrical characteristics of PVA: NaTf based solid polymer electrolytes: Role of lattice energy of salts on electrical DC conductivity," *Journal of Materials Science: Materials in Electronics,* 28(17): 12873-12884, 2017.

Aziz, S. B., Brza, M., Hamsan, M., Kadir, M., Muzakir, S. and Abdulwahid, R. T., "Effect of ohmic-drop on electrochemical performance of edlc fabricated from PVA: Dextran: NH_4I based polymer blend electrolytes," *Journal of Materials Research and Technology*, 2020.

Aziz, S. B., Woo, T. J., Kadir, M. and Ahmed, H. M., "A conceptual review on polymer electrolytes and ion transport models," *Journal of Science: Advanced Materials and Devices,* 3(1): 1-17, 2018.

Bai, Z W, "Investigation to $NaLiFePO_4F$ for high voltage cathode material of lithium-ion battery," The degree of doctor of philosophy, The Hong Kong University of Science and Technology, 2019.

Bai, Z. W., Shao, M. and Chen, G., "New insight of $NaLiFePO_4F$ as a high voltage cathode material for lithium-ion battery," Meeting Abstracts, The Electrochemical Society, 2019.

Balducci, A., Bardi, U., Caporali, S., Mastragostino, M. and Soavi, F., "Ionic liquids for hybrid supercapacitors," *Electrochemistry Communications,* 6(6): 566-570, 2004.

Baskoro, F., Wong, H. Q. and Yen, H. J., "Strategic structural design of a gel polymer electrolyte toward a high efficiency lithium-ion battery," *ACS Applied Energy Materials,* 2(6): 3937-3971, 2019.

Batisse, N. and Raymundo P, E., "A self-standing hydrogel neutral electrolyte for high voltage and safe flexible supercapacitors," *Journal of Power Sources,* 348: 168-174, 2017.

Bhargav, P. B., Mohan, V., Sharma, A. and Rao, V., "Characterization of poly (vinyl alcohol)/sodium bromide polymer electrolytes for electrochemical cell applications," *Journal of Applied Polymer Science,* 108(1): 510-517, 2008.

Bhide, A., Hofmann, J., Dürr, A. K., Janek, J. and Adelhelm, P., "Electrochemical stability of non-aqueous electrolytes for sodium-ion batteries and their compatibility with $Na_{0.7}CoO_2$," *Physical Chemistry Chemical Physics,* 16(5): 1987-1998, 2014.

Boschin, A. and Johansson, P., "Characterization of NaX (X: TFSI, FSI)-PEO based solid polymer electrolytes for sodium batteries," *Electrochimica Acta,* 175: 124-133, 2015.

Bresser, D., Hosoi, K., Howell, D., Li, H., Zeisel, H., Amine, K. and Passerini, S., "Perspectives of automotive battery R&D in China, Germany, Japan, and the USA," *Journal of Power Sources,* 382: 176-178, 2018.

Bridel, J. S., Azaïs, T., Morcrette, M., Tarascon, J. M. and Larcher, D., "Key parameters governing the reversibility of Si/carbon/CMC electrodes for li-ion batteries†," *Chemistry of Materials,* 22(3): 1229-1241, 2010.

Cao, W. and Zheng, J., "Li-ion capacitors with carbon cathode and hard carbon/stabilized lithium metal powder anode electrodes," *Journal of Power Sources,* 213: 180-185, 2012.

Cao, Y., Qi, X., Hu, K., Wang, Y., Gan, Z., Li, Y., Hu, G., Peng, Z. and Du, K., "Conductive polymers encapsulation to enhance electrochemical performance of Ni-rich cathode materials for li-ion batteries," *ACS Appllied Materials & Interfaces,* 10(21): 18270-18280, 2018.

Chan, C. K., Peng, H., Liu, G., McIlwrath, K., Zhang, X. F., Huggins, R. A. and Cui, Y., "High-performance lithium battery anodes using silicon nanowires," *Nature Nanotechnology,* 3(1): 31-35, 2008.

Chen, G., Song, X. and Richardson, T. J., "Electron microscopy study of the $LiFePO_4$ to $FePO_4$ phase transition," *Electrochemical and Solid-State Letters,* 9(6): A295-A298, 2006.

Chen, N., Han, C., Shi, R., Xu, L., Li, H., Liu, Y., Li, J. and Li, B., "Carbon coated MoS_2 nanosheets vertically grown on carbon cloth as efficient anode for high-performance sodium ion hybrid capacitors," *Electrochimica Acta*, 2018.

Chen, R., Sun, K., Zhang, Q., Zhou, Y., Li, M., Sun, Y., Wu, Z., Wu, Y., Li, X. and Xi, J., "Sequential solution polymerization of poly (3, 4-ethylenedioxythiophene) using V_2O_5 as oxidant for flexible touch sensors," *iScience,* 12: 66-75, 2019.

Chen, S., He, T., Su, Y., Lu, Y., Bao, L., Chen, L., Zhang, Q., Wang, J., Chen, R. and Wu, F., "Ni-rich $LiNi_{0.8}Co_{0.1}Mn_{0.1}O_2$ oxide coated by dual-conductive layers as high performance cathode material for lithium-ion batteries," *ACS Applied Materials & Interfaces,* 9(35): 29732-29743, 2017.

Chen, X., He, W., Ding, L. X., Wang, S. and Wang, H., "Enhancing interfacial contact in all solid state batteries with a cathode-supported solid electrolyte membrane framework," *Energy & Environmental Science*, 2019.

Chen, Y., Chen, H., Lin, F. and Chen, C., "Polyacrylonitrile electrolytes: 1. A novel high-conductivity composite polymer electrolyte based on PAN, $LiClO_4$ and α-Al_2O_3," *Solid State Ionics,* 150(3-4): 327-335, 2002.

Chen, Y., Du, N., Zhang, H. and Yang, D., "Facile synthesis of uniform MWCNT@Si nanocomposites as high-performance anode materials for lithium-ion batteries," *Journal of Alloys and Compounds,* 622: 966-972, 2015.

Chen, Y., Liu, L., Xiong, J., Yang, T., Qin, Y. and Yan, C., "Porous Si nanowires from cheap metallurgical silicon stabilized by a surface oxide layer for lithium ion batteries," *Advanced Functional Materials,* 25(43): 6701-6709, 2015.

Chen, Z., Augustyn, V., Jia, X., Xiao, Q., Dunn, B. and Lu, Y., "High-performance sodium-ion pseudocapacitors based on hierarchically porous nanowire composites," *ACS Nano,* 6(5): 4319-4327, 2012.

Chen, Z., Lu, Z. and Dahn, J., "Staging phase transitions in Li_xCoO_2," *Journal of the Electrochemical Society,* 149(12): A1604-A1609, 2002.

Cheng, S., Smith, D. M., Pan, Q., Wang, S. and Li, C. Y., "Anisotropic ion transport in nanostructured solid polymer electrolytes," *RSC Advances,* 5(60): 48793-48810, 2015.

Cheng, X., Pan, J., Zhao, Y., Liao, M. and Peng, H., "Gel polymer electrolytes for electrochemical energy storage," *Advanced Energy Materials,* 8(7): 1702184, 2018.

Chew, S. Y., Guo, Z. P., Wang, J. Z., Chen, J., Munroe, P., Ng, S. H., Zhao, L. and Liu, H. K., "Novel nano-silicon/polypyrrole composites for lithium storage," *Electrochemistry Communications,* 9(5): 941-946, 2007.

Chun, S. E., Evanko, B., Wang, X., Vonlanthen, D., Ji, X., Stucky, G. D. and Boettcher, S. W., "Design of aqueous redox-enhanced electrochemical capacitors with high specific energies and slow self-discharge," *Nature Communications,* 6: 7818, 2015.

Chung, K. Y. and Kim, K. B., "Investigation of structural fatigue in spinel electrodes using in situ laser probe beam deflection technique," *Journal of the Electrochemical Society,* 149(1): A79-A85, 2002.

Croce, F., Appetecchi, G., Persi, L. and Scrosati, B., "Nanocomposite polymer electrolytes for lithium batteries," *Nature,* 394(6692): 456, 1998.

Cui, D., Chen, S., Han, C., Ai, C. and Yuan, L., "Carbothermal reduction synthesis of carbon coated Na_2FePO_4F for lithium ion batteries," *Journal of Power Sources,* 301: 87-92, 2016.

Cui, S., Wei, Y., Liu, T., Deng, W., Hu, Z., Su, Y., Li, H., Li, M., Guo, H. and Duan, Y., "Optimized temperature effect of Li-ion diffusion with layer distance in $Li(Ni_xMn_yCo_z)O_2$ cathode materials for high performance Li-ion battery," *Advanced Energy Materials,* 6(4): 1501309, 2016.

Cui, Y., Liang, X., Chai, J., Cui, Z., Wang, Q., He, W., Liu, X., Liu, Z., Cui, G. and Feng, J., "High performance solid polymer electrolytes for rechargeable batteries: A self-catalyzed strategy toward facile synthesis," *Advanced Science,* 4(11): 1700174, 2017.

Das, P. R., Komsiyska, L., Osters, O. and Wittstock, G., "PEDOT: PSS as a functional binder for cathodes in lithium ion batteries," *Journal of the Electrochemical Society,* 162(4): A674-A678, 2015.

Das, S. and Ghosh, A., "Effect of plasticizers on ionic conductivity and dielectric relaxation of PEO-$LiClO_4$ polymer electrolyte," *Electrochimica Acta,* 171: 59-65, 2015.

Delmas, C., Maccario, M., Croguennec, L., Le Cras, F. and Weill, F. "Lithium deintercalation in $LiFePO_4$ nanoparticles via a domino-cascademodel," Materials for sustainable energy: A collection of peer-reviewed research and review articles from nature publishing group, World Scientific**:** 180-186, 2011.

Deshpande, R., Cheng, Y. T. and Verbrugge, M. W., "Modeling diffusion-induced stress in nanowire electrode structures," *Journal of Power Sources,* 195(15): 5081-5088, 2010.

Dhumal, N. R. and Gejji, S. P., "Theoretical studies on blue versus red shifts in diglyme-M^+-X^-(M= Li, Na, and K and X= CF_3SO_3, PF_6, and $(CF_3SO_2)_2N$)," *The Journal of Physical Chemistry A,* 110(1): 219-227, 2006.

Di Noto, V., Lavina, S., Giffin, G. A., Negro, E. and Scrosati, B, "Polymer electrolytes: Present, past and future," *Electrochimica Acta*, 57: 4-13, 2011.

Ding, C., Nohira, T., Kuroda, K., Hagiwara, R., Fukunaga, A., Sakai, S., Nitta, K. and Inazawa, S., "NaFSA-C_1C_3pyrFSA ionic liquids for sodium secondary battery operating over a wide temperature range," *Journal of Power Sources,* 238: 296-300, 2013.

Du, F. H., Li, B., Fu, W., Xiong, Y. J., Wang, K. X. and Chen, J. S., "Surface binding of polypyrrole on porous silicon hollow nanospheres for Li-ion battery anodes with high structure stability," *Advanced Materials,* 26(35): 6145-6150, 2014.

Du, F. H., Wang, K. X. and Chen, J. S., "Strategies to succeed in improving the lithium-ion storage properties of silicon nanomaterials," *Journal of Materials Chemistry A,* 4(1): 32-50, 2016.

Dunn, B., Kamath, H. and Tarascon, J. M., "Electrical energy storage for the grid: A battery of choices," *Science,* 334(6058): 928-935, 2011.

Edman, L., Doeff, M. M., Ferry, A., Kerr, J. and De Jonghe, L. C., "Transport properties of the solid polymer electrolyte system $P(EO)_n$ LiTFSI," *The Journal of Physical Chemistry B,* 104(15): 3476-3480, 2000.

Egashira, M., Takahashi, H., Okada, S. and Yamaki, J.I., "Measurement of the electrochemical oxidation of organic electrolytes used in lithium batteries by microelectrode," *Journal of Power Sources,* 92(1-2): 267-271, 2001.

Eikady, M. F., Ihns, M., Li, M., Hwang, J. Y., Mousavi, M. F., Chaney, L., Lech, A. T. and Kaner, R. B., "Engineering three-dimensional hybrid supercapacitors and microsupercapacitors for high-performance integrated energy storage," *Proceedings of the National Academy of Sciences,* 112(14): 4233-4238, 2015.

Ellis, B. L., Lee, K. T. and Nazar, L. F., "Positive electrode materials for Li-ion and Li-batteries," *Chemistry of Materials,* 22(3): 691-714, 2010.

Evans, J., Vincent, C. A. and Bruce, P. G., "Electrochemical measurement of transference numbers in polymer electrolytes," *Polymer,* 28(13): 2324-2328, 1987.

Fan, L. Q., Zhong, J., Wu, J. H., Lin, J. M. and Huang, Y. F., "Improving the energy density of quasi-solid-state electric double-layer capacitors by introducing redox additives into gel polymer electrolytes," *Journal of Materials Chemistry A,* 2(24): 9011-9014, 2014.

Fan, L., Wei, S., Li, S., Li, Q. and Lu, Y., "Recent progress of the solid-state electrolytes for high-energy metal-based batteries," *Advanced Energy Materials,* 8(11): 1702657, 2018.

Fan, X., Luo, C., Lamb, J., Zhu, Y., Xu, K. and Wang, C., "PEDOT encapsulated feof nanorod cathodes for high energy lithium-ion batteries," *Nano Letters,* 15(11): 7650-7656, 2015.

Feng, K., Li, M., Liu, W., Kashkooli, A. G., Xiao, X., Cai, M. and Chen, Z., "Silicon-based anodes for lithium-ion batteries: From fundamentals to practical applications," *Small,* 14(8), 2018.

Feuillade, G. and Perche, P., "Ion-conductive macromolecular gels and membranes for solid lithium cells," *Journal of Applied Electrochemistry,* 5(1): 63-69, 1975.

Fic, K., Meller, M. and Frackowiak, E., "Interfacial redox phenomena for enhanced aqueous supercapacitors," *Journal of the Electrochemical Society,* 162(5): A5140-A5147, 2015.

Flandrois, S. and Simon, B., "Carbon materials for lithium-ion rechargeable batteries," *Carbon,* 37(2): 165-180, 1999.

Francis, C. F., Kyratzis, I. L. and Best, A. S., "Lithium-ion battery separators for ionic-liquid electrolytes: A review," *Advanced Materials*: 1904205, 2020.

Fukata, N., Mitome, M., Bando, Y., Wu, W. and Wang, Z. L., "Lithium ion battery anodes using Si-Fe based nanocomposite structures," *Nano Energy,* 26: 37-42, 2016.

Gao, H., Guo, B., Song, J., Park, K. and Goodenough, J. B., "A composite gel-polymer/glass-fiber electrolyte for sodium-ion batteries," *Advanced Energy Materials,* 5(9): 1402235, 2015.

Gao, H. and Lian, K., "Proton-conducting polymer electrolytes and their applications in solid supercapacitors: A review," *RSC Advances,* 4(62): 33091-33113, 2014.

Gao, J., Qiu, G., Li, H., Li, M., Li, C., Qian, L. and Yang, B., "Boron-doped graphene/TiO_2 nanotube-based aqueous lithium ion capacitors with high energy density," *Electrochimica Acta,* 329: 135175, 2020.

Gao, R., Tang, J., Yu, X., Tang, S., Ozawa, K., Sasaki, T. and Qin, L. C., "In situ synthesis of MOF-derived carbon shells for silicon anode with improved lithium-ion storage," *Nano Energy*: 104444, 2020.

Gao, X. W., Deng, Y. F., Wexler, D., Chen, G. H., Chou, S. L., Liu, H. K., Shi, Z. C. and Wang, J. Z., "Improving the electrochemical performance of the $LiNi_{0.5}Mn_{1.5}O_4$ spinel by polypyrrole coating as a cathode material for the lithium-ion battery," *Journal of Materials Chemistry A,* 3(1): 404-411, 2015.

Geng, C. L., Fan, L. Q., Wang, C. Y., Wang, Y. L., Sun, S. J., Song, Z. Y., Liu, N. and Wu, J. H., "High energy density and high working voltage of a quasi-solid-state supercapacitor with a redox-active ionic liquid added gel polymer electrolyte," *New Journal of Chemistry,* 43(47): 18935-18942, 2019.

Ghosh, S. and Inganäs, O., "Conducting polymer hydrogels as 3D electrodes: Applications for supercapacitors," *Advanced Materials,* 11(14): 1214-1218, 1999.

Giffin, G. A., Moretti, A., Jeong, S. and Passerini, S., "Decoupling effective Li^+ ion conductivity from electrolyte viscosity for improved room-temperature cell performance," *Journal of Power Sources,* 342: 335-341, 2017.

Goodenough, J. B., "Rechargeable batteries: Challenges old and new," *Journal of Solid State Electrochemistry,* 16(6): 2019-2029, 2012.

Goodenough, J. B. and Kim, Y., "Challenges for rechargeable batteries," *Journal of Power Sources,* 196(16): 6688-6694, 2011.

Gordin, C., Rusu, M., Delaite, C., Salhi, S., Elzein, T. and Brogly, M., "Crystalinity behaviour in poly (ε-caprolactone)-b-poly (dimethylsiloxane) diblock and triblock copolymers through FTIR and DSC," *Materiale Plastice,* 46(1): 37, 2009.

Guo, R., Shi, P., Cheng, X. and Sun, L., "Effect of ZnO modification on the performance of $LiNi_{0.5}Co_{0.25}Mn_{0.25}O_2$ cathode material," *Electrochimica Acta,* 54(24): 5796-5803, 2009.

Guo, S., Li, H., Bai, H., Tao, Z. and Chen, J., "Ti/Si/Ti sandwich-like thin film as the anode of lithium-ion batteries," *Journal of Power Sources,* 248: 1141-1148, 2014.

Han, B., Key, B., Lapidus, S. H., Garcia, J. C., Iddir, H., Vaughey, J. T. and Dogan, F., "From coating to dopant: How the transition metal composition affects alumina coatings on Ni-rich cathodes," *ACS Appllied Matererials & Interfaces,* 9(47): 41291-41302, 2017.

Han, D., Zhang, J., Weng, Z., Kong, D., Tao, Y., Ding, F., Ruan, D. and Yang, Q. H., "Two-dimensional materials for lithium/sodium-ion capacitors," *Materials today energy,* 11: 30-45, 2019.

Han, X. Y., Zhao, D. L., Meng, W. J., Yang, H. X., Zhao, M., Duan, Y. J. and Tian, X. M., "Graphene caging silicon nanoparticles anchored on graphene sheets for high performance Li-ion batteries," *Applied Surface Science,* 484: 11-20, 2019.

Hao, Y., Wang, S., Shao, Y., Wu, Y. and Miao, S., "High-energy density li-ion capacitor with layered SnS_2/reduced graphene oxide anode and BCN nanosheet cathode," *Advanced Energy Materials*: 1902836, 2019.

Hashim, M., Majid, S., Ibrahim, Z. and Arof, A., "Electrochemical double layer capacitor based on cellulose-PVA hybrid electrolyte," *Ionics,* 11(5-6): 464-467, 2005.

He, L. J., Hong, J. L. and Chang, C. C., "Preparation and electrochemical characterizations of poly(3,4-dioxyethylenethiophene)/$LiCoO_2$ composite cathode in lithium-ion battery," *Journal of Power Sources,* 157(1): 457-463, 2006.

Heubner, C., Heiden, S., Matthey, B., Schneider, M. and Michaelis, A., "Sodiation vs. Lithiation of $FePO_4$: A comparative kinetic study," *Electrochimica Acta,* 216: 412-419, 2016.

Honary, S. and Orafai, H., "The effect of different plasticizer molecular weights and concentrations on mechanical and thermomechanical properties of free films," *Drug Development and Industrial Pharmacy,* 28(6): 711-715, 2002.

Hong, S. Y., Kim, Y., Park, Y., Choi, A., Choi, N. S. and Lee, K. T., "Charge carriers in rechargeable batteries: Na ions vs. Li ions," *Energy & Environmental Science,* 6(7): 2067-2081, 2013.

Hu, B., Shkrob, I. A., Zhang, S., Zhang, L., Zhang, J., Li, Y., Liao, C., Zhang, Z., Lu, W. and Zhang, L., "The existence of optimal molecular weight for poly (acrylic acid) binders in silicon/graphite composite anode for lithium-ion batteries." *Journal of Power Sources,* 378: 671-676, 2018.

Hu, K., Qi, X., Lu, C., Du, K., Peng, Z., Cao, Y. and Hu, G., "Enhanced electrochemical performance of $LiNi_{0.8}Co_{0.1}Mn_{0.1}O_2$ cathode materials via $Li_4P_2O_7$ surface modification for Li-ion batteries," *Ceramics International,* 44(12): 14209-14216, 2018.

Hu, Z., Zhang, S., Dong, S., Li, W., Li, H., Cui, G. and Chen, L., "Poly (ethyl α-cyanoacrylate)-based artificial solid electrolyte interphase layer for enhanced interface stability of Li metal anodes," *Chemistry of materials,* 29(11): 4682-4689, 2017.

Huang, J. L., Fan, L. Q., Gu, Y., Geng, C. L., Luo, H., Huang, Y. F., Lin, J. M. and Wu, J. H., "One-step solvothermal synthesis of high-capacity Fe_3O_4/reduced graphene oxide composite for use in Li-ion capacitor," *Journal of Alloys and Compounds,* 788: 1119-1126, 2019.

Idris, N. H., Rahman, M. M., Wang, J. Z. and Liu, H. K., "Microporous gel polymer electrolytes for lithium rechargeable battery application," *Journal of Power Sources,* 201: 294-300, 2012.

Inceoglu, S., Rojas, A. A., Devaux, D., Chen, X. C., Stone, G. M. and Balsara, N. P., "Morphology-conductivity relationship of single-ion-conducting block copolymer electrolytes for lithium batteries," *ACS Macro Letters,* 3(6): 510-514, 2014.

Isa, K. M., Othman, L., Hambali, D. and Osman, Z., "Electrical and electrochemical studies on sodium ion-based gel polymer electrolytes," AIP Conference Proceedings, AIP Publishing, 2017.

Islam, M. S. and Fisher, C. A., "Lithium and sodium battery cathode materials: Computational insights into voltage, diffusion and nanostructural properties," *Chemical Society Reviews,* 43(1): 185-204, 2014.

Jia, H., Zheng, J., Song, J., Luo, L., Yi, R., Estevez, L., Zhao, W., Patel, R., Li, X. and Zhang, J. G., "A novel approach to synthesize micrometer-sized porous silicon as a high performance anode for lithium-ion batteries," *Nano Energy,* 50: 589-597, 2018.

Jiang, S., Hu, B., Shi, Z., Chen, W., Zhang, Z. and Zhang, L., "Re‐Engineering Poly (Acrylic Acid) Binder toward Optimized Electrochemical Performance for Silicon Lithium‐Ion Batteries: Branching Architecture Leads to Balanced Properties of Polymeric Binders." *Advanced Functional Materials*, 30(10): 1908558, 2020.

Jin, Y., Zhu, B., Lu, Z., Liu, N. and Zhu, J., "Challenges and recent progress in the development of Si anodes for lithium-ion battery," *Advanced Energy Materials,* 7(23), 2017.

Jung, H., Park, M., Yoon, Y. G., Kim, G. B. and Joo, S. K., "Amorphous silicon anode for lithium-ion rechargeable batteries," *Journal of Power Sources,* 115(2): 346-351, 2003.

Kadir, M. and Arof, A., "Application of PVA-chitosan blend polymer electrolyte membrane in electrical double layer capacitor," *Materials Research Innovations,* 15(2): s217-s220, 2011.

Kalami, S., Khani, H. and Goodenough, J. B., "A microporous gel polymer electrolyte for sodium batteries," Meeting Abstracts, The Electrochemical Society, 2019.

Kang, Y., Lee, J., Suh, D. H. and Lee, C., "A new polysiloxane based cross-linker for solid polymer electrolyte," *Journal of Power Sources,* 146(1-2): 391-396, 2005.

Karaman, B. and Bozkurt, A., "Enhanced performance of supercapacitor based on boric acid doped PVA-H_2SO_4 gel polymer electrolyte system," *International Journal of Hydrogen Energy,* 43(12): 6229-6237, 2018.

Kayser, L. V. and Lipomi, D. J., "Stretchable conductive polymers and composites based on pedot and PEDOT: PSS," *Advanced Materials,* 31(10): 1806133, 2019.

Kayser, L. V., Russell, M. D., Rodriquez, D., Abuhamdieh, S. N., Dhong, C., Khan, S., Stein, A. N., Ramírez, J. and Lipomi, D. J., "RAFT polymerization of an intrinsically stretchable water-soluble block copolymer scaffold for PEDOT," *Chemistry of Materials*, 30(13): 4459-4468, 2018.

Khasanova, N. R., Drozhzhin, O. A., Storozhilova, D. A., Delmas, C. and Antipov, E. V., "New form of Li_2FePO_4F as cathode material for Li-ion batteries," *Chemistry of Materials,* 24(22): 4271-4273, 2012.

Kim, H., Kim, M. G., Jeong, H. Y., Nam, H. and Cho, J., "A new coating method for alleviating surface degradation of $LiNi_{0.6}Co_{0.2}Mn_{0.2}O_2$ cathode material: Nanoscale surface treatment of primary particles," *Nano Letters,* 15(3): 2111-2119, 2015.

Kim, H., Seo, M., Park, M. H. and Cho, J., "A critical size of silicon nano-anodes for lithium rechargeable batteries," *Angewandte Chemie International Edition,* 49(12): 2146-2149, 2010.

Kim, J., Choi, S., Jo, S., Lee, W. and Kim, B., "Characterization and properties of P(VDF-HFP)-based fibrous polymer electrolyte membrane prepared by electrospinning," *Journal of the Electrochemical Society,* 152(2): A295-A300, 2005.

Kim, J., Yoo, J. K., Jung, Y. S. and Kang, K., "$Li_3V_2(PO_4)_3$/conducting polymer as a high power 4 V-class lithium battery electrode," *Advanced Energy Materials,* 3(8): 1004-1007, 2013.

Kim, J. U., Jeong, I. S., Moon, S. I. and Gu, H. B., "Electrochemical characteristics of $LiMn_2O_4$-polypyrrole composite cathode for lithium polymer batteries," *Journal of Power Sources,* 97: 450-453, 2001.

Kim, J. W., Ryu, J. H., Lee, K. T. and Oh, S. M., "Improvement of silicon powder negative electrodes by copper electroless deposition for lithium secondary batteries," *Journal of Power Sources,* 147(1-2): 227-233, 2005.

Kim, M. G. and Cho, J., "Air stable Al_2O_3-coated Li_2NiO_2 cathode additive as a surplus current consumer in a Li-ion cell," *Journal of Materials Chemistry,* 18(48): 5880-5887, 2008.

Klasner, S. A., Metto, E. C., Roman, G. T. and Culbertson, C. T., "Synthesis and characterization of a poly (dimethylsiloxane)-poly (ethylene oxide) block copolymer for fabrication of amphiphilic surfaces on microfluidic devices," *Langmuir,* 25(17): 10390-10396, 2009.

Klinsmann, M., Rosato, D., Kamlah, M. and McMeeking, R. M., "Modeling crack growth during Li extraction in storage particles using a fracture phase field approach," *Journal of the Electrochemical Society,* 163(2): A102-A118, 2016.

Klonos, P., Sulym, I. Y., Borysenko, M., Gun'ko, V., Kripotou, S., Kyritsis, A. and Pissis, P., "Interfacial interactions and complex segmental dynamics in systems based on silica-polydimethylsiloxane core-shell nanoparticles: Dielectric and thermal study," *Polymer,* 58: 9-21, 2015.

Krause, L. J., Lamanna, W., Summerfield, J., Engle, M., Korba, G., Loch, R. and Atanasoski, R., "Corrosion of aluminum at high voltages in non-aqueous electrolytes containing perfluoroalkylsulfonyl imides; new lithium salts for lithium-ion cells," *Journal of Power Sources,* 68(2): 320-325, 1997.

Kumar, D. and Hashmi, S., "Ion transport and ion-filler-polymer interaction in poly (methyl methacrylate)-based, sodium ion conducting, gel polymer electrolytes dispersed with silica nanoparticles," *Journal of Power Sources,* 195(15): 5101-5108, 2010.

Kumar, D. and Hashmi, S., "Ionic liquid based sodium ion conducting gel polymer electrolytes," *Solid State Ionics,* 181(8-10): 416-423, 2010.

Kumar, D., Suleman, M. and Hashmi, S., "Studies on poly (vinylidene fluoride-co-hexafluoropropylene) based gel electrolyte nanocomposite for sodium-sulfur batteries," *Solid State Ionics,* 202(1): 45-53, 2011.

Kumar, M. and Srivastava, N., "Conductivity and dielectric investigation of NH_4I-doped synthesized polymer electrolyte system," *Ionics,* 21(5): 1301-1310, 2015.

Kvarnström, C., Neugebauer, H., Blomquist, S., Ahonen, H., Kankare, J. and Ivaska, A., "In situ spectroelectrochemical characterization of poly (3, 4-ethylenedioxythiophene)," *Electrochimica Acta,* 44(16): 2739-2750, 1999.

Laheäär, A., Przygocki, P., Abbas, Q. and Béguin, F., "Appropriate methods for evaluating the efficiency and capacitive behavior of different types of supercapacitors," *Electrochemistry Communications,* 60: 21-25, 2015.

Lang, U., Müller, E., Naujoks, N. and Dual, J., "Microscopical investigations of pedot: Pss thin films," *Advanced Functional Materials,* 19(8): 1215-1220, 2009.

Lee, S. and Gleason, K. K., "Enhanced optical property with tunable band gap of cross-linked PEDOT copolymers via oxidative chemical vapor deposition," *Advanced Functional Materials,* 25(1): 85-93, 2015.

Lee, S., Paine, D. C. and Gleason, K. K., "Heavily doped poly (3, 4-ethylenedioxythiophene) thin films with high carrier mobility deposited using oxidative CVD: Conductivity stability and carrier transport," *Advanced Functional Materials,* 24(45): 7187-7196, 2014.

Lee, S. H., Yoon, C. S., Amine, K. and Sun, Y. K., "Improvement of long-term cycling performance of $Li[Ni_{0.8}Co_{0.15}Al_{0.05}]O_2$ by AlF_3 coating," *Journal of Power Sources,* 234: 201-207, 2013.

Lee, S. J., Lee, J. K., Chung, S. H., Lee, H. Y., Lee, S. M. and Baik, H. K., "Stress effect on cycle properties of the silicon thin-film anode," *Journal of Power Sources,* 97: 191-193, 2001.

Lee, S. M., Oh, S. H., Ahn, J. P., Cho, W. I. and Jang, H., "Electrochemical properties of ZrO_2-coated $LiNi_{0.8}Co_{0.2}O_2$ cathode materials," *Journal of Power Sources,* 159(2): 1334-1339, 2006.

Li, C., Zhang, H., Fu, L., Liu, H., Wu, Y., Rahm, E., Holze, R. and Wu, H., "Cathode materials modified by surface coating for lithium ion batteries," *Electrochimica Acta,* 51(19): 3872-3883, 2006.

Li, H., Huang, X., Chen, L., Zhou, G., Zhang, Z., Yu, D., Mo, Y. J. and Pei, N., "The crystal structural evolution of nano-Si anode caused by lithium insertion and extraction at room temperature," *Solid State Ionics,* 135(1-4): 181-191, 2000.

Li, H., Sun, M., Zhang, T., Fang, Y. and Wang, G., "Improving the performance of PEDOT-PSS coated sulfur@ activated porous graphene composite cathodes for lithium–sulfur batteries," *Journal of Materials Chemistry A,* 2(43): 18345-18352, 2014.

Li, J., Cassagnau, P., Da Cruz-Boisson, F., Mélis, F., Alcouffe, P. and Bounor-Legaré, V., "Efficient hydrosilylation reaction in polymer blending: An original approach to structure PA12/PDMS blends at multiscales," *Polymer,* 112: 10-25, 2017.

Li, W., Yang, J., Wu, Z., Wang, J., Li, B., Feng, S., Deng, Y., Zhang, F. and Zhao, D., "A versatile kinetics-controlled coating method to construct uniform porous TiO_2 shells for multifunctional core-shell structures," *Journal of the American Chemical Society,* 134(29): 11864-11867, 2012.

Li, W., Zhang, Q., Zheng, G., Seh, Z. W., Yao, H. and Cui, Y., "Understanding the role of different conductive polymers in improving the nanostructured sulfur cathode performance," *Nano Letters,* 13(11): 5534-5540, 2013.

Liao, Y., Rao, M., Li, W., Yang, L., Zhu, B., Xu, R. and Fu, C., "Fumed silica-doped poly (butyl methacrylate-styrene)-based gel polymer electrolyte for lithium ion battery," *Journal of Membrane Science,* 352(1-2): 95-99, 2010.

Lim, C. S., Teoh, K., Liew, C. W. and Ramesh, S., "Capacitive behavior studies on electrical double layer capacitor using poly (vinyl alcohol)–lithium perchlorate based polymer electrolyte incorporated with TiO_2," *Materials Chemistry and Physics,* 143(2): 661-667, 2014.

Lin, D., Liu, W., Liu, Y., Lee, H. R., Hsu, P.-C., Liu, K. and Cui, Y., "High ionic conductivity of composite solid polymer electrolyte via in situ synthesis of monodispersed SiO_2 nanospheres in poly (ethylene oxide)," *Nano Letters,* 16(1): 459-465, 2015.

Lin, X., Salari, M., Arava, L. M. R., Ajayan, P. M. and Grinstaff, M. W., "High temperature electrical energy storage: Advances, challenges, and frontiers," *Chemical Society Reviews,* 45(21): 5848-5887, 2016.

Lin, Z., Guo, X. and Yu, H., "Amorphous modified silyl-terminated 3D polymer electrolyte for high-performance lithium metal battery," *Nano Energy,* 41: 646-653, 2017.

Liu, H., Gao, P., Fang, J. and Yang, G., "$Li_3V_2(PO_4)_3$/graphene nanocomposites as cathode material for lithium ion batteries," *Chemical Communications,* 47(32): 9110-9112, 2011.

Liu, H., Zhang, F., Li, W., Zhang, X., Lee, C. S., Wang, W. and Tang, Y., "Porous tremella-like MoS_2/polyaniline hybrid composite with enhanced performance for lithium-ion battery anodes," *Electrochimica Acta,* 167: 132-138, 2015.

Liu, J., Chen, H., Xie, J., Sun, Z., Wu, N. and Wu, B., "Electrochemical performance studies of Li-rich cathode materials with different primary particle sizes," *Journal of Power Sources,* 251: 208-214, 2014.

Liu, J., Li, N., Goodman, M. D., Zhang, H. G., Epstein, E. S., Huang, B., Pan, Z., Kim, J., Choi, J. H. and Huang, X., "Mechanically and chemically robust sandwich-structured C@Si@C nanotube array Li-ion battery anodes," *ACS Nano,* 9(2): 1985-1994, 2015.

Liu, J., Zheng, Q., Goodman, M. D., Zhu, H., Kim, J., Krueger, N. A., Ning, H., Huang, X., Liu, J., Terrones, M. and Braun, P. V., "Graphene sandwiched mesostructured li-ion battery electrodes," *Advanced Materials,* 28(35): 7696-7702, 2016.

Liu, M., Gao, H., Hu, G., Zhu, K. and Huang, H., "Facile preparation of core-shell si@ $Li_4Ti_5O_{12}$ nanocomposite as large-capacity lithium-ion battery anode," *Journal of Energy Chemistry,* 40: 89-98, 2020.

Liu, N., Lu, Z., Zhao, J., McDowell, M. T., Lee, H. W., Zhao, W. and Cui, Y., "A pomegranate-inspired nanoscale design for large-volume-change lithium battery anodes," *Nature Nanotechnology,* 9(3): 187, 2014.

Liu, N., Wu, H., McDowell, M. T., Yao, Y., Wang, C. and Cui, Y., "A yolk-shell design for stabilized and scalable Li-ion battery alloy anodes," *Nano Letters,* 12(6): 3315-3321, 2012.

Liu, S., Wu, H., Huang, L., Xiang, M., Liu, H. and Zhang, Y., "Synthesis of $Li_2Si_2O_5$-coated $LiNi_{0.6}Co_{0.2}Mn_{0.2}O_2$ cathode materials with enhanced high-voltage electrochemical properties for lithium-ion batteries," *Journal of Alloys and Compounds,* 674: 447-454, 2016.

Liu, T., Lin, L., Bi, X., Tian, L., Yang, K., Liu, J., Li, M., Chen, Z., Lu, J. and Amine, K., "In situ quantification of interphasial chemistry in Li-ion battery," *Nature Nanotechnology,* 14(1): 50, 2019.

Liu, W., Lee, S. W., Lin, D., Shi, F., Wang, S., Sendek, A. D. and Cui, Y., "Enhancing ionic conductivity in composite polymer electrolytes with well-aligned ceramic nanowires," *Nature Energy,* 2(5): 17035, 2017.

Liu, W., Li, X., Xiong, D., Hao, Y., Li, J., Kou, H., Yan, B., Li, D., Lu, S. and Koo, A., "Significantly improving cycling performance of cathodes in lithium ion batteries: The effect of Al_2O_3 and $LiAlO_2$ coatings on $LiNi_{0.6}Co_{0.2}Mn_{0.2}O_2$," *Nano Energy,* 44: 111-120, 2018.

Liu, W., Liu, N., Sun, J., Hsu, P. C., Li, Y., Lee, H. W. and Cui, Y., "Ionic conductivity enhancement of polymer electrolytes with ceramic nanowire fillers," *Nano Letters,* 15(4): 2740-2745, 2015.

Liu, X. H., Fan, L. L., Yang, H., Zhang, S. L., Huang, J. Y., Zhu, Ting., "Self-limiting lithiation in silicon nanowires," *ACS Nano,* 7(2): 1495-1503, 2013.

Liu, X. H., Zheng, H., Zhong, L., Huang, S., Karki, K., Zhang, L. Q., Liu, Y., Kushima, A., Liang, W. T., Wang, J. W., Cho, J. H., Epstein, E., Dayeh, S. A., Picraux, S. T., Zhu, T., Li, J., Sullivan, J. P., Cumings, J., Wang, C., Mao, S. X., Ye, Z. Z., Zhang, S. and Huang, J. Y., "Anisotropic swelling and fracture of silicon nanowires during lithiation," *Nano Letters,* 11(8): 3312-3318, 2011.

Liu, X. H., Zhong, L., Huang, S., Mao, S. X., Zhu, T. and Huang, J. Y., "Size-dependent fracture of silicon nanoparticles during lithiation," *ACS Nano,* 6(2): 1522-1531, 2012.

Lotfabad, E. M., Kalisvaart, P., Kohandehghan, A., Cui, K., Kupsta, M., Farbod, B. and Mitlin, D., "Si nanotubes ald coated with TiO_2, TiN or Al_2O_3 as high performance lithium ion battery anodes," *Journal of Materials Chemistry A,* 2(8): 2504-2516, 2014.

Lu, B., Yuk, H., Lin, S., Jian, N., Qu, K., Xu, J. and Zhao, X., "Pure PEDOT:PSS hydrogels," *Nature Communications,* 10(1): 1-10, 2019.

Luo, F., Liu, B., Zheng, J., Chu, G., Zhong, K., Li, H., Huang, X. and Chen, L., "Review-nano-silicon/carbon composite anode materials towards practical application for next generation Li-ion batteries," *Journal of the Electrochemical Society,* 162(14): A2509-A2528, 2015.

Luo, W., Chen, X., Xia, Y., Chen, M., Wang, L., Wang, Q., Li, W. and Yang, J., "Surface and interface engineering of silicon-based anode materials for lithium-ion batteries," *Advanced Energy Materials,* 7(24), 2017.

Luo, W., Gong, Y., Zhu, Y., Fu, K. K., Dai, J., Lacey, S. D., Wang, C., Liu, B., Han, X. and Mo, Y., "Transition from superlithiophobicity to superlithiophilicity of garnet solid-state electrolyte," *Journal of the American Chemical Society,* 138(37): 12258-12262, 2016.

Luo, W., Wang, Y., Wang, L., Jiang, W., Chou, S. L., Dou, S. X., Liu, H. K. and Yang, J., "Silicon/mesoporous carbon/crystalline TiO_2 nanoparticles for highly stable lithium storage," *ACS Nano,* 10(11): 10524-10532, 2016.

Luo, Y., Li, X., Zhang, Y., Ge, L., Chen, H. and Guo, L., "Electrochemical properties and structural stability of Ga-and Y-co-doping in $Li_7La_3Zr_2O_{12}$ ceramic electrolytes for lithium-ion batteries," *Electrochimica Acta,* 294: 217-225, 2019.

Ma, D., Cao, Z. and Hu, A., "Si-based anode materials for li-ion batteries: A mini review," *Nano-Micro Letters,* 6(4): 347-358, 2014.

Ma, G., Li, J., Sun, K., Peng, H., Mu, J. and Lei, Z., "High performance solid-state supercapacitor with PVA-KOH-$K_3[Fe(CN)_6]$ gel polymer as electrolyte and separator," *Journal of Power Sources,* 256: 281-287, 2014.

Ma, H., Cheng, F., Chen, J. Y., Zhao, J. Z., Li, C. S., Tao, Z. L. and Liang, J., "Nest-like silicon nanospheres for high-capacity lithium storage," *Advanced Materials,* 19(22): 4067-4070, 2007.

Ma, Y., Chang, H., Zhang, M. and Chen, Y., "Graphene-based materials for lithium-ion hybrid supercapacitors," *Advanced Materials,* 27(36): 5296-5308, 2015.

Ma, Y., Li, L., Gao, G., Yang, X. and You, Y., "Effect of montmorillonite on the ionic conductivity and electrochemical properties of a composite solid polymer electrolyte based on polyvinylidenedifluoride/polyvinyl alcohol matrix for lithium ion batteries," *Electrochimica Acta,* 187: 535-542, 2016.

Ma, Y., Martinez de la Hoz, J. M., Angarita, I., Berrio-Sanchez, J. M., Benitez, L., Seminario, J. M., Son, S. B., Lee, S. H., George, S. M., Ban, C. and Balbuena, P. B., "Structure and reactivity of alucone-coated films on Si and Li_xSi_y surfaces," *ACS Appllied Materials & Interfaces,* 7(22): 11948-11955, 2015.

Makhlooghiazad, F., Guazzagaloppa, J., O'Dell, L. A., Yunis, R., Basile, A., Howlett, P. C. and Forsyth, M., "The influence of the size and symmetry of cations and anions on the physicochemical behavior of organic ionic plastic crystal electrolytes mixed with sodium salts," *Physical Chemistry Chemical Physics,* 20(7): 4721-4731, 2018.

McDonald, M. B. and Hammond, P. T., "Efficient transport networks in a dual electron/lithium-conducting polymeric composite for electrochemical applications," *ACS Applied Materials & Interfaces,* 10(18): 15681-15690, 2018.

McDowell, M. T., Lee, S. W., Nix, W. D. and Cui, Y., "25th anniversary article: Understanding the lithiation of silicon and other alloying anodes for lithium-ion batteries," *Advanced Materials,* 25(36): 4966-4985, 2013.

McDowell, M. T., Lee, S. W., Ryu, I., Wu, H., Nix, W. D., Choi, J. W. and Cui, Y., "Novel size and surface oxide effects in silicon nanowires as lithium battery anodes," *Nano Letters,* 11(9): 4018-4025, 2011.

Mindemark, J., Mogensen, R., Smith, M. J., Silva, M. M. and Brandell, D., "Polycarbonates as alternative electrolyte host materials for solid-state sodium batteries," *Electrochemistry Communications,* 77: 58-61, 2017.

Mishra, K., Garg, A., Sharma, R., Gautam, R. and Pundir, S., "Effect of blending of pmma on PVDF-HFP+$NaCF_3SO_3$-EC-PC gel polymer electrolyte," *Materials Today: Proceedings,* 12: 621-627, 2019.

Mishra, R. and Rao, K. J., "On the formation of poly (ethyleneoxide)-poly (vinylalcohol) blends," *European Polymer Journal,* 35(10): 1883-1894, 1999.

Mohapatra, S. R., Thakur, A. K. and Choudhary, R., "Effect of nanoscopic confinement on improvement in ion conduction and stability properties of an intercalated polymer nanocomposite electrolyte for energy storage applications," *Journal of Power Sources,* 191(2): 601-613, 2009.

Moreno, J. S., Maresca, G., Panero, S., Scrosati, B. and Appetecchi, G., "Sodium-conducting ionic liquid-based electrolytes," *Electrochemistry Communications,* 43: 1-4, 2014.

Moskwiak, M., Giska, I., Borkowska, R., Zalewska, A., Marczewski, M., Marczewska, H. and Wieczorek, W., "Physico-and electrochemistry of composite electrolytes based on PEODME-LiTFSI with TiO_2," *Journal of Power Sources,* 159(1): 443-448, 2006.

Muldoon, J., Bucur, C. B., Boaretto, N., Gregory, T. and Di Noto, V., "Polymers: Opening doors to future batteries," *Polymer Reviews,* 55(2): 208-246, 2015.

Munaoka, T., Yan, X., Lopez, J., To, J. W., Park, J., Tok, J. B. H., Cui, Y. and Bao, Z., "Ionically conductive self-healing binder for low cost Si microparticles anodes in Li-ion batteries," *Advanced Energy Materials,* 8(14): 1703138, 2018.

Murugan, A. V., Muraliganth, T. and Manthiram, A., "Rapid microwave-solvothermal synthesis of phospho-olivine nanorods and their coating with a mixed conducting polymer for lithium ion batteries," *Electrochemistry Communications,* 10(6): 903-906, 2008.

Naik, J., Bhajantri, R., Hebbar, V. and Rathod, S. G., "Influence of ZrO_2 filler on physico-chemical properties of PVA/$NaClO_4$ polymer composite electrolytes," *Advanced Composites and Hybrid Materials,* 1(3): 518-529, 2018.

Naoi, K., Ishimoto, S., Isobe, Y. and Aoyagi, S., "High-rate nano-crystalline $Li_4Ti_5O_{12}$ attached on carbon nano-fibers for hybrid supercapacitors," *Journal of Power Sources,* 195(18): 6250-6254, 2010.

Nie, M., Abraham, D. P., Chen, Y., Bose, A. and Lucht, B. L., "Silicon solid electrolyte interphase (SEI) of lithium ion battery characterized by microscopy and spectroscopy," *The Journal of Physical Chemistry C,* 117(26): 13403-13412, 2013.

Noh, J. S., "Highly conductive and stretchable poly (dimethylsiloxane): poly (3, 4-ethylenedioxythiophene): poly (styrene sulfonic acid) blends for organic interconnects," *Rsc Advances,* 4(4): 1857-1863, 2014.

Noor, S. A. M., Howlett, P. C., MacFarlane, D. R. and Forsyth, M., "Properties of sodium-based ionic liquid electrolytes for sodium secondary battery applications," *Electrochimica Acta,* 114: 766-771, 2013.

Novák, P., Müller, K., Santhanam, K. and Haas, O., "Electrochemically active polymers for rechargeable batteries," *Chemical Reviews,* 97(1): 207-282, 1997.

Oh, H., Xu, K., Yoo, H. D., Kim, D. S., Chanthad, C., Yang, G., Jin, J., Ayhan, I. A., Oh, S. M. and Wang, Q., "Poly (arylene ether)-based single-ion conductors for lithium-ion batteries," *Chemistry of Materials,* 28(1): 188-196, 2015.

Pal, B., Yang, S., Ramesh, S., Thangadurai, V. and Jose, R., "Electrolyte selection for supercapacitive devices: A critical review," *Nanoscale Advances,* 1(10): 3807-3835, 2019.

Park, M. H., Kim, M. G., Joo, J., Kim, K., Kim, J., Ahn, S., Cui, Y. and Cho, J., "Silicon nanotube battery anodes," *Nano Letters,* 9(11): 3844-3847, 2009.

Park, M. S., Lee, J. W., Choi, W., Im, D., Doo, S. G. and Park, K. S., "On the surface modifications of high-voltage oxide cathodes for lithium-ion batteries: New insight and significant safety improvement," *Journal of Materials Chemistry,* 20(34), 2010.

Park, S. B., Shin, H. C., Lee, W. G., Cho, W. I. and Jang, H., "Improvement of capacity fading resistance of $LiMn_2O_4$ by amphoteric oxides," *Journal of Power Sources,* 180(1): 597-601, 2008.

Patel, M., Chandrappa, K. G. and Bhattacharyya, A. J., "Increasing ionic conductivity of polymer-sodium salt complex by addition of a non-ionic plastic crystal," *Solid State Ionics,* 181(17-18): 844-848, 2010.

Peng, L., Peng, X., Liu, B., Wu, C., Xie, Y. and Yu, G., "Ultrathin two-dimensional MnO_2/graphene hybrid nanostructures for high-performance, flexible planar supercapacitors," *Nano Letters,* 13(5): 2151-2157, 2013.

Phattharasupakun, N., Wutthiprom, J., Ma, N., Chanlek, N. and Sawangphruk, M., "Sodium-ion diffusion and charge transfer kinetics of sodium-ion hybrid capacitors using bio-derived hierarchical porous carbon," *Electrochimica Acta,* 286: 55-64, 2018.

Ponrouch, A., Monti, D., Boschin, A., Steen, B., Johansson, P. and Palacin, M., "Non-aqueous electrolytes for sodium-ion batteries," *Journal of Materials Chemistry A,* 3(1): 22-42, 2015.

Pu, X., Li, L., Liu, M., Jiang, C., Du, C., Zhao, Z., Hu, W. and Wang, Z. L., "Wearable self-charging power textile based on flexible yarn supercapacitors and fabric nanogenerators," *Advanced Materials,* 28(1): 98-105, 2016.

Quartarone, E. and Mustarelli, P., "Electrolytes for solid-state lithium rechargeable batteries: Recent advances and perspectives," *Chemical Society Reviews,* 40(5): 2525-2540, 2011.

Ramesh Babu, J., Ravindhranath, K. and Vijaya Kumar, K., "Preparation and characterization of nano-Dy_2O_3-doped PVA+$Na_3C_6H_5O_7$ polymer electrolyte films for battery applications," *Advances in Materials Science and Engineering*, 2018.

Ravi, M., Song, S., Wang, J., Wang, T. and Nadimicherla, R., "Ionic liquid incorporated biodegradable gel polymer electrolyte for lithium ion battery applications," *Journal of Materials Science: Materials in Electronics,* 27(2): 1370-1377, 2016.

Risangud, N., Li, Z., Anastasaki, A., Wilson, P., Kempe, K. and Haddleton, D. M., "Hydrosilylation as an efficient tool for polymer synthesis and modification with methacrylates." *RSC Advances,* 5(8): 5879-5885, 2015.

Rivas, B. L., Pereira, E. D. and Moreno-Villoslada, I., "Water-soluble polymer-metal ion interactions," *Progress in Polymer Science,* 28(2): 173-208, 2003.

Rohan, R., Pareek, K., Cai, W., Zhang, Y., Xu, G., Chen, Z., Gao, Z., Dan, Z. and Cheng, H., "Melamine-terephthalaldehyde-lithium complex: A porous organic network based single ion electrolyte for lithium ion batteries," *Journal of Materials Chemistry A,* 3(9): 5132-5139, 2015.

Roldán, S., Blanco, C., Granda, M., Menéndez, R. and Santamaría, R., "Towards a further generation of high-energy carbon-based capacitors by using redox-active electrolytes," *Angewandte Chemie International Edition,* 50(7): 1699-1701, 2011.

Roldán, S., Granda, M., Menéndez, R., Santamaría, R. and Blanco, C., "Supercapacitor modified with methylene blue as redox active electrolyte," *Electrochimica Acta,* 83: 241-246, 2012.

Rozier, P. and Tarascon, J. M., "Li-rich layered oxide cathodes for next-generation li-ion batteries: Chances and challenges," *Journal of the Electrochemical Society,* 162(14): A2490-A2499, 2015.

Ruffo, R., Hong, S. S., Chan, C. K., Huggins, R. A. and Cui, Y., "Impedance analysis of silicon nanowire lithium ion battery anodes," *The Journal of Physical Chemistry C,* 113(26): 11390-11398, 2009.

Ryu, I., Choi, J. W., Cui, Y. and Nix, W. D., "Size-dependent fracture of si nanowire battery anodes," *Journal of the Mechanics and Physics of Solids,* 59(9): 1717-1730, 2011.

Ryu, J. H., Kim, J. W., Sung, Y. E. and Oh, S. M., "Failure modes of silicon powder negative electrode in lithium secondary batteries," *Electrochemical and Solid-State Letters,* 7(10): A306-A309, 2004.

Saha, P., Datta, M. K., Velikokhatnyi, O. I., Manivannan, A., Alman, D. and Kumta, P. N., "Rechargeable magnesium battery: Current status and key challenges for the future," *Progress in Materials Science,* 66: 1-86, 2014.

Saikia, D., Wu, H. Y., Pan, Y. C., Lin, C. P., Huang, K. P., Chen, K. N., Fey, G. T. and Kao, H. M., "Highly conductive and electrochemically stable plasticized blend polymer electrolytes based on PVDF-HFP and triblock copolymer PPG-PEG-PPG diamine for Li-ion batteries," *Journal of Power Sources,* 196(5): 2826-2834, 2011.

Schmidt, O., Hawkes, A., Gambhir, A. and Staffell, I., "The future cost of electrical energy storage based on experience rates," *Nature Energy,* 2(8): 1-8, 2017.

Selulos, B. M., "Effect of dimethyl carbonate plasticizer on ionic conductivity of methyl cellulose-based polymer electrolytes," *Malaysian Journal of Analytical Sciences,* 16(3): 283-289, 2012.

Senthilkumar, S., Selvan, R. K., Ponpandian, N., Melo, J. and Lee, Y., "Improved performance of electric double layer capacitor using redox additive (VO^{2+}/VO^{2+}) aqueous electrolyte," *Journal of Materials Chemistry A,* 1(27): 7913-7919, 2013.

Shamsipur, M., Beigi, A. A. M., Teymouri, M., Pourmortazavi, S. M. and Irandoust, M., "Physical and electrochemical properties of ionic liquids 1-ethyl-3-methylimidazolium tetrafluoroborate, 1-butyl-3-methylimidazolium trifluoromethanesulfonate and 1-butyl-1-methylpyrrolidinium bis (trifluoromethylsulfonyl) imide," *Journal of Molecular Liquids,* 157(1): 43-50, 2010.

Sharma, P., Patel, D. K., Kancharlapalli, S., Magdassi, S. and Sasson, Y., "Facile combined experimental & computational study: G-C_3N_4@ pdms assisted knoevenagel condensation reaction under phase transfer conditions," *ACS Sustainable Chemistry & Engineering*, 2019.

Shen, L., Lv, H., Chen, S., Kopold, P., van Aken, P. A., Wu, X., Maier, J. and Yu, Y., "Peapod-like Li_3VO_4/N-doped carbon nanowires with pseudocapacitive properties as advanced materials for high-energy lithium-ion capacitors," *Advanced Materials,* 29(27): 1700142, 2017.

Shi, S., Lu, P., Liu, Z., Qi, Y., Hector, L. G., Jr., Li, H. and Harris, S. J., "Direct calculation of Li-ion transport in the solid electrolyte interphase," *Journal of the American Chemical Society,* 134(37): 15476-15487, 2012.

Shim, J. H., Lee, S. and Park, S. S., "Effects of MgO coating on the structural and electrochemical characteristics of $LiCoO_2$ as cathode materials for lithium ion battery," *Chemistry of Materials,* 26(8): 2537-2543, 2014.

Sim, L., Majid, S. and Arof, A., "Effects of 1-butyl-3-methyl imidazolium trifluoromethanesulfonate ionic liquid in poly (ethyl methacrylate)/poly (vinylidenefluoride-co-hexafluoropropylene) blend based polymer electrolyte system," *Electrochimica Acta,* 123: 190-197, 2014.

Sim, S., Oh, P., Park, S. and Cho, J., "Critical thickness of SiO_2 coating layer on core@shell bulk@nanowire si anode materials for Li-ion batteries," *Advanced Materials,* 25(32): 4498-4503, 2013.

Singh, V. K. and Singh, R. K., "Development of ion conducting polymer gel electrolyte membranes based on polymer PVDF-HFP, BMIMTFSI ionic liquid and the Li-salt with improved electrical, thermal and structural properties," *Journal of Materials Chemistry C,* 3(28): 7305-7318, 2015.

Snook, G. A., Kao, P. and Best, A. S., "Conducting-polymer-based supercapacitor devices and electrodes," *Journal of Power Sources,* 196(1): 1-12, 2011.

Son, I. H., Park, J. H. and Mun, J., "Surface modification of over-lithiated layered oxide by low-temperature chemical vapor deposition for high energy lithium-ion batteries," *Energy Storage Materials,* 4: 137-144, 2016.

Soulintzis, A., Kontos, G., Karahaliou, P., Psarras, G., Georga, S. and Krontiras, C., "Dielectric relaxation processes in epoxy resin-ZnO composites," *Journal of Polymer Science Part B: Polymer Physics,* 47(4): 445-454, 2009.

Stephan, A. M., Kumar, T. P., Kulandainathan, M. A. and Lakshmi, N. A., "Chitin-incorporated poly (ethylene oxide)-based nanocomposite electrolytes for lithium batteries," *The Journal of Physical Chemistry B,* 113(7): 1963-1971, 2009.

Su, L. H., Zhang, X. G., Mi, C. H., Gao, B. and Liu, Y., "Improvement of the capacitive performances for co-Al layered double hydroxide by adding hexacyanoferrate into the electrolyte," *Physical Chemistry Chemical Physics,* 11(13): 2195-2202, 2009.

Tang, X., Lui, Y. H., Chen, B. and Hu, S., "Functionalized carbon nanotube based hybrid electrochemical capacitors using neutral bromide redox-active electrolyte for enhancing energy density," *Journal of Power Sources,* 352: 118-126, 2017.

Taracson, J. and Armand, M., "Issues and challenges facing lithium ion batteries," *Nature,* 414: 359-367, 2001.

Tarascon, J. M. and Armand, M, "Issues and challenges facing rechargeable lithium batteries," Materials for sustainable energy: A collection of peer-reviewed research and review articles from nature publishing group, World Scientific**:** 171-179, 2011.

Tarascon, J. M., Rozier, P. and Zhang, B, "Method for producing a positive electrode composite material for Na ion battery," Patents, 2018.

Thakur, V. K., Ding, G., Ma, J., Lee, P. S. and Lu, X., "Hybrid materials and polymer electrolytes for electrochromic device applications," *Advanced Materials,* 24(30): 4071-4096, 2012.

Tian, H., Tan, X., Xin, F., Wang, C. and Han, W., "Micro-sized nano-porous Si/C anodes for lithium ion batteries," *Nano Energy,* 11: 490-499, 2015.

Trinh, N. D., Saulnier, M., Lepage, D. and Schougaard, S. B., "Conductive polymer film supporting $LiFePO_4$ as composite cathode for lithium ion batteries," *Journal of Power Sources,* 221: 284-289, 2013.

Tsuji, F., Tanibata, N., Sakuda, A., Hayashi, A. and Tatsumisago, M., "Preparation of sodium ion conductive $Na_{10}GeP_2S_{12}$ glass-ceramic electrolytes," *Chemistry Letters,* 47(1): 13-15, 2018.

Verma, H., Mishra, K. and Rai, D., "Sodium ion conducting nanocomposite polymer electrolyte membrane for sodium ion batteries," *Journal of Solid State Electrochemistry*: 1-12, 2020.

Vignarooban, K., Badami, P., Dissanayake, M., Ravirajan, P. and Kannan, A. M., "Poly-acrylonitrile-based gel-polymer electrolytes for sodium-ion batteries," *Ionics,* 23(10): 2817-2822, 2017.

Wang, G., Lu, X., Ling, Y., Zhai, T., Wang, H., Tong, Y. and Li, Y., "LiCl/PVA gel electrolyte stabilizes vanadium oxide nanowire electrodes for pseudocapacitors," *ACS Nano,* 6(11): 10296-10302, 2012.

Wang, H., Jang, Y. I., Huang, B., Sadoway, D. R. and Chiang, Y. M., "Tem study of electrochemical cycling-induced damage and disorder in $LiCoO_2$ cathodes for rechargeable lithium batteries," *Journal of the Electrochemical Society,* 146(2): 473-480, 1999.

Wang, J., Chen, G. and Song, S., "Na-ion conducting gel polymer membrane for flexible supercapacitor application." *Electrochimica Acta* 330: 135322, 2020.

Wang, J., Li, S., Zhao, Y., Shi, J., Lv, L., Wang, H., Zhang, Z. and Feng, W., "The influence of different Si:C ratios on the electrochemical performance of silicon/carbon layered film anodes for lithium-ion batteries," *RSC Advances,* 8(12): 6660-6666, 2018.

Wang, J., Liao, L., Li, Y., Zhao, J., Shi, F., Yan, K., Pei, A., Chen, G., Li, G. and Lu, Z., "Shell-protective secondary silicon nanostructures as pressure-resistant high-volumetric-capacity anodes for lithium-ion batteries," *Nano Letters,* 18(11): 7060-7065, 2018.

Wang, J., Zhao, Z., Muchakayala, R. and Song, S., "High-performance mg-ion conducting poly (vinyl alcohol) membranes: Preparation, characterization and application in supercapacitors," *Journal of Membrane Science,* 555: 280-289, 2018.

Wang, J., Zhao, Z., Song, S., Ma, Q. and Liu, R., "High performance poly (vinyl alcohol)-based Li-ion conducting gel polymer electrolyte films for electric double-layer capacitors," *Polymers,* 10(11): 1179, 2018.

Wang, L., Liu, J., Yuan, S., Wang, Y. and Xia, Y., "To mitigate self-discharge of lithium-sulfur batteries by optimizing ionic liquid electrolytes," *Energy & Environmental Science,* 9(1): 224-231, 2016.

Wang, M., Wang, W., Wang, A., Yuan, K., Miao, L., Zhang, X., Huang, Y., Yu, Z. and Qiu, J., "A multi-core-shell structured composite cathode material with a conductive polymer network for Li-S batteries," *Chemical Communications,* 49(87): 10263-10265, 2013.

Wang, M. S., Wang, G. L., Wang, S., Zhang, J., Wang, J., Zhong, W., Tang, F., Yang, Z.-L., Zheng, J. and Li, X., "In situ catalytic growth 3D multi-layers graphene sheets coated nano-silicon anode for high performance lithium-ion batteries," *Chemical Engineering Journal,* 356: 895-903, 2019.

Wang, W. and Alexandridis, P., "Composite polymer electrolytes: Nanoparticles affect structure and properties," *Polymers,* 8(11): 387, 2016.

Wang, W., Ruiz, I., Ahmed, K., Bay, H. H., George, A. S., Wang, J., Butler, J., Ozkan, M. and Ozkan, C. S., "Silicon decorated cone shaped carbon nanotube clusters for lithium ion battery anodes," *Small,* 10(16): 3389-3396, 2014.

Wang, W., Yin, Z., Wang, J., Wang, Z., Li, X. and Guo, H., "Effect of heat-treatment on Li_2ZrO_3-coated $LiNi_{1/3}Co_{1/3}Mn_{1/3}O_2$ and its high voltage electrochemical performance," *Journal of Alloys and Compounds,* 651: 737-743, 2015.

Wang, X., Liu, Z., Zhang, C., Kong, Q., Yao, J., Han, P., Jiang, W., Xu, H. and Cui, G., "Exploring polymeric lithium tartaric acid borate for thermally resistant polymer electrolyte of lithium batteries," *Electrochimica Acta,* 92: 132-138, 2013.

Wang, Y., Song, S., Xu, C., Hu, N., Molenda, J. and Lu, L., "Development of solid-state electrolytes for sodium-ion battery-a short review," *Nano Materials Science*, 2019.

Wei, B., Liu, J., Ouyang, L. and Martin, D. C., "POSS-ProDOT crosslinking of PEDOT," *Journal of Materials Chemistry B,* 5(25): 5019-5026, 2017.

Wieczorek, W., Stevens, J. and Florjańczyk, Z., "Composite polyether based solid electrolytes. The lewis acid-base approach," *Solid State Ionics,* 85(1-4): 67-72, 1996.

Woodford, W. H., Chiang, Y. M. and Carter, W. C., "“Electrochemical shock” of intercalation electrodes: A fracture mechanics analysis," *Journal of the Electrochemical Society,* 157(10): A1052-A1059, 2010.

Wu, F., Liu, J., Li, L., Zhang, X., Luo, R., Ye, Y. and Chen, R., "Surface modification of li-rich cathode materials for lithium-ion batteries with a PEDOT:PSS conducting polymer," *ACS Appllied Materials & Interfaces,* 8(35): 23095-23104, 2016.

Wu, H., Chan, G., Choi, J. W., Ryu, I., Yao, Y., McDowell, M. T., Lee, S. W., Jackson, A., Yang, Y. and Hu, L., "Stable cycling of double-walled silicon nanotube battery anodes through solid-electrolyte interphase control," *Nature Nanotechnology,* 7(5): 310, 2012.

Wu, H. and Cui, Y., "Designing nanostructured si anodes for high energy lithium ion batteries," *Nano Today,* 7(5): 414-429, 2012.

Wu, H., Yu, G., Pan, L., Liu, N., McDowell, M. T., Bao, Z. and Cui, Y., "Stable Li-ion battery anodes by in-situ polymerization of conducting hydrogel to conformally coat silicon nanoparticles," *Nature Communications,* 4: 1943, 2013.

Xi, J., Qiu, X., Li, J., Tang, X., Zhu, W. and Chen, L., "PVDF-PEO blends based microporous polymer electrolyte: Effect of peo on pore configurations and ionic conductivity," *Journal of Power Sources,* 157(1): 501-506, 2006.

Xiao, B., Liu, H., Liu, J., Sun, Q., Wang, B., Kaliyappan, K., Zhao, Y., Banis, M. N., Liu, Y., Li, R., Sham, T. K., Botton, G. A., Cai, M. and Sun, X., "Nanoscale manipulation of spinel lithium nickel manganese oxide surface by multisite Ti occupation as high-performance cathode," *Advanced Materials,* 29(47), 2017.

Xiao, B. and Sun, X., "Surface and subsurface reactions of lithium transition metal oxide cathode materials: An overview of the fundamental origins and remedying approaches," *Advanced Energy Materials,* 8(29): 1802057, 2018.

Xiao, Q., Deng, C., Wang, Q., Zhang, Q., Yue, Y. and Ren, S., "In situ cross-linked gel polymer electrolyte membranes with excellent thermal stability for lithium ion batteries," *ACS Omega,* 4(1): 95-103, 2019.

Xie, Y., Zhao, H., Cheng, H., Hu, C., Fang, W., Fang, J., Xu, J. and Chen, Z., "Facile large-scale synthesis of core–shell structured sulfur@ polypyrrole composite and its application in lithium–sulfur batteries with high energy density," *Applied Energy,* 175: 522-528, 2016.

Xiong, L., Xu, Y., Tao, T., Du, X. and Li, J., "Double roles of aluminium ion on surface-modified spinel $LiMn_{1.97}Ti_{0.03}O_4$," *Journal of Materials Chemistry,* 21(13), 2011.

Xu, D., Hu, W., Sun, X. N., Cui, P. and Chen, X. Y., "Redox additives of Na_2MoO_4 and KI: Synergistic effect and the improved capacitive performances for carbon-based supercapacitors," *Journal of Power Sources,* 341: 448-456, 2017.

Xu, G. L., Amine, R., Abouimrane, A., Che, H., Dahbi, M., Ma, Z. F., Saadoune, I., Alami, J., Mattis, W. L. and Pan, F., "Challenges in developing electrodes, electrolytes, and diagnostics tools to understand and advance sodium-ion batteries," *Advanced Energy Materials,* 8(14): 1702403, 2018.

Xu, G. L., Liu, J., Amine, R., Chen, Z. and Amine, K., "Selenium and selenium-sulfur chemistry for rechargeable lithium batteries: Interplay of cathode structures, electrolytes, and interfaces," *ACS Energy Letters,* 2(3): 605-614, 2017.

Xu, R., Guo, F., Cui, X., Zhang, L., Wang, K. and Wei, J., "High performance carbon nanotube based fiber-shaped supercapacitors using redox additives of polypyrrole and hydroquinone," *Journal of Materials Chemistry A,* 3(44): 22353-22360, 2015.

Xu, R. C., Xia, X. H., Wang, X. I., Xia, Y. and Tu, J. P., "Tailored Li_2S-P_2S_5 glass-ceramic electrolyte by mos_2 doping, possessing high ionic conductivity for all-solid-state lithium-sulfur batteries," *Journal of Materials Chemistry A*, 2017.

Xu, Y. D., Xiang, W., Wu, Z. G., Xu, C. L., Li, Y. C., Guo, X. D., Lv, G. P., Peng, X. and Zhong, B. H., "Improving cycling performance and rate capability of Ni-rich $LiNi_{0.8}Co_{0.1}Mn_{0.1}O_2$ cathode materials by $Li_4Ti_5O_{12}$ coating," *Electrochimica Acta,* 268: 358-365, 2018.

Xun, Z., Liu, Y., Gu, J., Liu, L. and Huo, P., "A biomass-based redox gel polymer electrolyte for improving energy density of flexible supercapacitor," *Journal of the Electrochemical Society,* 166(10): A2300-A2312, 2019.

Yan, P., Zheng, J., Chen, T., Luo, L., Jiang, Y., Wang, K., Sui, M., Zhang, J. G., Zhang, S. and Wang, C., "Coupling of electrochemically triggered thermal and mechanical effects to aggravate failure in a layered cathode," *Nature Communications,* 9(1): 2437, 2018.

Yan, P., Zheng, J., Gu, M., Xiao, J., Zhang, J. G. and Wang, C. M., "Intragranular cracking as a critical barrier for high-voltage usage of layer-structured cathode for lithium-ion batteries," *Nature Communications,* 8: 14101, 2017.

Yan, S. X., Luo, S.H., Feng, J., Li, P. W., Guo, R., Wang, Q., Zhang, Y. H., Liu, Y.G. and Bao, S., "Rational design of flower-like $FeCo_2S_4$/reduced graphene oxide films: Novel binder-free electrodes with ultra-high conductivity flexible substrate for high-performance all-solid-state pseudocapacitor," *Chemical Engineering Journal,* 381: 122695, 2020.

Yang, J., Wang, Y., Li, W., Wang, L., Fan, Y., Jiang, W., Luo, W., Wang, Y., Kong, B. and Selomulya, C., "Amorphous TiO_2 shells: A vital elastic buffering layer on silicon nanoparticles for high-performance and safe lithium storage," *Advanced Materials,* 29(48): 1700523, 2017.

Yang, M., Zhong, Y., Ren, J., Zhou, X., Wei, J. and Zhou, Z., "Fabrication of high-power Li-ion hybrid supercapacitors by enhancing the exterior surface charge storage," *Advanced Energy Materials,* 5(17): 1500550, 2015.

Yang, W., Yang, W., Feng, J. and Qin, X., "A polypyrrole-coated acetylene black/sulfur composite cathode material for lithium–sulfur batteries," *Journal of Energy Chemistry,* 27(3): 813-819, 2018.

Yang, Y., Chang, Z., Li, M., Wang, X. and Wu, Y., "A sodium ion conducting gel polymer electrolyte," *Solid State Ionics,* 269: 1-7, 2015.

Yang, Y., Liao, X. Z., Ma, Z. F., Wang, B. F., He, L. and He, Y. S., "Superior high-rate cycling performance of $LiFePO_4$/C-PPY composite at 55°C," *Electrochemistry Communications,* 11(6): 1277-1280, 2009.

Ye, L., Liang, Q., Lei, Y., Yu, X., Han, C., Shen, W., Huang, Z. H., Kang, F. and Yang, Q. H., "A high performance li-ion capacitor constructed with $Li_4Ti_5O_{12}$/C hybrid and porous graphene macroform," *Journal of Power Sources,* 282: 174-178, 2015.

Yin, J., Qi, L. and Wang, H., "Sodium titanate nanotubes as negative electrode materials for sodium-ion capacitors," *ACS Applied Materials & Interfaces,* 4(5): 2762-2768, 2012.

Yoshio, M., Kugino, S. and Dimov, N., "Electrochemical behaviors of silicon based anode material," *Journal of Power Sources,* 153(2): 375-379, 2006.

Yu, Y., Gu, L., Wang, C., Dhanabalan, A., Van Aken, P. A. and Maier, J., "Encapsulation of Sn@ carbon nanoparticles in bamboo-like hollow carbon nanofibers as an anode material in lithium-based batteries," *Angewandte Chemie International Edition,* 48(35): 6485-6489, 2009.

Yuan, C., Zhang, X., Wu, Q. and Gao, B., "Effect of temperature on the hybrid supercapacitor based on nio and activated carbon with alkaline polymer gel electrolyte," *Solid State Ionics,* 177(13-14): 1237-1242, 2006.

Zeng, X. X., Yin, Y. X., Li, N. W., Du, W. C., Guo, Y. G. and Wan, L. J., "Reshaping lithium plating/stripping behavior via bifunctional polymer electrolyte for room-temperature solid Li metal batteries," *Journal of the American Chemical Society,* 138(49): 15825-15828, 2016.

Zengin, A., Badak, M. U., Bilici, M., Suludere, Z. and Aktas, N., "Preparation of molecularly imprinted PDMS elastomer for selective detection of folic acid in orange juice," *Applied Surface Science,* 471: 168-175, 2019.

Zhan, L., Song, Z., Zhang, J., Tang, J., Zhan, H., Zhou, Y. and Zhan, C., "PEDOT: Cathode active material with high specific capacity in novel electrolyte system," *Electrochimica Acta,* 53(28): 8319-8323, 2008.

Zhang, H., Qin, G., Lin, Y., Zhang, D., Liao, H., Li, Z., Tian, J. and Wu, Q., "A novel flexible electrode with coaxial sandwich structure based polyaniline-coated MoS_2 nanoflakes on activated carbon cloth," *Electrochimica Acta,* 264: 91-100, 2018.

Zhang, L., Deng, J., Liu, L., Si, W., Oswald, S., Xi, L., Kundu, M., Ma, G., Gemming, T. and Baunack, S., "Hierarchically designed SiO_x/SiO_y bilayer nanomembranes as stable anodes for lithium ion batteries," *Advanced Materials,* 26(26): 4527-4532, 2014.

Zhang, R., Du, Y., Li, D., Shen, D., Yang, J., Guo, Z., Liu, H. K., Elzatahry, A. A. and Zhao, D., "Highly reversible and large lithium storage in mesoporous Si/C nanocomposite anodes with silicon nanoparticles embedded in a carbon framework," *Advanced Materials,* 26(39): 6749-6755, 2014.

Zhang, W. J., "Lithium insertion/extraction mechanism in alloy anodes for lithium-ion batteries," *Journal of Power Sources,* 196(3): 877-885, 2011.

Zhang, Y., Rohan, R., Sun, Y., Cai, W., Xu, G., Lin, A. and Cheng, H., "A gel single ion polymer electrolyte membrane for lithium-ion batteries with wide-temperature range operability," *RSC Advances,* 4(40): 21163-21170, 2014.

Zhang, Y., Zhao, Y., Bakenov, Z., Gosselink, D. and Chen, P., "Poly (vinylidene fluoride-co-hexafluoropropylene)/poly (methylmethacrylate)/nanoclay composite gel polymer electrolyte for lithium/sulfur batteries," *Journal of Solid State Electrochemistry,* 18(4): 1111-1116, 2014.

Zhao, C. Z., Zhang, X. Q., Cheng, X. B., Zhang, R., Xu, R., Chen, P. Y., Peng, H. J., Huang, J. Q. and Zhang, Q., "An anion-immobilized composite electrolyte for dendrite-free lithium metal anodes," *Proceedings of the National Academy of Sciences,* 114(42): 11069-11074, 2017.

Zhao, C., Liu, L., Qi, X., Lu, Y., Wu, F., Zhao, J., Yu, Y., Hu, Y. S. and Chen, L., "Solid-state sodium batteries," *Advanced Energy Materials,* 8(17): 1703012, 2018.

Zhao, Y., Ding, Y., Li, Y., Peng, L., Byon, H. R., Goodenough, J. B. and Yu, G., "A chemistry and material perspective on lithium redox flow batteries towards high-density electrical energy storage," *Chemical Society Reviews,* 44(22): 7968-7996, 2015.

Zhou, P., Meng, H., Zhang, Z., Chen, C., Lu, Y., Cao, J., Cheng, F. and Chen, J., "Stable layered Ni-rich $LiNi_{0.9}Co_{0.07}Al_{0.03}O_2$ microspheres assembled with nanoparticles as high-performance cathode materials for lithium-ion batteries," *Journal of Materials Chemistry A,* 5(6): 2724-2731, 2017.

Zhou, Y., Lu, J., Deng, C., Zhu, H., Chen, G. Z., Zhang, S. and Tian, X., "Nitrogen-doped graphene guided formation of monodisperse microspheres of $LiFePO_4$ nanoplates as the positive electrode material of lithium-ion batteries," *Journal of Materials Chemistry A,* 4(31): 12065-12072, 2016.

Zhu, B., Jin, Y., Hu, X., Zheng, Q., Zhang, S., Wang, Q. and Zhu, J., "Poly (dimethylsiloxane) thin film as a stable interfacial layer for high-performance lithium-metal battery anodes," *Advanced Materials,* 29(2): 1603755, 2017.

Zhu, M., Wu, J., Wang, Y., Song, M., Long, L., Siyal, S. H., Yang, X. and Sui, G., "Recent advances in gel polymer electrolyte for high-performance lithium batteries," *Journal of Energy Chemistry,* 37: 126-142, 2019.

Zhu, P., Zhu, J., Yan, C., Dirican, M., Zang, J., Jia, H., Li, Y., Kiyak, Y., Tan, H. and Zhang, X., "In situ polymerization of nanostructured conductive polymer on 3D sulfur/carbon nanofiber composite network as cathode for high-performance lithium–sulfur batteries," *Advanced Materials Interfaces,* 5(10): 1701598, 2018.

Zhu, Y., Gao, X., Wang, X., Hou, Y., Liu, L. and Wu, Y., "A single-ion polymer electrolyte based on boronate for lithium ion batteries," *Electrochemistry Communications,* 22: 29-32, 2012.

Zhu, Y., Wang, X., Hou, Y., Gao, X., Liu, L., Wu, Y. and Shimizu, M., "A new single-ion polymer electrolyte based on polyvinyl alcohol for lithium ion batteries," *Electrochimica Acta,* 87: 113-118, 2013.

Zuo, X., Zhu, J., Müller-Buschbaum, P. and Cheng, Y. J., "Silicon based lithium-ion battery anodes: A chronicle perspective review," *Nano Energy,* 31: 113-143, 2017.